Universidade de Aveiro Departamento de Engenharia Mecânica
2019

Filipe José Matos de Almeida

Exploratory design of a heterogeneous mechanical test using topology optimisation

Projeto exploratório de um ensaio heterogéneo recorrendo a otimização topológica

Universidade de Aveiro Departamento de Engenharia Mecânica
2019

Filipe José Matos de Almeida

Exploratory design of a heterogeneous mechanical test using topology optimisation

Projeto exploratório de um ensaio heterogéneo recorrendo a otimização topológica

Dissertação apresentada à Universidade de Aveiro para cumprimento dos requisitos necessários para a obtenção do grau de Mestre em Engenharia Mecânica, realizada sob orientação científica do António Gil d'Orey de Andrade Campos, Professor auxiliar do Departamento de Engenharia Mecânica da Universidade de Aveiro, e de João Alexandre Dias de Oliveira, Professor auxiliar do Departamento de Engenharia Mecânica da Universidade de Aveiro.

Esta dissertação teve o apoio dos projetos UID/EMS/00481/2019-FCT - FCT - Fundacão para a Ciência e a Tecnologia; e CENTRO-01-0145-FEDER-022083 - Programa Operacional Regional do Centro (Centro2020), através do Portugal 2020 e do Fundo Europeu de Desenvolvimento Regional

o júri/ the jury

presidente / president

Prof. Doutor Joaquim Alexandre Mendes de Pinho da Cruz
Professor Auxiliar do Departamento de Engenharia Mecânica da Universidade de Aveiro

Prof. Doutor Pedro André Dias Prates
Professor auxiliar do Departamento de Engenharia Mecânica da Universidade de Coimbra (arguente)

Prof. Doutor João Alexandre Dias de Oliveira
Professor auxiliar do Departamento de Engenharia Mecânica da Universidade de Aveiro (co-orientador)

agradecimentos / acknowledgements

Os meus sinceros agradecimentos ao meu orientador professor Gil Campos e ao meu coorientador professor João Oliveira, pela disponibilidade, boa disposição, pelo constante rigor e por todo o conhecimento que me trasmitiram ao longo do meu percurso académico. Pelo acompanhamento constante nesta etapa final, e, sobretudo, por me tornarem num melhor engenheiro. Um agradecimento especial também ao grupo de investigação, TherMechCharxsteels, pela disponibilidade, simpatia e por todo o conhecimento e ideias que me foram transmitindo.

Aos meus pais, João e Elisabete, e às minhas irmãs, Daniela e Raquel, por sempre acreditarem nas minhas capacidades, por me aturarem e me fazerem feliz. Por me moldarem enquanto ser humano e, com sacrifício, me darem as condições necessárias para ser bem sucedido.

À minha namorada Salomé, pelo constante apoio, motivação e paciência nos momentos mais difíceis. Por me fazer sair da zona de conforto e por me tornar numa pessoa melhor. Por me fazer acreditar nas minhas capacidades, e por fazer parte da minha vida.

À minha familia, em especial ao Hugo, ao Lúcio e ao Pedro Jorge, por serem uma constante no meu crescimento.

A todos os meus amigos, da Gafanha e da universidade, pela constante aprendizagem pessoal, pelos bons momentos e por me ajudarem a desenvolver uma espécie de personalidade.

keywords Heterogeneous specimen; Topology optimisation; Characterisation of sheet metals; Mechanical tests

abstract

The frequent development and production of new metals in the sheet metal forming industry results in an ever-increasing demand for an accurate prediction of the material's behavior and, particularly, its behavior on sheet forming processes. Heterogeneous tests are crucial to swiftly characterise numerically the material and identify the parameters of the constitutive models, as they provide a wider spectrum of stress and strain states per test.

In the present work, a novel approach is proposed for the design of a heterogeneous specimen. Using topology optimisation, the goal is to find the optimal geometry of the specimen which maximises the incidence of all stress states over the area. A number of formulations were developed and an accurate criterion was developed with one of these objective functions for the purpose of measuring the heterogeneity value of a test. The boundary conditions were defined as a uniaxial tensile test, and the goal was to obtain maximum heterogeneity on a single test.

A novel algorithm that combines different optimisation approaches was developed for one of the formulations that requires sensitivity analysis, while the remaining formulations make use of the Propotinal Topology Optimization (PTO) algorithm. This latter algorithm does not calculate the sensitivities, which is favorable because sensitivity calculation is computationally expensive.

The resulting heterogeneous specimens' designs were analyzed, evaluated and ranked under the defined criterion for comparison purposes. These solutions ranked significantly close to some of the state of the art specimens. However, there is still progress to be made, given the potential of topology optimisation for this application. The efficiency of the objective functions, when formulated individualy, is lacking. That is due to the fact that the present problem is highly non-linear and complex, and relying on a formulation that is aimed entirely at enhancing the heterogeneity of a specimen resulted mostly in greatly heterogeneous non-manufacturable solutions. Therefore, it is concluded that allying these heterogeneous formulations with a structural segment, either by adding a structural restriction or a multiobjective approach, shows promissing results and valuable heterogeneous solutions to the industry.

palavras-chave

Provete heterogéneo; Otimização topológica; Caracterização de chapas metálicas; Ensaios mecânicos

resumo

O recorrente desenvolvimento e produção de novos metais por parte da indústria de chapas metálicas resulta num aumento constante da necessidade de prever corretamente o comportamento destes materiais e, consequentemente, o comportamento dos processos de conformação de metais. Os ensaios mecânicos heterogéneos são cruciais para a rápida caracterização numérica destes materiais e para identificar os respetivos parâmetros dos modelos constitutivos, sendo que estes proporcionam um espectro abrangente de estados de tensão e deformação por ensaio.

No presente trabalho, é proposta uma nova metodologia para o desenvolvimento de um provete mecânico heterogéneo. Recorrendo a otimização topológica, o objetivo é encontrar a geometria ótima que maximize a incidência de estados de tensão na área do provete num só ensaio. Foi desenvolvida uma coletânea de formulações por forma a obter uma solução ótima, de onde resultou um indicador preciso com o intuito de avaliar o grau de heterogeneidade de um ensaio mecânico. As condições de fronteira foram definidas como sendo as de um ensaio mecânico uniaxial.

Um novo algoritmo que combina diferentes metodologias de otimização foi desenvolvido para a formulação que necessita de análise de sensibilidade, enquanto que as restantes foram implementadas no algoritmo PTO (*Proportinal Topology Optimization*). Este último não necessita do cálculo das sensibilidades, pelo que o torna menos pesado computacionalmente.

Os provetes heterogéneos obtidos foram analisados, avaliados e classificados de acordo com o indicador de heterogeneidade desenvolvido com o intuito de estabelecer comparação entre diferentes topologias. Estas soluções mostraram-se bastante perto em termos de heterogeneidade de alguns designs presentes na literatura. No entanto, tendo em conta o potencial que a otimização topológica apresenta nesta aplicação, ainda existe margem para progredir. A eficiência das funções objetivo desenvolvidas não é ideal quando formuladas individualmente. Isto deve-se ao facto de o presente problema ser extremamente não-linear e complexo, e depender de uma formulação cujo objetivo é exclusivamente aumentar a heterogeneidade do provete, o que resulta maioritariamente em geometrias extremamente heterogéneas e não fabricáveis. Deste modo, conclui-se que aliar estas formulações heterogégeneas a uma parcela estrutural, adicionando uma restrição estrutural ou utilizando uma abordagem multiobjetivo, apresenta resultados promissores e soluções heterogéneas relevantes para a indústria.

Contents

List of Tables

Intentionally blank page.

List of Figures

Chapter 1

Introduction

1.1 Framework

The sheet metal forming industry frequently develops new materials with different sets of properties. As a result, there is an increasing demand for the accurate and fast characterization of steels. It is imperative to precisely identify the parameters of the material's constitutive models in order to accurately predict their behaviour and improve the numerical representation of the mechanical properties. These are obtained by performing mechanical tests on sheet samples, which are time consuming.

When characterising a mechanical test, there are some key aspects to be taken into account. Firstly, the type of load performed on the specimen needs to be addressed, such as whether it is a uniaxial or biaxial tensile test, compression or pressure test, for example. Secondly, within these tests, the specimen's geometry and test conditions must be defined. Thirdly, the methods of identification of constitutive parameteres must be considered.

Some of the homogeneous classical tests presented in the literature do not allow for a full characterisation of metal materials on a single test. A multitude of tests is required to characterise a single material, which reduces their economical competitiveness. It is in the industry's interest to find a better solution in order to save time and reduce costs. Heterogeneous tests provide an advantageous solution, because these are richer in terms of the variety of stress and strain fields. Thus, fewer tests are needed to characterise a material. The heterogeneous strain fields observed in mechanical tests are extremely valuable for the identification of constitutive parameters, in comparison to homogeneous ones. For example, considering the cruciform test developed by Cooreman et al. [2], the material parameters identified with only one heterogeneous test were similar to a homogeneous approach considering eight classical experiments [3]. Nonetheless, heterogeneous tests require relatively complex inverse parameter identification strategies. Inverse identification strategies allow for the identification of the parameters from complex heterogeneous tests [1]. Regarding inverse methods of identification, these are usually seen as an optimisation problem, where the objective is to minimise the difference between computed and experimental results of one or more experiments [1].

On the present work, efforts are made towards the design by optimisation of the geometry of a sample, which results in the maximisation of the heterogeneity of the strain and stress fields. Regarding heterogeneous mechanical tests, there are some examples present in the literature that address different specimen's geometries. Whether it is

using a trial and error approach by changing the overall geometry [4], such as the *TIX* test [3], or by using a more refined method like, for example, shape optimisation used in the *Butterfly specimen* [3]. According to the author, topology optimisation would be an asset to the maximisation of the heterogeneity of strain and stress fields, as it does not depend on a predefined shape to reach an optimal solution. Despite this statement, topology optimisation in regards to heterogeneity seems to have not been yet addressed on the literature.

1.2 Objectives and motivation

The current state-of-the-art specimens, presented in Section 2.1, can be surpassed in terms of the heterogeneity levels attained. Therefore, the goal of this work is to develop a methodology for the design of a new geometry of a sample for mechanical tests. With the purpose of maximising the heterogeneity of the strain and stress fields, this specimen will allow for the creation an optimal framework for the characterisation of the constitutive models of metals. Thus, the information taken from a single test is richer and, thereafter, able to fully represent the behaviour of the targeted material with minimal wastage of time. To create this new geometry, a novel approach was used: topology optimisation. Topology optimisation presents an advantage over the optimisation procedures found in the literature, as it is not limited by a predefined geometry definition to reach its optimal solution. Nonetheless, to the author's knowledge, topology optimisation is not addressed in the literature regarding the specimen design problem. This work is limited to a plane stress 2D approach, as inverse methods of identification only allow for the extraction of information from a planar surface, considering material isotropy and elastic behaviour.

Chapter 2

Material testing and sample design

2.1 Mechanical tests

Nowadays, mechanical tests are performed on sheet metal specimens with the objective of characterising the behaviour of the material and, therefore, predicting sheet forming processes. Obtaining the parameters of the constitutive models of materials has become essential to fully characterise these materials in terms of finite element analysis [3]. Regarding these experiments, the factors that can influence the characterisation of metal sheets are the sample's geometry, testing conditions and analysis methodologies [1]. Different stress states within the specimen gauge section can be achieved by changing its geometry or by changing the direction and orientation of the displacement loading [5]. In Figure 2.1, an overview on some well-known tests is presented, each representing a specific stress state on the yield locus [6]. These strain and stress states are defined by the $\varepsilon_2/\varepsilon_1$ and σ_2/σ_1 ratios, respectively. The range of these ratios can be used to define a heterogeneity indicator. Some of the mechanical tests that have been proposed over the years exhibit the same stress state (see equibiaxial tension and simple shear tests in Figure 2.1). The prediction capability of the simulations depends on the constitutive model chosen and on the suitable identification of their material parameters.

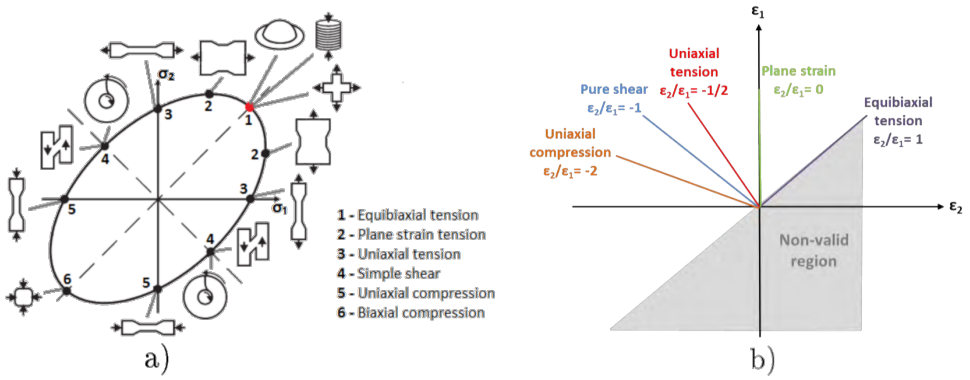

Figure 2.1: a) Different tests concerning its yield surface in terms of major and minor stress in plane stress; b) Strain states of sheet forming processes concerning $\varepsilon_2/\varepsilon_1$ and considering material isotropy [3].

2.1.1 Plane stress state condition

Plane stress state is a special case in three-dimensional stress states, and can be used when studying specimens of relatively thin thickness. Being very common in engineering problems, plane stress states are present in most classical tests [4]. Considering a rectangular planar element in a thin-walled structure, three non-zero stress components may be present: two normal stresses, σ_{xx} and σ_{yy}, and one shear stress, τ_{xy}. Also, these stresses vary with the angle φ of rotation according to the coordinate system, as shown in Figure 2.2 [4]. The experimental principal stresses can be determined by the measurement of the strains, through a linear elastic constitutive relation, and can be calculated accordingly, as

$$\varepsilon_{1,2} = \frac{(\varepsilon_{xx} + \varepsilon_{yy})}{2} \pm \sqrt{\left(\frac{\varepsilon_{xx} - \varepsilon_{yy}}{2}\right)^2 + \varepsilon_{xy}^2}, \tag{2.1}$$

$$\sigma_1 = \frac{E}{(1-\nu^2)}(\varepsilon_1 + \nu\varepsilon_2) \quad \text{and} \quad \sigma_2 = \frac{E}{(1-\nu^2)}(\varepsilon_2 + \nu\varepsilon_1), \tag{2.2}$$

where ε_1 and ε_2 represent the principal strains, σ_1 and σ_2 represent the principal stresses, E is the Young's modulus and ν is the Poisson's ratio [4]. Principal stresses, maximum (σ_1) and minimum (σ_2), can also be calculated directly from stress components σ_{xx}, σ_{yy} and τ_{xy}, as

$$\sigma_{1,2} = \frac{(\sigma_{xx} + \sigma_{yy})}{2} \pm \sqrt{\left(\frac{\sigma_{xx} - \sigma_{yy}}{2}\right)^2 + \tau_{xy}^2}. \tag{2.3}$$

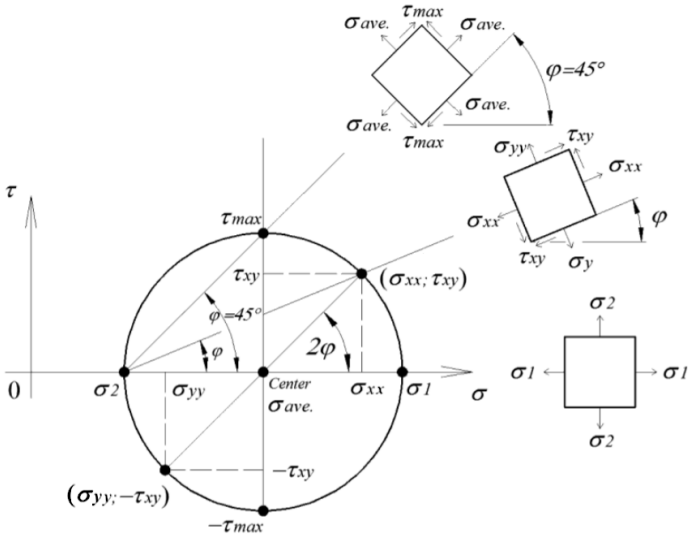

Figure 2.2: Mohr's circle for a plane stress state [4].

2.1.2 Homogeneous tests

Usually, material parameters are identified by a set of classical mechanical tests which develop homogeneous strain fields. These simpler tests return stress and strain fields for a fixed stress state and allow for a simple material's parameter identification, suitable for

simple constitutive models. Despite being relatively simple, some of the cons of homogeneous testing is that it requires a high number of tests for more complex constitutive models, which do not resemble metal forming operations accurately [3]. Some examples of homogeneous tests encompass uniaxial tension, simple shear, plane strain tension, hydraulic bulge test and disk compression. These are presented on the following sections and studied in terms of their stress and strain states.

Tensile test

Uniaxial tensile tests are very easy to perform and are mainly utilized to determine the flow curves under uniaxial stress state as well as anisotropy coefficients [3, 7](see Figure 2.3). This specific test exhibits homogeneous deformation of the specimen in the gauge region/area until necking, which allows for the accurate representation of the behaviour of the material in terms of analytical equations. One of the drawbacks is the non-homogeneity of the gauge area after necking. Regarding the Cauchy stress and strain tensors, in elasticity and in plane stress, where there are only stress components in one plane (no stress in *0z* direction), they show the following tensors [3],

$$\boldsymbol{\sigma} = \begin{bmatrix} \sigma_{xx} & 0 & 0 \\ 0 & 0 & 0 \\ 0 & 0 & 0 \end{bmatrix} \quad \text{and} \quad \boldsymbol{\varepsilon} = \begin{bmatrix} \varepsilon_{xx} & 0 & 0 \\ 0 & \varepsilon_{yy} & 0 \\ 0 & 0 & \varepsilon_{zz} \end{bmatrix}. \tag{2.4}$$

Using Equation 2.3, principal stresses are calculated, as $\sigma_1 = \sigma_{xx}$ and $\sigma_2 = 0$.

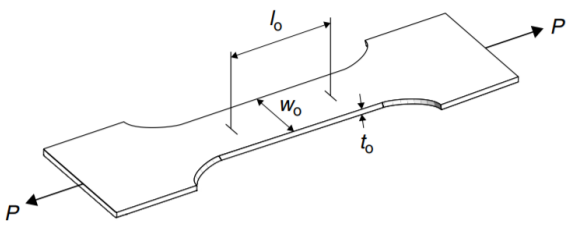

Figure 2.3: An example of a simple tensile test [7] .

Shear test

The shear test (represented in Figure 2.4) allows for a characterisation of the hardening effect, similarly to the uniaxial tensile test. Also, higher levels of deformation are obtained due to the absence of necking.

In terms of the stress and strain tensors, in elasticity and in plane stress, non-diagonal components appear and $\sigma_{xx} = \sigma_{yy} = 0$, as shown in

$$\boldsymbol{\sigma} = \begin{bmatrix} 0 & \tau_{xy} & 0 \\ \tau_{xy} & 0 & 0 \\ 0 & 0 & 0 \end{bmatrix} \quad \text{and} \quad \boldsymbol{\varepsilon} = \begin{bmatrix} 0 & \varepsilon_{xy} & 0 \\ \varepsilon_{xy} & 0 & 0 \\ 0 & 0 & 0 \end{bmatrix}. \tag{2.5}$$

Also, in terms of principal stresses, using Equation 2.3, it is observed that $\sigma_1 = \tau_{xy}$ and $\sigma_2 = -\tau_{xy}$.

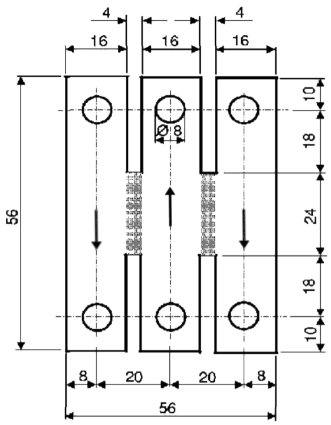

Figure 2.4: A representation of a simple shear test [3, 8].

Plane strain tensile test

As seen in Figure 2.1, the plane strain tensile test (represented in Figure 2.5) characterises a material in-between uniaxial and equibiaxial tension. Some real life examples involving these types of material's behaviour are the bending of wide sheets and the tension in a cylindrical cup wall. The in-plane stress state can be defined as

$$\boldsymbol{\sigma} = \begin{bmatrix} \sigma_{xx} & 0 & 0 \\ 0 & \sigma_{yy} & 0 \\ 0 & 0 & 0 \end{bmatrix} \quad \text{and} \quad \boldsymbol{\varepsilon} = \begin{bmatrix} \varepsilon_{xx} & 0 & 0 \\ 0 & 0 & 0 \\ 0 & 0 & \varepsilon_{zz} \end{bmatrix}. \tag{2.6}$$

Regarding the principal stresses in this example, using Equation 2.3, it is observed that $\sigma_1 = \sigma_{xx}$ and $\sigma_2 = \sigma_{yy}$.

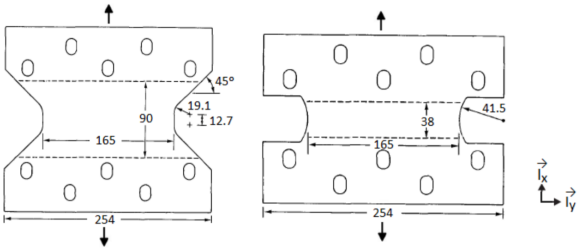

Figure 2.5: A geometry used for a plane strain test [3].

Hydraulic bulge test

The hydraulic bulge test (represented in Figure 2.6) is a reliable test for the characterization of the behaviour of materials in complex sheet forming processes, such as deep drawing. Concerning this experiment, the Cauchy stress and logarithmic strain tensors can be written as

$$\boldsymbol{\sigma} = \begin{bmatrix} \sigma_{xx} & 0 & 0 \\ 0 & \sigma_{yy} & 0 \\ 0 & 0 & 0 \end{bmatrix} \quad \text{and} \quad \boldsymbol{\varepsilon} = \begin{bmatrix} \varepsilon_{xx} & 0 & 0 \\ 0 & \varepsilon_{yy} & 0 \\ 0 & 0 & \varepsilon_{zz} \end{bmatrix}. \tag{2.7}$$

Regarding the principal stresses in this example, using Equation 2.3, it is also observed that $\sigma_1 = \sigma_{xx}$ and $\sigma_2 = \sigma_{yy}$.

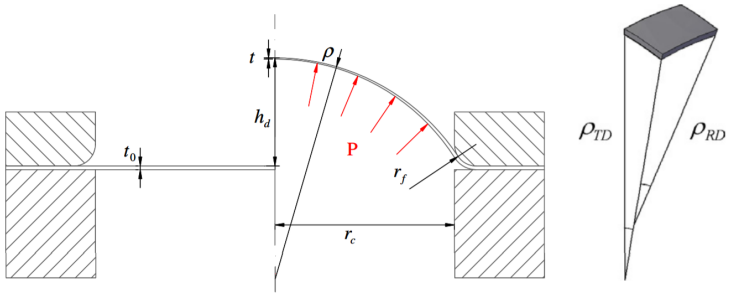

Figure 2.6: A representation of a bulge test [3].

2.1.3 Heterogeneous tests

Over the years, efforts have been made by the scientific community in order to balance time, material consumption and the number of tests required for the parametrization of constitutive models [1]. This statement endorses the focus on the study of heterogeneous tests. For non-homogeneous tests, several parameters of a constitutive model can be obtained from a single test, but they require inverse methods of identification. Some of those identification strategies encompass FFM (Full-Field Measurement methods) with DIC techniques, FEMU (Finite Element Model Updating), or VFM (Virtual Field Method). These are suited for complex mechanical tests with multi stress/strain states on a single specimen [3].

Most heterogeneous tests available in the literature are classical biaxial tension tests using a cruciform specimen. To obtain a more heterogeneous test, usually the design is changed by adding a hole, notching the specimen or promoting a shear-like tensile zone [3]. Comparing with homogeneous fields, it is noted that heterogeneous fields provide a richer canvas of information in terms of material parameters identification. Some alternatives are studied in the following sections.

Biaxial tensile test

Contrary to what is observed in uniaxial loading, sheet forming processes are subjected to multiple loadings. Biaxial tensile tests are usually characterised by a cruciform specimen, in which its arms are loaded in tension [3, 4]. This provides large strain heterogeneity over the whole cruciform and a variety of stress states and strain levels. It is observed that one single biaxial tensile test is able to promote a material characterisation quite similarly to 8 homogeneous classical experiments [3]. A representation of the mechanism and the geometry of the sample is presented in Figure 2.7.

Biaxial fixture

The Arcan fixture was proposed by Arcan et al. [9] with the intent of producing biaxial states of stress with applications to fiber-reinforced materials under uniform plane-stress conditions. A modified Arcan fixture is proposed by El-Hajjar et al. [10] with a butterfly

Figure 2.7: A representation of the mechanism and geometry used in a biaxial tensile test [4].

specimen geometry, which was designed in order to measure in-plane shear response of thick-section pultruded FRP composites. Both shear and axial forces are applied in the butterfly specimen, as shown in Figure 2.8.

D.Mohr et al. [5] introduced a basic design based on the Arcan apparatus, where the universal biaxial testing device is used. The objective was to develop a flat specimen in order to predict the crack initiation in metals. The displacement loading is applied to the specimen in order to perform tests over a wide range of stress triaxialities, by changing the direction and orientation of the displacement loading [5].

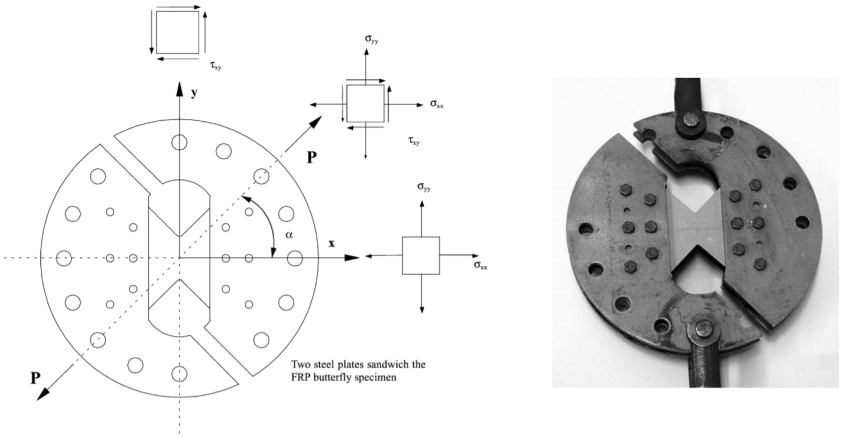

Figure 2.8: Representation of the Arcan fixture test, the butterfly specimen and the biaxial states of stress [10].

Tubular specimen

In this test, a thin walled tubular specimen is loaded with an axial tension force and an inertial pressure from the inside, as shown in Figure 2.9, and plane stress is inforced in the specimen. The device used in this experiment is very complex. Actually, all of the previous heterogeneous tests are quite expensive and complex [4].

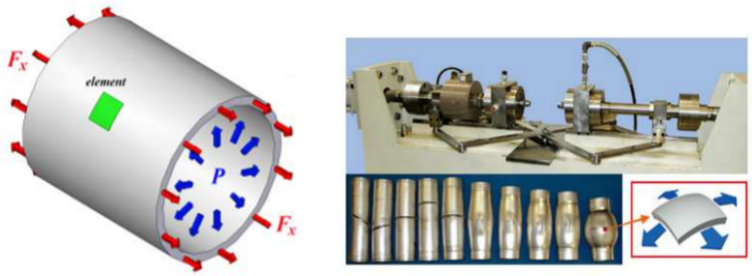

Figure 2.9: A depiction of the tubular test [4].

Other designs

One good example is the specimen designed in [4]. The main advantage of this sample is that it can be tested by a universal tensile testing machine, without the aid of any special equipment. As seen in Figure 2.10, the vertical arm is loaded in tension, while the horizontal arm is loaded in compression.

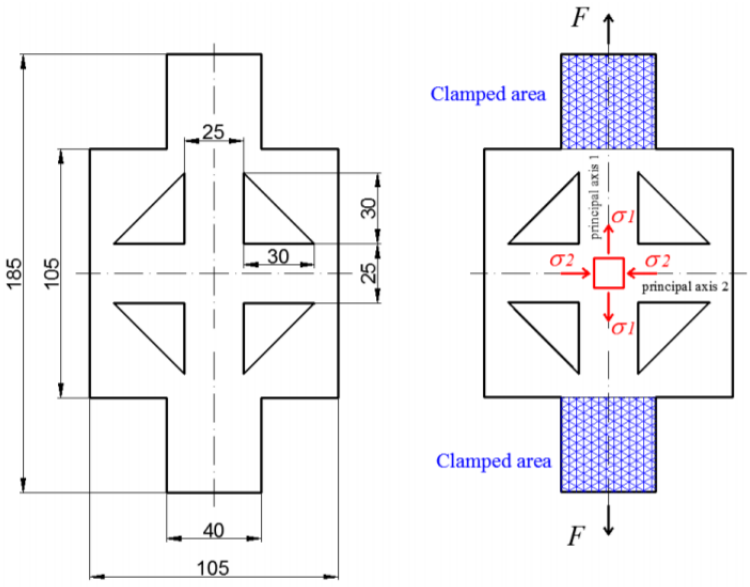

Figure 2.10: Representation of the geometry of the specimen present in [4] and the respective load directions.

The heterogeneous TIX test is another new design for the specimen and loading, introduced by Pottier et al. [3, 11]. Based on an uniaxial device, the punch forces the sample out-of-plane. The specimen then exhibits several types of deformation in different places, as shown in Figure 2.11.

Butterfly specimen

Using design shape optimisation, a new specimen's geometry that promotes heterogeneous strain fields is proposed in [3]. The shape optimisation process of the butterfly

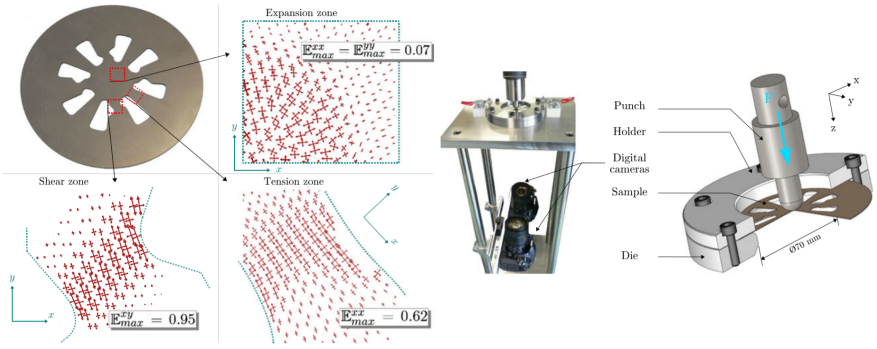

Figure 2.11: Geometry of the specimen and the respective strain directions [3].

specimen (see Figure 2.12) was dependent on the usage of cubic splines, by just changing the position of 7 control points using a *Matlab*® script (interface program) that links an *Abaqus* code, and a *Python* script used to create the numerical model [3]. The ob-

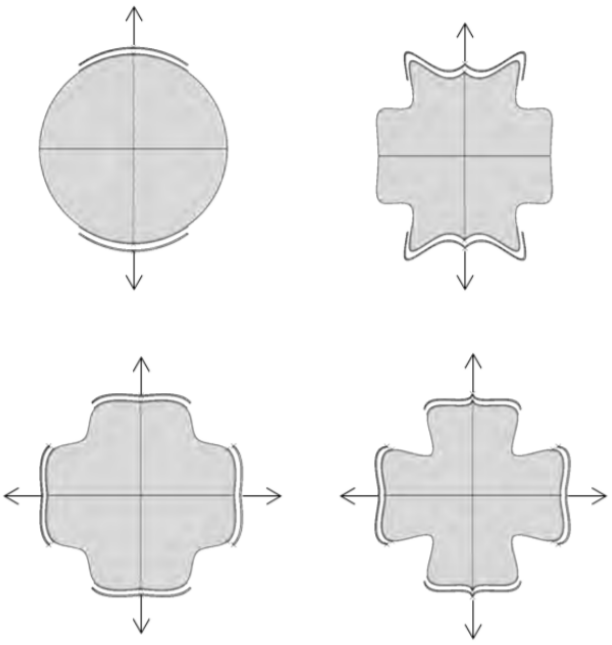

Figure 2.12: Representation of the initial(left) and final optimised shapes [3].

jective was to maximise the heterogeneity of the specimen, therefore an indicator I_t was developed by N. M. Souto [3]. A second approach was applied in [3], where a sequential incremental technique designing the specimen shape and the loading path of the specimen is considered, for local displacements, as shown in Figure 2.13. Comparing with other mechanical tests, Figure 2.14 provides an insight in terms of I_t values reached.

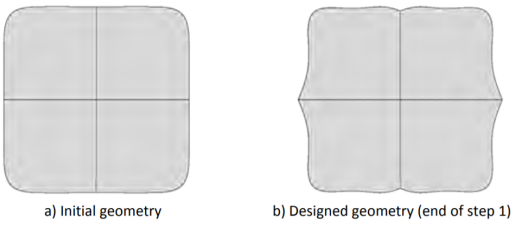

Figure 2.13: Test design based on local displacements, before and after the optimisation [3].

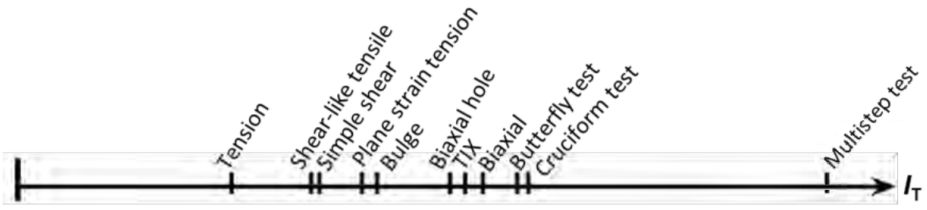

Figure 2.14: Representation of the indicator regarding different tests [3].

2.2 Topology optimisation

Topology optimisation is a field of structural optimisation and design which deals with the optimal distribution of material within a restricted area or volume, referred to as the *design domain*. Being defined as a binary programming problem, it is of interest to determine the optimal subset of elements in the design [12, 13]. Topology optimisation covers a multitude of areas in physics, ranging from structural rigidity to heat conduction, eletrical and magnetic problems. This field's relevance and popularity has been increasing, with the improvement of computational power/tools, and also with the recent appearance of popular additive manufacturing techniques, which allow for the manufacturing of porous structural designs with complex geometries [14]. This approach makes use of finite element method (*FEM*) with the intent of discretizing the design domain. Some techniques used for solving Topology optimisation problems encompass, as example, the optimality criteria (OC) method, the convex linearization method, the method of moving asymptotes (MMA), successive linear programming (SLP), evolutionary structural optimisation (ESO), and stochastic methods such as simulated annealing and the genetic algorithm.

The following sections focus on different applications, types of formulation and update methods regarding Topology Optimisation.

2.2.1 Structural problems

Minimum compliance problem — TOP99/SIMP

One of the most popular starting points for students and newcomers to the field of topology optimisation is the article "A 99 line topology optimisation code written in

Matlab®, developed by Sigmund et al. [15]". Concerning this paper, a concise *Matlab*® code was developed in order to solve a simple stiffness maximisation problem. In terms of formulation of the problem, the goal is to minimise the compliance of a component, whilst keeping a volume fraction restriction. Topology optimisation methods with continuous design variables are useful for the minimisation of the objective function. For this reason, continuum design variables combined with penalisation methods are highly favored, such as the SIMP (Solid Isotropic Material with Penalisation) method, represented in Equation 2.8 as $(\rho_{el})^p$, which is recalled in order to push the elements' density (design variable) to 1 (solid) or 0 (void) [14, 15]. Elements with intermediate densities are set to 0 or 1 by the usage of the penalisation power, p, as seen in Figure 2.15. Therefore, it is possible to minimise the weight whilst minimising the desired objective function. The formulation of the problem consists of

$$\min_{\rho} \quad c(\boldsymbol{\rho}) = \mathbf{U}^{\mathrm{T}}\mathbf{K}\mathbf{U} = \sum_{el=1}^{N} (\rho_{el})^p \mathbf{u}_{el}^{\mathrm{T}} \mathbf{k}_0 \mathbf{u}_{el}, \tag{2.8}$$

$$\text{subject to:} \quad \frac{V(\boldsymbol{\rho})}{V_0} = f, \tag{2.9}$$

$$\mathbf{F} = \mathbf{K}\mathbf{U}, \tag{2.10}$$

$$\mathbf{0} < \boldsymbol{\rho}_{\min} \leq \boldsymbol{\rho} \leq \mathbf{1}. \tag{2.11}$$

where c($\boldsymbol{\rho}$) represents the compliance (objective function) as a function of the design

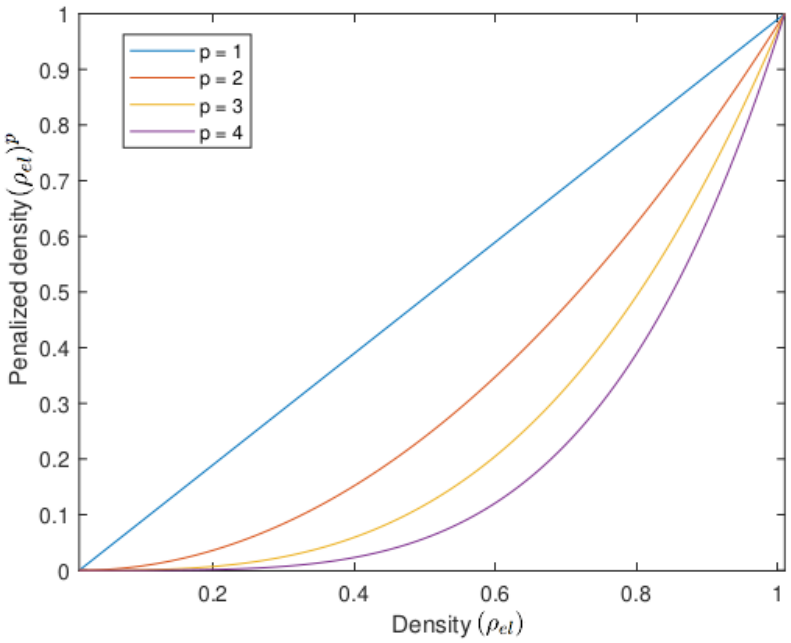

Figure 2.15: A representation of the SIMP penalisation for different values of penalisation power, p.

variable $\boldsymbol{\rho}$. $\mathbf{U}$ and $\mathbf{F}$ are, respectively, the global displacement and force vectors, $\mathbf{K}$ is the global stiffness matrix, ρ_{el} is the density of the element el, $\mathbf{u}_{el}$ is the element displacement

vector, p is the penalisation power (typically equal to 3), $\mathbf{k}_0$ the stiffness matrix of the element, N is the number of elements in the discretized design domain, $V(\rho)$ and V_0 are the material volume and design domain volume, respectively, f is the prescribed volume fraction, and $\rho_{\min}$ is a vector of minimum relative densities [15].

The optimisation problem is solved with a gradient-based algorithm, the standard optimality criteria (OC) method. However, other approaches such as Sequential Linear Programming (SLP) or the Method of Moving Asymptotes (MMA) could be used as well.

Stress constrained problem — Proportional topology optimisation

A proportional topology optimisation procedure was developed with the intent of both solving compliance minimisation and stress constrained problems efficiently and accurately, without the aid of sensitivity analysis [14]. Being relatively easy to solve, the compliance problem is addressed in the literature by various researchers (as stated previously). On the other hand, stress constrained problems are more complex and harder to solve. These are highly nonlinear, analytically difficult to derive (sensitivity analysis), computationally costly, and open source codes are scarce. Despite all these statements, there's always a trade-off between grandient and non-gradient methods in terms of efficiency and complexity, and for this reason a gradient based approach developed by Jeong et al. can be found in the literature [16].

The Proportional topology optimisation (PTO) non-gradient algorithm iteratively assigns the design variables to elements proportionally to the respective value of stress. For each iteration, it either adds material (density) to the system if the maximum elemental von Mises stress is surpassed, or subtracts material otherwise. It is noted that this method is highly heuristic and the employement of continuous density variables allows for a more flexible design and improves the search method. The formulation of the PTO algorithm applied to the stress problem, where the objective function is to minimise the mass of the design whilst satisfying a maximum stress constraint, is encompassed as

$$\begin{aligned} \min \quad & \sum_{el}^{N} \rho_{el} v_{el}, && (2.12)\\ \text{subject to :} \quad & \mathbf{F} = \mathbf{KU}, && (2.13)\\ & \sigma_{el} \leqslant \sigma_{\mathrm{l}} \quad \text{if} \quad \rho > 0, \quad \text{and} && (2.14)\\ & 0 \leqslant \rho_{\min} \leqslant \rho_{el} \leqslant \rho_{\max} \leqslant 1. && (2.15) \end{aligned}$$

where N is the total number of elements, x is the density (design variable), v_el is the volume/area of the element el, σ_{el} is the element von Mises stress measure and σ_{l} is the stress limit. Equation 2.15 limits the densities to avoid stiffness singularities.

2.2.2 Other problems

Topology optimisation is an efficient procedure to solve a broad range of problems in engineering design [12]. The present paragraph focuses on the formulation and solution procedures of some applications outside of the structural compliance problem. Starting with problems in dynamics, one of the first applications for topology optimisation is the eigenvalue optimisation for free vibrations, often used on machines or structures subjected to dynamic loads. Another case study is the maximisation of the dynamic

response of a structure, often applied in sensors and actuators [12]. One common problem is the maximisation of the eigenvalue of a dynamically loaded structure, and its formulation can be consulted in [12], as well as the formulation for the minimisation or maximisation of the response under forced vibrations. A selection of important problems in structural optimisation includes the maximisation of the fundamental buckling load of a structure, the inclusion of stress constraints, pressure loads, geometrically nonlinear problems, the synthesis of compliant mechanisms and the design of supports. Multiphysics problems can also be addressed, whether it is electrostatics and elasticity or coupled electric, thermal and elastic fields (electrothermal actuation). Other applications include the Stokes flow problem, multiple material phases, wave propagation problems, material design for maximum buckling load, crashworthiness and bio-mechanical simulations [12].

Regarding the topic of acoustics, R. Yang et al. [17] approached the topological design of a microstructure with the intent of minimising the sound power radiation from the boundaries of a vibrating macrostructure. A high frequency approximation model is employed and the macrostructure is excited by a time-harmonic mechanical loading vector [17]. Nandy et al. [18] proposed an approach for the reduction of radiated noise on vibrating structures (i.e. light-fluid loaded structures, such as structures vibrating in air). By minimising the dynamic compliance, the natural frequencies of the structure move away from the driving frequency, which reduces the vibration levels of the structure and, consequently, reduces the radiated sound power [18]. The optimisation problem consists of finding the optimal subset of design variables ρ (density) which minimises the dynamic compliance, subject to a volume constraint [18].

In terms of solving electric/magnetic based problems [19], periodic microstructures of two-phase composites with extremal electromagnetic permeability and permittivity were designed using a bidirectional evolutionary structural optimisation (BESO) method. The objective function is the permeability and the permittivity of an isotropic composite, and the goal is either to maximise or minimise these eletromagnetic properties subject to a volume fraction constraint. Another example is [20], in which the design of both the elastic and the piezoelectric material, present in energy harvesting devices (i.e. transducers), is taken into account. The objective function is to maximise the energy conversion factor (stored electric energy resultant from an external force which yields work) [20].

A relevant application for topology optimisation is laid on thermal dissipation problems. It has been shown in the literature that rearraging the distribution of material within a design can improve thermal systems. Some of these examples include a wing box, a thermal diffuser and cooling fins [21]. Several papers address these types of thermal problems recurring to topology optimisation. In [21], the objective function is to minimise the temperature at the control point for a volume constraint, and the design variable is the thermal conductivity of the element. The elements with the most negative sensitivity are removed and the ESO method is employed to minimise the objective function [21]. Another relevant example is in [22] where it is considered the optimal design of a steady heat conduction. The objective is to construct effective heat transport paths in order to keep the heat capacity to a minimum.

Chapter 3

Definition of the optimisation methodologies and formulations

The goal of this work is create a methodology to develop a specimen which maximises the heterogeneity of its stress field using topology optimisation. In order to solve the topology optimisation problem, the first step is to define an objective function that expresses the heterogeneity problem. The following indicator's purpose is to accurately quantify the level of heterogeneity of a mechanical test.

3.1 Heterogeneity definition

As seen in Section 2.1, classifying a specific mechanical test as homogeneous or heterogeneous depends on the range of the stress states exhibited by the specimen. The principal stress states can be evaluated by the ratio between the principal stresses σ_2 and σ_1, which can define a vector $\underset{\sim}{S}$ which expresses an angle with the σ_1 axis, as seen in Figure 3.1. This angle, θ_{el}, which is referred to as principal stress angle hereafter, is defined by

$$\theta_{el} = \frac{\arcsin\left(\frac{\sigma_{2,el}}{\sqrt{\sigma_{1,el}^2+\sigma_{2,el}^2}}\right)}{\left|\arcsin\left(\frac{\sigma_{2,el}}{\sqrt{\sigma_{1,el}^2+\sigma_{2,el}^2}}\right)\right|} \times \arccos\left(\frac{\mathbf{S}\cdot\hat{\mathbf{x}}}{|\mathbf{S}|\times|\hat{\mathbf{x}}|}\right) \times \frac{360}{2\pi}, \tag{3.1}$$

where $\mathbf{S}$ represents the principal stress tensor and $\hat{\mathbf{x}}$ is the unit vector in the horizontal σ_1 direction. The dot product between the stress vector and the unit vector on the σ_1 axis was used to calculate the magnitude of the angle from equation 3.1. But, because the angle θ is measured in the range of [-135,45] degrees, the sign of the value of the dot product is shifted in regards to its respective quadrant. In order to correct this, the dot product is multiplied by the cross product divided by its absolute value. The first portion of equation 3.1 returns the correct sign for the angle, and is composed by the inverse sine function of the principal stress vector divided by its magnitude. It is noticed that it is mathematically impossible to divide by zero, so the null values of the arcsin of the principal stress vector are replaced by 1. The second portion, regarding the cross product between the principal stress vector $\mathbf{S}$ and the unit vector $\hat{\boldsymbol{x}}$ in the x axis, returns the magnitude of the angle. It is noticed that it is possible to fully define a stress state

using θ_{el}, which is useful to quantify the heterogeneity level of a mechanical test. The author acknowledges that using the principal strain field would be equivalent to using the principal stress field, as the principal stresses and strains are a linear function of each other, as seen in Equation 2.2, in elasticity.

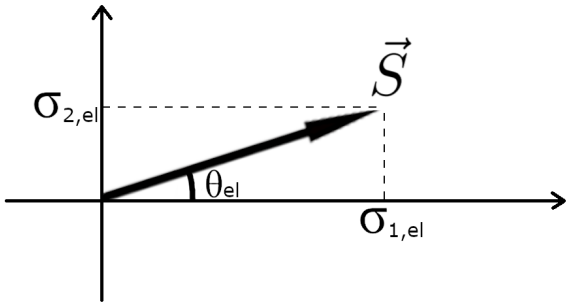

Figure 3.1: A visual representation of θ_{el}.

Figure 3.2 exhibits a comparison between a homogeneous and a heterogeneous test, regarding their stress fields. Subfigure 3.2a represents the homogeneous case. It shows a finite element analysis (FEA) performed on Matlab of a square specimen, discretized in 9 elements, where the boundary conditions are homogeneous, exhibiting a force spread on all nodes of the right edge, and symmetry conditions on all the nodes of the bottom and left edge. The principal stresses distribution on the homogeneous test exhibits that all stress states of the elements are overlapped on the same point, implying that their respective principal stress states and principal stress angle θ_{el} are equal. Also, the complete surface of the specimen is under the same stress state, meaning that the principal stress angle's vector resulting from the FEA is an array of zeros.

One of the main strategies to induce heterogeneity on a specimen is to change its geometry. Subfigure 3.2b shows a specimen where the middle element was removed by assigning its density to 0. Altering the previous homogeneous geometry forces some other elements to have a different response to the boundary conditions. This is corroborated by the principal stress distribution on Subfigure 3.2b, where the variance of stress states is higher in comparison to 3.2a, and the principal stress angle's θ_{el} vector is now composed of slightly different values. Therefore, the increase in the variance of the θ_{el} vector on the altered geometry from the specimen from Figure 3.2b is correlated to a higher level of heterogeneity in comparison to the one from Figure 3.2b.

The level of heterogeneity can be defined as a function of the vector composed by the principal stress angles θ_{el}. In topology optimisation, every discretized element has a density value assigned to it. Thus, the area of an element is proportional to its density value. The strategy adopted to measure the dispersion of stress states, and therefore its heterogeneity level, was to sum the densities of the elements, ρ_{el}, per interval of principal stress angle, recalled angle resolution a_{r}, for the required angle interval. The angle resolution represents the required angle accuracy at which the densities are summed, as seen in figure 3.3. Then the densities of the elements within the sections resulting from the intervals made using a_{r} on the principal stress diagram are summed for every interval, for which results a vector, the density per angle vector $dpa(\boldsymbol{\theta})$. This vector is represented in Figure 3.4 as the density histogram (the exhibited specimen was taken

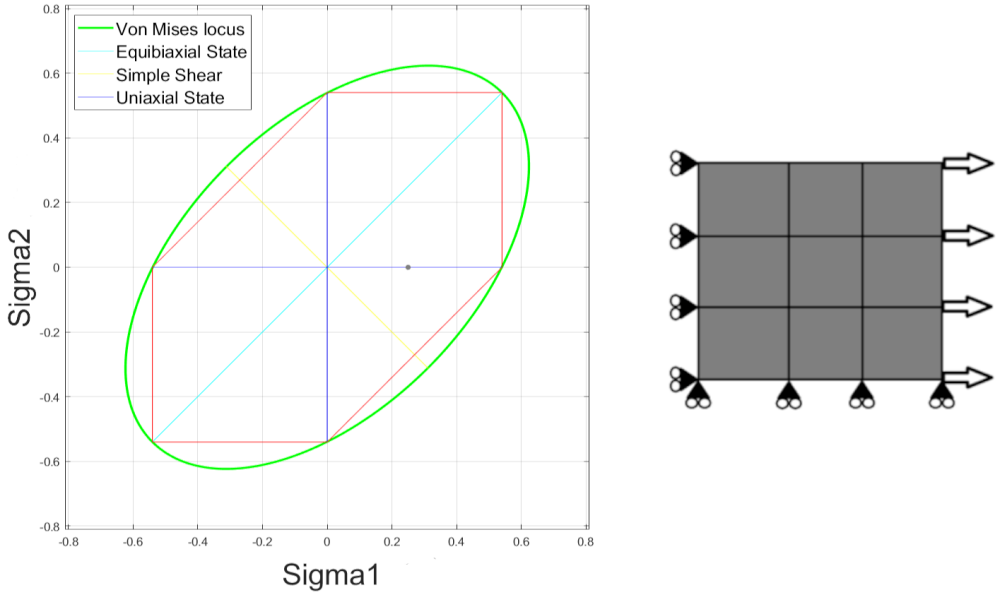

(a)

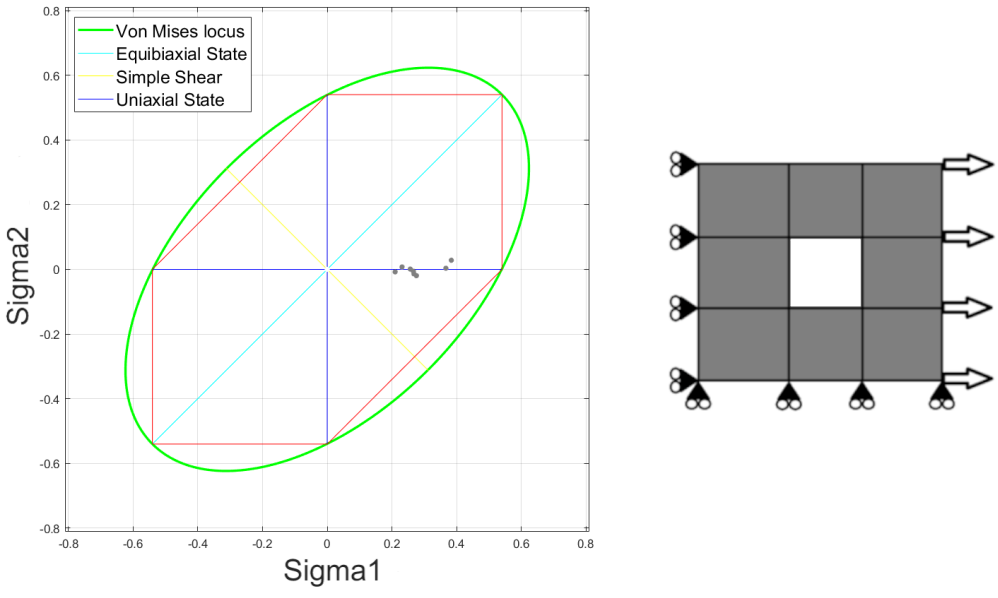

(b)

Figure 3.2: Comparison between a homogeneous and a heterogeneous test in terms of their principal stress fields: a) Principal stress field of a Homogeneous test; b) Principal stress field of a Heterogeneous test.

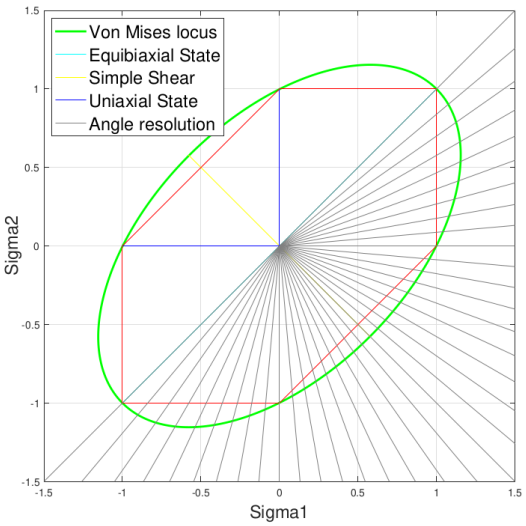

Figure 3.3: Representation of the angle resolution. In the present example a_{r} is set to 5 degrees.

from the literature [23]), and is defined as

$$dpa(\boldsymbol{\theta}) = \sum_{el \in \theta_{el}} \rho_{el} \times L^2, \qquad \theta \leq \theta_{el} \leq \theta + a_r, \tag{3.2}$$

where ρ_{el} is the element density and L is the size (length) of the square element. ALso, the length L is constant for every element.

In short, the heterogeneity level of a certain mechanical test is defined by the range and variance of the stress states yielded by its surface. Intuitively, high heterogeneity is depicted in the principal stresses diagrams a scattering of stress states, spread evenly, which results in an even representativity of the specimen's area in the principal stress diagram. The optimal case scenario of maximum heterogeneity is that of a specimen which every finite fraction of its area yields a unique stress state, and also which range of angles θ_{el} covers the interval of [-135,45] degrees on the principal stresses diagram. The stress diagram of a hypothetical optimal solution could be represented as the principal stress diagram in Figure 3.5. This optimal solution a_{o} is defined by

$$a_{\mathrm{o}} = \frac{V_{\mathrm{lim}} \times N \times L^2}{\frac{180}{a_{\mathrm{r}}}}, \tag{3.3}$$

where V_{lim} represents the prescribed volume fraction, N represents the number of elements of the specimen, L is the length of the square element, and the a_{r} is the angle resolution.

From an optimisation stand point, if the density histogram $dpa(\boldsymbol{\theta})$ is closer to the optimal solution a_{o}, it is depicted that the test is close to the optimal case of heterogeneity. The green line on the histogram 3.4 represents the utopian solution defined by a_{o}. Statistically speaking, this would result in a case were maximum variance or standard deviation are verified. However, statistical approaches should not be used in topology optimisation due to its discrete nature.

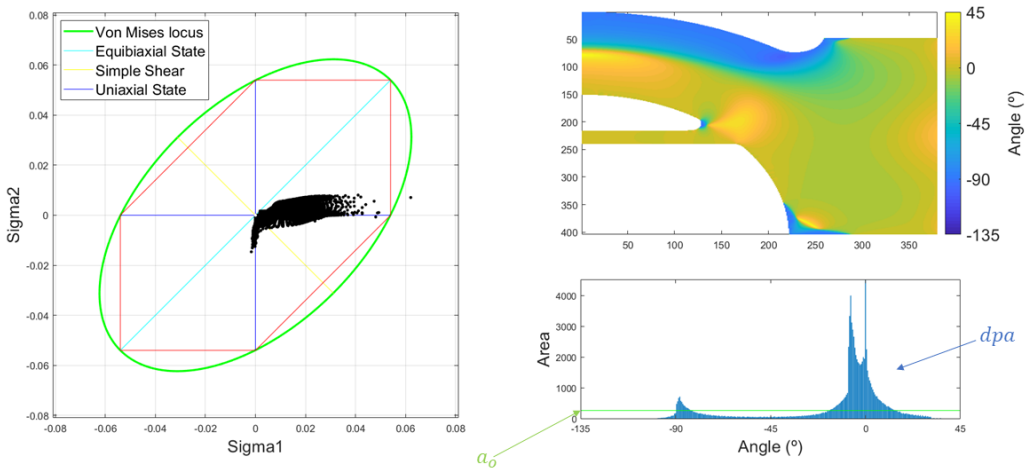

Figure 3.4: Representation of the heterogeneity level of the specimen present in [23]. It is noticed that the principal stresses, the von mises surface and their values represented across the present work are merely visual, and its magnitude has no relation to the actual tensile yield strength of the material, as this work only addresses the elastic behaviour of the specimen.

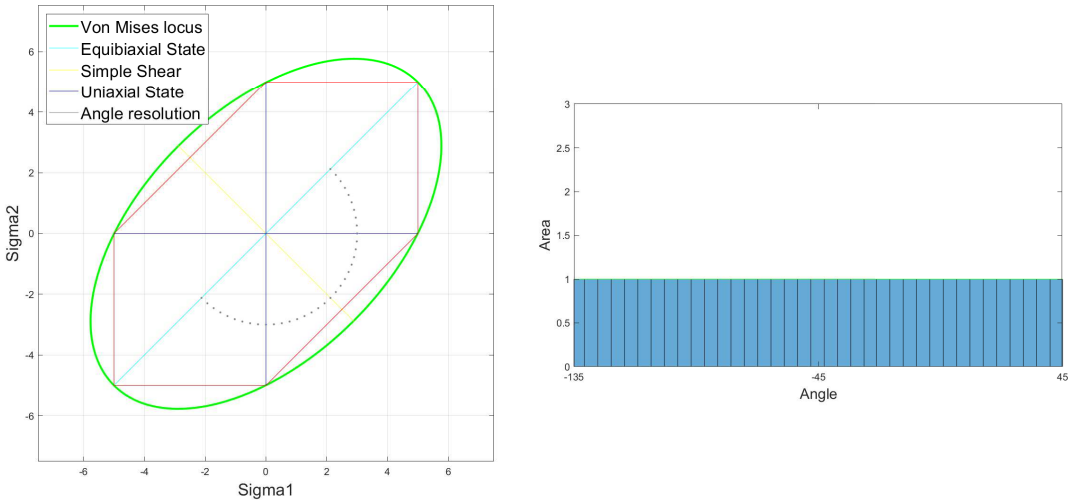

Figure 3.5: Principal stress diagram for a hypothetical optimal solution using a specimen with a mesh of 37 elements.

3.2 Statistics-based formulation

The first general formulation defined for the problem from the different methodologies developed on this work can be written as

$$\min_{\rho} \quad F_1(\boldsymbol{\rho}) \tag{3.4}$$

$$\text{subject to:} \quad \frac{V(\boldsymbol{\rho})}{V_0} = f, \tag{3.5}$$

$$\mathbf{F} = \mathbf{KU}, \tag{3.6}$$

$$0 \leq \boldsymbol{\rho} \leq 1. \tag{3.7}$$

where $F_1(\boldsymbol{\rho})$ represents a general objective function to be minimized.

The main composite objective function, $H(\boldsymbol{\rho})$, formulated according to the heterogeneity definition built in Section 3.1, is defined by the integral over θ of the quadratic euclidian distance between the density per angle vector, $dpa(\boldsymbol{\theta})$, and the optimal area, a_o (resembling a mean squared error approach). The histogram from Figure 3.4 ilustrates this concept, where the squared euclidian distance between the histogram and the utopian solution a_o expresses the objective function. The heterogeneity function $H(\boldsymbol{\rho})$ can be used as an objective function leading the optimisation process to a heterogeneous specimen. This function was developed using the concept of distribution of principal stresses angles θ as a statistical analysis (histogram) of the angle made by the vectors of the principal stresses σ_1 and σ_2. Therefore, this function is defined by

$$F_1(\boldsymbol{\rho}) = H(\boldsymbol{\rho}) = \int_\theta \left[dpa(\boldsymbol{\theta}) - a_\mathrm{o}\right]^2 \mathrm{d}\theta \simeq \sum_\theta \left[dpa(\boldsymbol{\theta}) - a_\mathrm{o}\right]^2, \tag{3.8}$$

As the stress states only exist in the range inbetween -135 and 45 degrees, due to the fact that σ_1 is always greater than σ_2 by definition, a_o is divided by 180, which is also divided by the a_r constant.

The principal stresses $\sigma_{1,2}$ are calculated using Equation 2.3. These resort to the stress tensor, which is represented by

$$\boldsymbol{\sigma}_{el} = \begin{bmatrix} \sigma_{xx} \\ \sigma_{yy} \\ \tau_{xy} \end{bmatrix}, \tag{3.9}$$

which is obtained from [14]

$$\boldsymbol{\sigma} = \mathbf{DBu}, \tag{3.10}$$

where $\mathbf{D}$ represents the constitutive matrix, $\mathbf{B}$ is the shape function derivative matrix and $\mathbf{u}$ is the displacement vector. The constitutive matrix for plane stress in 2-D is calculated as

$$\mathbf{D} = \frac{E}{1-\nu^2} \begin{bmatrix} 1 & \nu & 0 \\ \nu & 1 & 0 \\ 0 & 0 & \frac{1-\nu}{2} \end{bmatrix}, \tag{3.11}$$

where E is the Young's modulus and ν is the Poisson's ratio. For linear shape functions for a bilinear square element in 2-D, the matrix B is defined as

$$\mathbf{B} = \frac{1}{2L} \begin{bmatrix} -1 & 0 & 1 & 0 & 1 & 0 & -1 & 0 \\ 0 & -1 & 0 & -1 & 0 & 1 & 0 & 1 \\ -1 & -1 & -1 & 1 & 1 & 1 & 1 & -1 \end{bmatrix}, \tag{3.12}$$

and the displacement vector $\mathbf{u}$ is given by

$$\mathbf{u} = \begin{bmatrix} u_{1x} \\ u_{1y} \\ \vdots \\ u_{Nx} \\ u_{Ny} \end{bmatrix}. \tag{3.13}$$

where N represents the number of elements.

Lastly, the calculation of the Young's modulus comes from the modified SIMP approach, where the penalisation factor affects the stiffness of the square finite elements of the design domain [14]. It is represented by

$$E(\boldsymbol{\rho}) = E_{\min} + \rho^p (E_0 - E_{\min}), \tag{3.14}$$

where $E_{\min}$ is a very small value of stiffness assigned to void elements in order to avoid the singularity of the stiffness matrix, ρ is the design variable and represents the elemental density, p is the SIMP penalisation exponent, and E_0 is the stiffness of the material.

3.2.1 Sensitivity calculation

Regarding the formulation in Section 3.1, it is infered that the sensitivities are analytically cumbersome to derive. That's due to the fact that the objective function is a composite function composed by a number of operations (from Equation 3.8 to 3.14), including the eigenvalues of the stress tensor in Equation 2.3. Also, as this disseration is exploratory in nature, approximating the sensitivities is a plausible and efficient solution. Therefore, the forward finite difference method was employed to find the approximate sensitivities, which are expressed as

$$\frac{\mathrm{d}H}{\mathrm{d}\rho} = \frac{H(\rho + \mathrm{d}\rho) - H(\rho)}{\mathrm{d}\rho}, \tag{3.15}$$

where $d\rho$ represents the disturbance step.

3.3 Heterogeneity indicator

The formulation $H(\boldsymbol{\rho})$ turns out to be an accurate heterogeneity criterion. This is due to the fact that this objective function calculates the squared euclidian distance between the specimen subject of study, and the utopian point. This is revealed to be a great indicator of heterogeneity because it gauges how close a mechanical test is to the optimal solution. It is noticed that the smaller the indicator, the smaller the distance to the optimal solution and the larger the heterogeneity level. The formulation of $H(\boldsymbol{\rho})$ from Equation 3.8 was therefore used as a heterogeneity indicator, defined as

$$I_{\mathrm{h}} = \frac{H(\boldsymbol{\rho})}{V_{\mathrm{lim}} \times N}. \tag{3.16}$$

This indicator is normalized by dividing $H(\boldsymbol{\rho})$ by the mesh size and the volume fraction of the respective specimen, in order to have a fair comparison between the specimens.

3.4 Definition of the complementary formulations

Other formulations were tested for comparison purposes and as a way of obtaining complementary results. These formulations were developed using different approaches, always keeping in mind the goal of this work, which is to obtain a manufacturable and highly heterogeneous specimen.

3.4.1 Maximisation of the sum of the magnitudes of the principal stress tensors

The goal of this work is to find the geometry of a specimen which maximises the range of its principal stress states for a given set of boundary conditions. The objective with this complementary approach does directly maximize its heterogeneity as in $H(\boldsymbol{\rho})$. Also, the integral of the $H(\boldsymbol{\rho})$ objective function is not defined over the design domain, which is one of the defining aspects in the formulation of topology optimisation problems.

The strategy adopted was to assign more weight to the stress states where the magnitude of the stress vector is higher. Assuming that the effect of continuum mechanics is verified, the shift in the stress states between neighbour elements must be continuous. Also, the boundary conditions force some portion of the specimen into the uniaxial state. So, the goal is to develop an objective function that, with the iterative design update, forces the stress states into the equibiaxial stress state, and in the meantime, maintain some representativity of the specimen's area in the intermediate stress states.

The remainder general formulations developed on this work can be written as

$$\max_{\rho} \quad F_2(\boldsymbol{\rho}). \tag{3.17}$$

$$\text{subject to:} \quad \frac{V(\boldsymbol{\rho})}{V_0} = f, \tag{3.18}$$

$$\mathbf{F} = \mathbf{KU}, \tag{3.19}$$

$$0 \leq \boldsymbol{\rho} \leq 1. \tag{3.20}$$

where $F_2(\boldsymbol{\rho})$ represents a general objective function to be maximised. A first approach to formulate this problem is to define the objective function $S_{\mathrm{m1}}(\boldsymbol{\rho})$ as the integral over the design domain Ω of the product of the absolute value of the principal stress states, as seen in

$$F_2(\boldsymbol{\rho}) = S_{\mathrm{m1}}(\boldsymbol{\rho}) = \int_{\Omega} |\sigma_1 \times \sigma_2| \, \mathrm{d}\Omega \quad = \quad \sum_{el=1}^{N} |\sigma_{1,el} \times \sigma_{2,el}|. \tag{3.21}$$

where $|\sigma_{1,el}|$ and $|\sigma_{2,el}|$ represent the absolute value of the elemental principal stress tensors, and N is the total number of elements used to discretize the design domain.

In a similar way, $S_{\mathrm{m2}}(\boldsymbol{\rho})$ presents a slight modification to this objective function with the purpose of enabling and facilitating the search for a maximum value on the biaxial stress state. The square root is employed in order to shape the objective function into a function that is maximised when both of the principal stresses are maximised, and not just one of them. This formulation is expressed as

$$F_2(\boldsymbol{\rho}) = S_{\mathrm{m2}}(\boldsymbol{\rho}) = \int_{\Omega} \sqrt{|\sigma_1 \times \sigma_2|} \, \mathrm{d}\Omega \quad = \quad \sum_{el=1}^{N} (|\sigma_{1,el} \times \sigma_{2,el}|)^{\frac{1}{2}}. \tag{3.22}$$

3.4.2 Maximisation of the sum of the angles formed by the principal stress tensors

The formulation in Section 3.4.1 does not completely express the search for the most heterogeneous specimen, as it maximises the magnitude of the stress states. Another strategy is to attribute more weight to the stress states distant from the uniaxial state. This concept is expressed in Figure 3.6. The formulation consists of maximising the sum of the absolute values of the principal stress angles θ using the dot product (regardless of the quadrant the vector is in). Said formulation is defined as

$$F_2(\boldsymbol{\rho}) = T_1(\boldsymbol{\rho}) = \int_\Omega \arccos\left(\frac{\mathbf{S}\cdot\hat{\mathbf{x}}}{|\mathbf{S}|\times|\hat{\mathbf{x}}|}\right) \quad = \quad \sum_{el=1}^{N} \arccos\left(\frac{\mathbf{S}_{el}\cdot\hat{\mathbf{x}}}{|\mathbf{S}_{el}|\times|\hat{\mathbf{x}}|}\right), \tag{3.23}$$

where $\mathbf{S}_{el}$ represents the principal stress vector of an element.

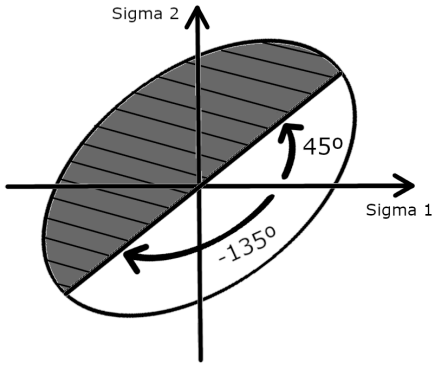

Figure 3.6: A visual representation of the objective expressed by the formulations in Section 3.4.2.

On the other hand, function T_2 expresses an alternative way to formulate the maximization of the sum of the principal stress angles, as seen in

$$F_2(\boldsymbol{\rho}) = T_2(\boldsymbol{\rho}) = \int_\Omega \arctan\left(\left|\frac{\sigma_2}{\sigma_1}\right|\right). \tag{3.24}$$

3.5 Multiobjective approach

The exploratory procedure on this work called for a multiobjective approach, which comes as an asset to the previous objective functions, functioning as a constraint to the optimisation problem and pushing the geometry of the specimen into a structure that not only is manufacturable, but also that can withstand the occuring stresses caused by the applied force. From the exploratory procedure, it was concluded that adding a structural function to the problem would be benefitial. This multiobjective function is formulated with the weighted sum of the separate objective functions.

Due to the fact that $H(\boldsymbol{\rho})$ on its own is not sufficient to solve the proposed problem, formulation $M_1(\boldsymbol{\rho})$ makes use of the heterogeneity function $H(\boldsymbol{\rho})$ and the compliance

formulation $c(\boldsymbol{\rho})$ with a modified SIMP method from [24]. The compliance formulation is defined as

$$c(\boldsymbol{\rho}) \;=\; \mathbf{U}^{\mathrm{T}}\mathbf{K}\mathbf{U} \;=\; \sum_{el=1}^{N} E_{el}(\rho_{el})\mathbf{u}_{el}^{\mathrm{T}}\mathbf{k}_0\mathbf{u}_{el}. \tag{3.25}$$

where $E_{el}(\rho_{el})$ is equal to Equation 3.14, and $\mathbf{k}_0$ is the element stiffness matrix for an element with unit Young's modulus. Formulation $M_1(\boldsymbol{\rho})$ is expressed as

$$F_1(\boldsymbol{\rho}) = M_1(\boldsymbol{\rho}) = w_1 \times \frac{H(\boldsymbol{\rho})}{H_0} \quad + \quad (1-w_1) \times \frac{c(\boldsymbol{\rho})}{c_0}, \qquad w_1 \epsilon [0,1], \tag{3.26}$$

where w_1 and $(1-w_1)$ represent the weights of the separate objective functions, H_0 is its respective initial solution and c_0 is its respective initial solution. Regarding the sensitivity calculation, $\partial H/\partial\rho_{el}$ is calculated using the finite difference method, and $\partial c/\partial\rho_{el}$ is calculated by

$$\text{with} \quad \frac{\partial c}{\partial \rho_{el}} \;=\; -p\rho_{el}^{p-1}(E_0 - E_{\min})\mathbf{u}_{el}^{T}\mathbf{k}_0\mathbf{u}. \tag{3.27}$$

The second multiobjective approach $M_2(\boldsymbol{\rho})$ combines both the $T_2(\boldsymbol{\rho})$ function and the structural problem $c(\boldsymbol{\rho})$, for the same reasons. It is expressed as

$$F_2(\boldsymbol{\rho}) = M_2(\boldsymbol{\rho}) = w_1 \times \frac{T_2(\boldsymbol{\rho})}{T_{2_{\max}}} \quad + \quad (1-w_1) \times \left(\frac{c(\boldsymbol{\rho})}{c_0}\right)^{-1}. \tag{3.28}$$

where w_1 and $(1-w_1)$ represent the weights of the separate objective functions, $T_{2_{\max}}$ represents its maximum solution (not the initial solution because it is equal to zero) and c_0 is its respective initial solution. The compliance parcel is inverted due to the fact that this is a maximisation multiobjective formulation.

Chapter 4

Implementation

The set of formulations defined in Chapter 3 required two different algorithms, one of them being the PTO algorithm, from [14], and the other being a novel SIMP based algorithm developed by the author in order to accomodate the formulation $H(\boldsymbol{\rho})$. This is due to the nature of these functions and their respective sensitivities.

4.1 Testing conditions

The testing conditions are defined by the boundary conditions and the geometry/mesh of the specimen. The boundary conditions used on this work are those of a uniaxial test. There are two main approaches to define them. On the one hand, these can be defined by two symmetry conditions and one distributed load on an edge, as seen in Figure 4.1a. These boundary conditions are defined as homogeneous. On the other hand, a more heterogeneous way to define the boundary conditions of the same test is represented in Figure 4.1b, where an encastre is set on one edge and the nodes on the distributed load are confined to horizontal movement.

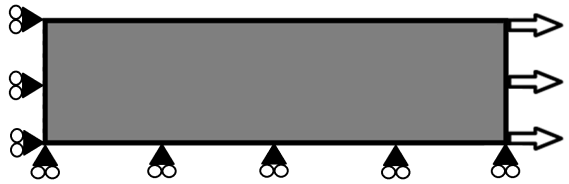

(a)

(b)

Figure 4.1: A representation of the testing conditions: (a) BC1 – Homogeneous boundary conditions; (b) BC2 – Boundary conditions emulating an encastre with holders.

Regarding the geometries used for the specimens, they were either squared or rectangular, and the size of the meshes varied according to each particular test.

4.2 Implementation of the statistics-based function

The heterogeneity formulation $H(\boldsymbol{\rho})$ was implemented using a novel algorithm, represented in Figures 4.2 and 4.3, due to the nature of its objective function and sensitivities. The inital segment of the code, shown in Figure 4.2, is focused on setting up the iterative process, which includes the constants, the Finite Element Analysis (FEA, explained in Section 3.2), the respective boundary conditions and the density filter. Also, the plot figure is initialized, the optimal objective function is calculated and the iterative procedure is initialized.

The second segment of the code is layed on the iterative process itself. The objective function of the current iteration is calculated, as well as the sensitivity values of the current design. The figure is plotted, and then the new design is updated using the scheme from Section 4.2.1, and the new density matrix is obtained. This loop is then repeated until a termination criterion is satisfied, which stops the iterative process if the change in the density matrix between two successive iterations is smaller than a prescribed tolerance, which is equal to 0.01. The $dpa(\boldsymbol{\theta})$ segment from Figure 4.3 represents a separate *Matlab*® function which is used in order to calculate representativity of density per angle, $dpa(\boldsymbol{\theta})$, which is used to obtain the objective function. This function consists of calculating the FEA and, therefore, obtaining the element principal stresses, which are then used to calculate their respective element stress angles. Lastly, the density representativity per interval of angle is obtained.

4.2.1 Updating scheme

The updating scheme is the segment of the code where the variables are updated in order to guide the optimisation problem, respecting its constraints. The adopted updating scheme is a very simple additive one, represented by

$$\rho_{i+1} = \rho_i - \frac{\mathrm{d}H}{\mathrm{d}\rho}\delta, \tag{4.1}$$

where ρ_{i+1} represents the design variable matrix of the current iteration, ρ_i is the variable matrix of the previous iteration, δ is the updating step, and $\mathrm{d}H/\mathrm{d}\rho$ represents the sensitivity matrix. A scaling procedure was applied over the sensitivity values, where the values of $\mathrm{d}H/\mathrm{d}\rho$ were normalized in relation to their maximum value, for the purpose of keeping the updating scheme controlled and within the desired limits.

The updating scheme is guided by the sensitivity values of the problem, whilst satisfying the constraints of volume fraction and limits of density. The updating scheme adopted was based on the OC method. With the intent of accomodating its constraints, some changes were made to the algorithm, in order to be effective over a sensitivity matrix which values range from negative to positive in sign. For instance, in Equation 4.1, the current density matrix is calculated with the previous values of the density matrix and a step which is proportional to the value of its sensitivity, in order to assign density values to the elements accordingly. This methodology differs from the optimality criteria (OC) method present in the TOP99 algorithm [15], which finds the Lagrange multiplier

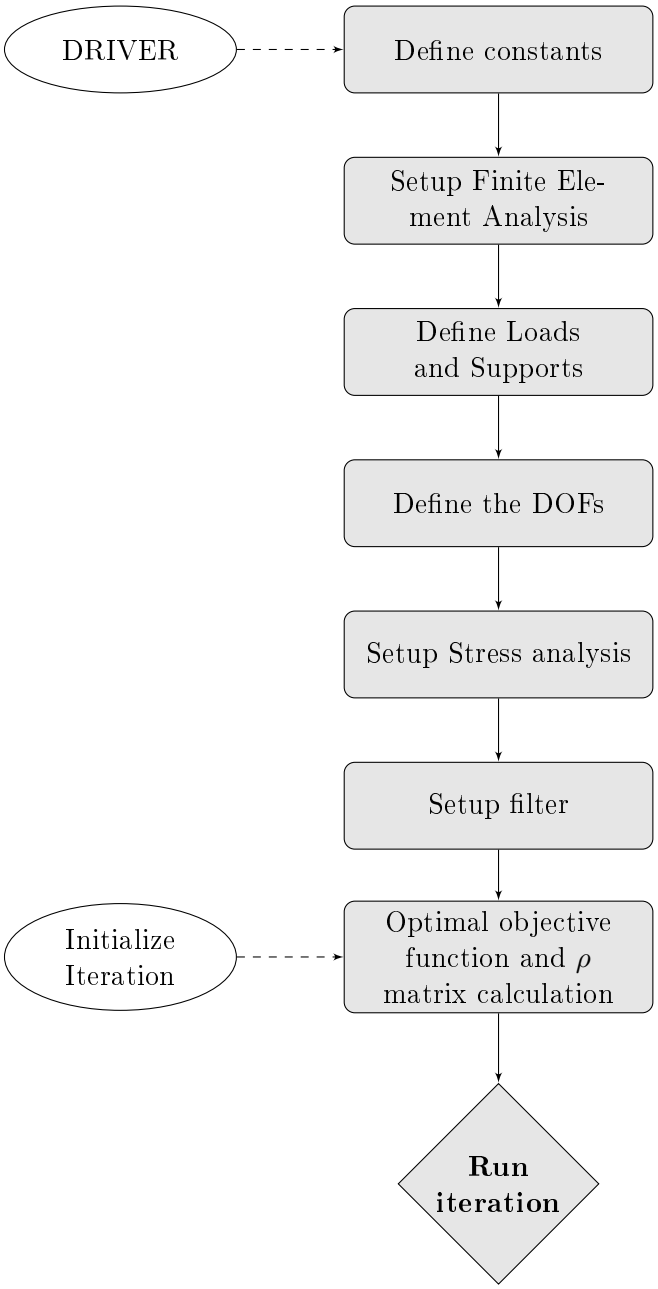

Figure 4.2: Flow chart representing the initialization process on the code regarding $H(\boldsymbol{\rho})$.

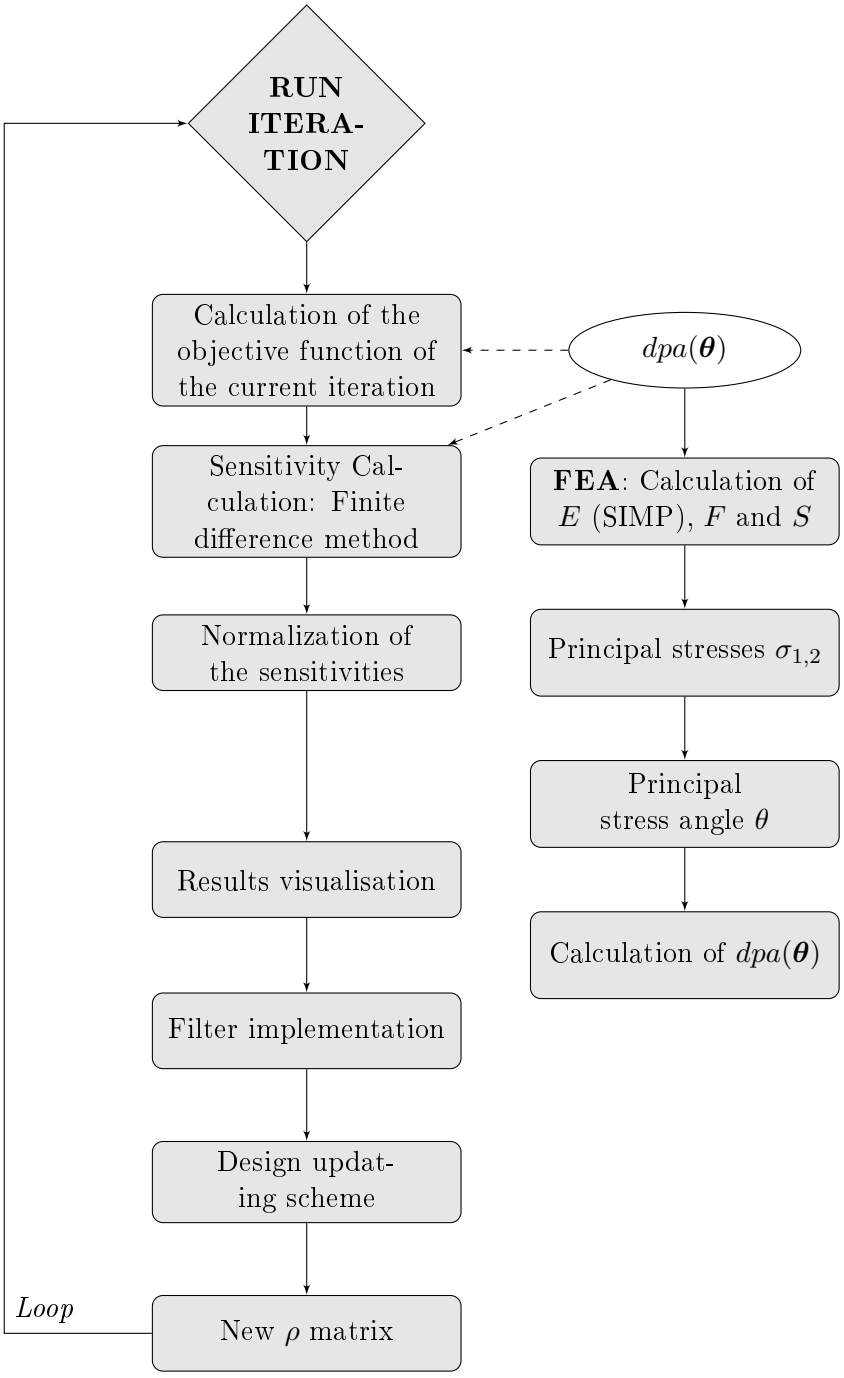

Figure 4.3: Flow chart representing the iterative process on the code regarding $H(\boldsymbol{\rho})$.

instead of an additive constant. The second part of the equation is subtracted due to the fact that, on the one hand, this is a minimisation problem, and on the other hand, the sensitivities are calculated using a progressive finite difference method. Meaning that, when the sign of the derivative is negative, it is of interest to increase the value of the respective variable.

Coding wise, as seen in Algorithm 1, the sequence of the design updating scheme starts with the implementation of the sensitivity filter, W, on the sensitivity matrix, $norm$. The updating scheme, represented in Equation 4.1 does not preserve the volume fraction. As the sensitivity values can be positive or negative, this updating scheme either adds or subtracts material to the system. So, it is necessary to append a constant, add_{mid}, to the derivatives of the updating scheme in order to keep the volume fraction. To do so, the difference between the ρ matrix from the previous iteration (for which the mean is equal to the prescribed volume fraction), represented in pseudocode as x, and the ρ_{i+1} matrix from the current iteration (Equation 4.1), represented as *xNew_ original* (for which the volume fraction is not preserved) is calculated. This difference, defined as *xChange_ original*, indicates whether the balance of mass is positive or negative using the current sensitivities, and indicates whether the updating scheme needs to add or subtract material in order to keep the volume fraction. Afterwards, the updating scheme utilizes the bissection algorithm, expressed in Algorithm 1 as the while loop, with the intent of finding *add_ mid* (represented as add_{mid} in Equation 4.2), similarly to the optimality criteria (OC) method. This constant is then added to the sensitivity matrix dif_new, to account for the constraints of the problem. The new corrected sensitivity matrix is expressed as

$$\left(\frac{\mathrm{d}H}{\mathrm{d}\rho}\right)_{\text{corrected}} = \frac{\mathrm{d}H}{\mathrm{d}\rho} \pm add_{\text{mid}} \tag{4.2}$$

where add_{mid} is the added constant which is found by the bissection algorithm. Finally, the new density matrix is updated using Equation 4.1 with the corrected sensitivity matrix from 4.2.

4.3 Implementation of the PTO – complementary objective functions

The nature of the complementary formulations from Section 3.4 allows for the usage of a non-gradient algorithm, such as the PTO algorithm from Section 2.2.1. As this algorithm does not require the calculation of the derivatives, the optimisation procedure is computationally less expensive than the algorithm used on the implementation of $H(\boldsymbol{\rho})$ from Section 4.2. The main difference between the two is the updating scheme. The PTO defines the proportion of the local objective function values per element in order to define an equivalent to the sensitivity matrix, which is then used to update the design variables. As an example, according to the formulation in Equation 3.21, it is optimal to favour the elements of which the product of the principal stress tensors is greater. So, a greater value of sensitivity, or proportion, is assigned to those elements, and, hopefully, the algorithm is naturally drawn to the optimal solution. However, it is observed that this proportion violates the volume constraint. In order to correct this, the PTO, represented in Algorithm 2, loops the amount of material that exceeds the density limits and redistributes it until the remaining material amount is small enough [14].

```
norm(:) = W × norm(:);
xNew_original = max(xlim(1),min(xlim(2),x - delta_move × norm));
xChange_original = xNew_original - x;
add_min = 0;
add_max = 1e9;
while (add_max - add_min) / (add_max + add_min) > 1e-6 do
    add_mid = (add_max + add_min) / 2;
    if sum(xChange_original(:)) > 0 then
        dif_new = norm + add_mid;
        xnew = max( xlim(1), min( xlim(2), x - delta_move × dif_new) );
        xChange = xnew - x;
        if sum(xChange(:)) < 0 then
            add_max = add_mid;
        else
            add_min = add_mid;
        end
    else if sum(xChange_original(:)) < 0 then
        dif_new = norm - add_min;
        xnew = max( xlim(1), min( xlim(2), x - delta_move × dif_new) );
        xChange = xnew - x;
        if sum(xChange(:)) < 0 then
            add_min = add_mid;
        else
            add_max = add_mid;
        end
    else
        xnew = xnew_original;
        break
    end
end
x = xnew;
```

Algorithm 1: A representation of the updating scheme developed by the author, in pseudo-code.

```
xTarget = nelx × nely × vlim;
xRemaining = xTarget;
xNew(:) = 0;
ObjFunc_proportion = ObjFunc / sum(ObjFunc(:));
ObjFunc_proportion(:) = W × ObjFunc_proportion(:);
while xRemaining > 0.001 do
    xDist = xRemaining × ObjFunc_proportion;
    xNew(:) = xNew(:) + xDist(:);
    xNew = max( min( xNew, xlim(2) ), xlim(1) );
    xRemaining = xTarget-sum(xNew(:));
end
x = alpha × x + (1-alpha) × xNew;
```

Algorithm 2: A representation of the updating scheme on the PTO algorithm [14], in pseudo-code.

This algorithm initially sets the value of the desired amount of material, *xTarget*, and defines the remaining material that is yet to be spread across the elements, *xRemaining*. Then it defines the proportion matrix, *ObjFunc_proportion*, where for each element a proportional magnitude of the objective function is assigned. The proportion matrix is filtered by the density filter, *W*. The remaining material is then spread across the elements, represented by *xDist*. The operation on *xDist* does not meet the density constraints, so a loop is used in order to correct that. Finally, *xNew* is returned. When the loop is over, the design variable matrix x is updated, using the history coefficient *alpha*. For a more detailed explanation, the reader is referred to [14].

Intentionally blank page.

Chapter 5

Results

5.1 Results regarding the statistics-based formulation

5.1.1 Analysis of the applied methodologies and parameters

The present section is focused on analysing the behaviour of the objective function $H(\boldsymbol{\rho})$ under certain methodologies and parameters, and describing the iterative process up until the development of the final code. Some of these parameters include the size of the mesh, the filter implementation, the penalisation factor from SIMP, the updating step, and the specimen's geometry. Each one of these parameters was tested individually, whilst keeping the remainder constant. Table 5.1 exhibits the constants used in the following analyses (most of them taken from the PTO code). The program is unitless, similar to the PTO, except from the units of the angles, which are expressed in degrees.

Table 5.1: List of constants of the driver of the algorithm, where the ones in asterisks represent the parameters that were studied furthermore.

Constants		Description
E0	1	Young's Modulus
Emin	1×10^{-9}	Minimum value of the Young's Modulus
L	1	Element edge length
lv	1	Load value
*nelx**	40	Number of elements in x dimension
*nely**	10	Number of elements in y dimension
nu	0.3	Poisson's ratio
*penal**	3	SIMP penalisation
rmin	1.5	Filter radius
vmslim	1.08	Stress limit
xlim	[0, 1]	Lower and upper bounds of density
ld	*nely*+1	Number of nodes the displacement and loads are distributed on
*vlim**	0.5	Volume fraction
*ar**	0.5°	Resolution of the principal stress angle (degrees)
*step_fin_dif**	0.0001	Disturbance step – finite difference method
*delta_move**	0.2	Updating step
*filter**	0	Filter – boolean

Initially, the values of the constants from Table 5.1 were either taken from [14] or chosen heuristically. Then, these parameters were carefully and individually analysed, in an iterative process, in order to choose the best possible values and obtain the optimal results.

5.1.2 Objective function and sensitivity analyses

An in depth analysis was made regarding the objective function $H(\boldsymbol{\rho})$ and the respective sensitivities for the purpose of better understanding the problem and develop strategies to solve it. As defined in Section 3.1, $H(\boldsymbol{\rho})$ describes the quadratic difference between the resulting histogram of the density matrix and the optimal distribution across the angles θ. It is noticed that the magnitude of the objective function varies with both the prescribed volume fraction and the design domain ($nelx \times nely$), as seen in Equation 3.8.

For the purpose of evaluating the behaviour of the objective function in distinct locations of the specimen, a study was made by sweeping the value of the design variables between 0 and 1, on 3 different elements individually. Figure 5.1 represents a study on a homogeneous test (the matrix of the design variables is equal to 0.5, with size $nelx$=40 by $nely$=10) regarding the objective function, where three different elements were strategically chosen (represented as green squares on the respective figures) in different places in regards to the boundary conditions. For the purpose of obtaining reliable conclusions, the number of points used on the plot of the objective function was 10000.

By analysing the plots of the objective functions in Figure 5.1, it is concluded that the function is not continuous when the value of density of the element in study is equal to the surrounding elements. This discontinuity might be due to the fact that, on top of having a discrete problem of finite element analysis, for the calculation of the objective function, the measurement of the density per angle is also of discrete nature. The objective function has a maximum peak if all the elements have equal density, because the worst case scenario is that of a homogeneous specimen. The objective function dramatically decreases if the density of the element in study changes, making it more heterogeneous. Also, by analysing the principal stress diagram on the same figure, it is observed that if the density of the element gets closer to 1 (the stress states are presented on grayscale for a better visualization of the variation of the density), the stress state strays away from the uniaxial stress state, making the specimen more heterogeneous, as the objective function decreases. The same is verified when the density of the element gets closer to 0 (the element is void), as the stress state gets closer to the origin, the objective function also decreases.

In order to verify if the function $H(\boldsymbol{\rho})$ is discontinuous when the variable is equal to the density of the surrounding elements, a study was made with a beam with 3 different density values (equal to 0.5, 0.6 and 0.7). As seen in Figure 5.2, no conclusions were drawn regarding this statement, as the plots don't appear to present a pattern that corroborates that.

The same study was performed on a heterogeneous specimen with different values of density over the elements. Figure 5.3 exhibits a highly non-linear objective function. In topology optimisation this non-linearity is not ideal for two reasons. First, in the initial iterations, when the variables are updated, their values are of intermediate densities. If the sensitivity values are too volatile, the updating method is not able to push the design variables to 0 and 1 efficiently, and the SIMP method becomes ineffective. In this case,

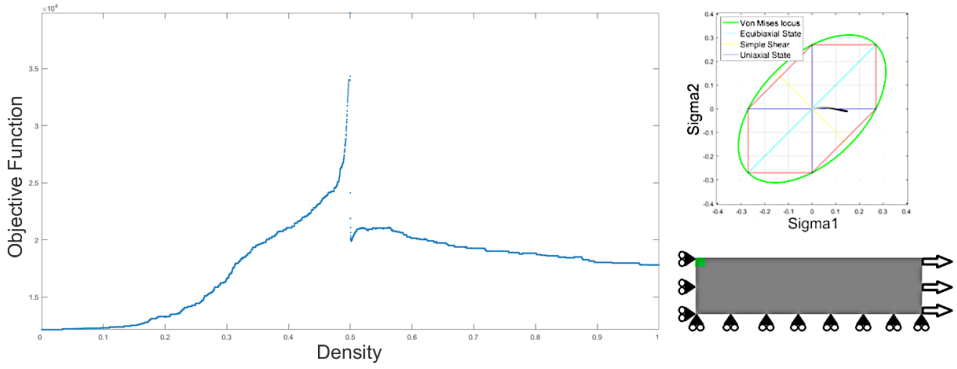

(a)

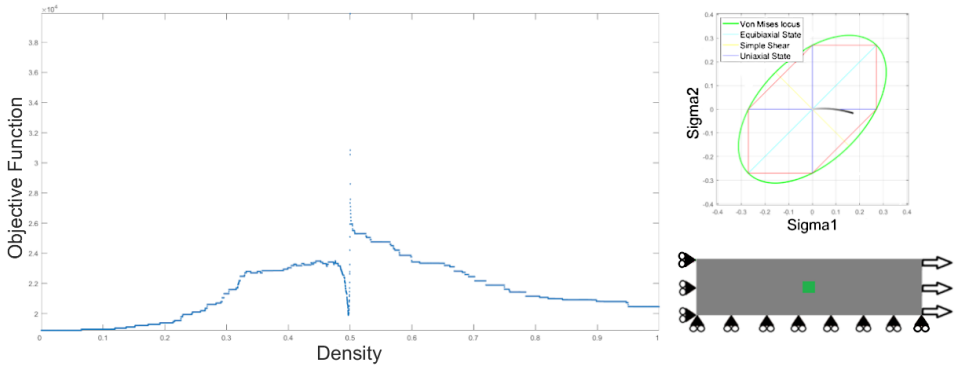

(b)

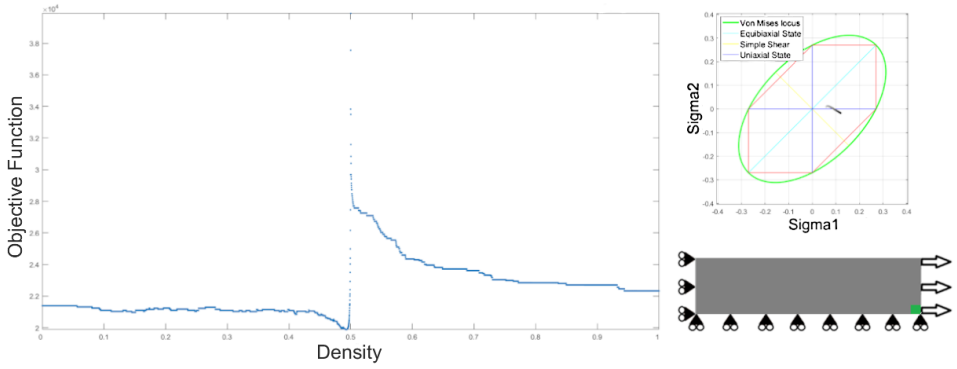

(c)

Figure 5.1: A study on one of the design variables of a sample with homogeneous geometry, where all the elements present a density equal to 0.5, and boundary conditions regarding the behaviour of the objective function: (a) Upper left element; (b) Middle element; (c) Lower right element.

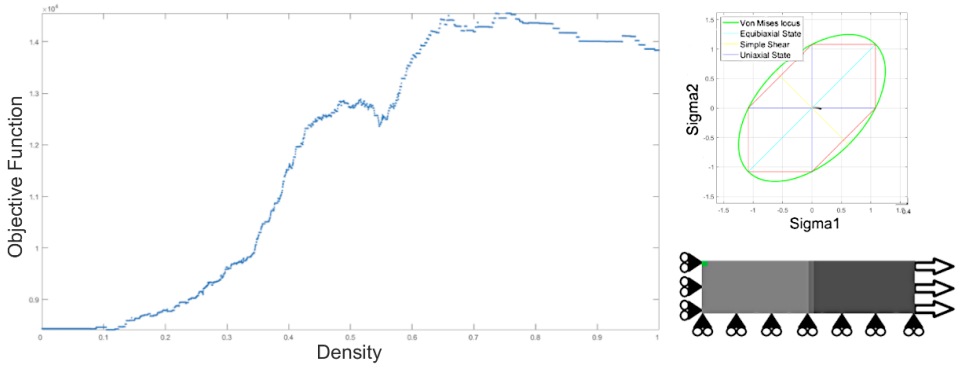

(a)

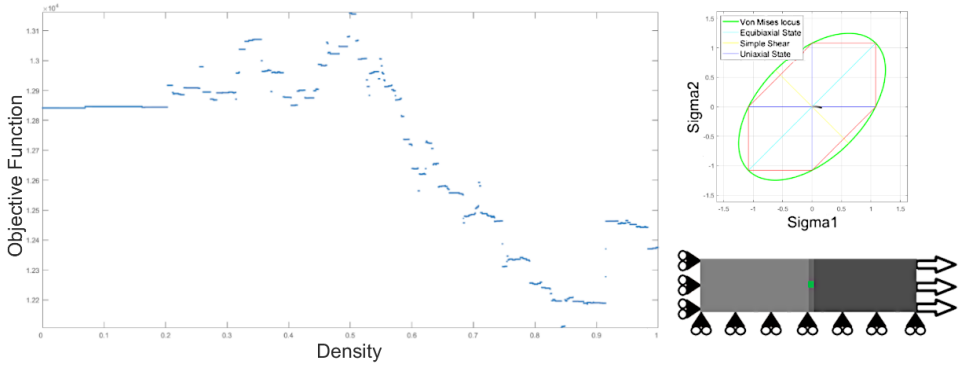

(b)

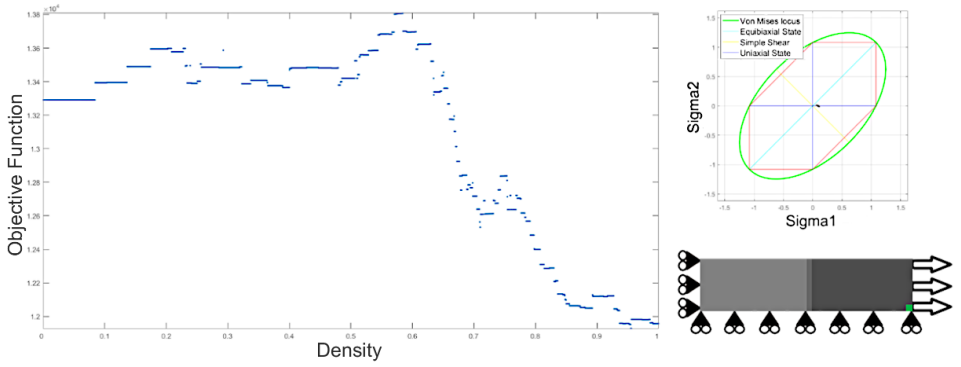

(c)

Figure 5.2: A study on one of the design variables regarding the behaviour of the objective function, on a specimen with 3 different levels of density and homogeneous boundary conditions: (a) Upper left element; (b) Middle element; (c) Lower right element.

as seen in the plot of the objective functions, it is not possible to obtain an accurate gradient based algorithm, as the function is discrete and presents a lot of local minima.

A final evaluation was made, regarding this objective function using a solution of a heterogeneous specimen found in the literature [25], to verify if this geometry would be an effective initial solution. Analysing Figure 5.4, it is concluded that the function has a nonlinear nature and unpredictable behaviour.

This objective function may not be ideal as a topology optimisation formulation. The objective function is not continuous and nonlinear, which may make it not suitable for the topology optimisation problem. Nonetheless, it is an efficient heterogeneity indicator. Another important conclusion involves the magnitude of the sensitivity values. As the objective function is full of spikes and dips, the magnitudes of its gradient are very large, which presents huge challenges in terms of normalization.

5.1.3 Starting solution of the statistics-based formulation

The starting solution is that of a homogeneous specimen with the boundary conditions set to BC1 (represented in Figure 4.1a), with a geometry composed of a rectangle with 1200 elements, which represents the homogeneous case. Initially, it is observed that the stress states of all the elements of the specimen are overlapped in one point in the principal stress diagram, corresponding to the uniaxial stress state, as seen in Figure 5.5. The algorithm then proceeds to update the design variables in the direction of the optimal heterogeneous solution. All the constants used are present in Table 5.1.

5.1.4 Implementation and analysis of the filter

The filter assessed is the one present in [14]. It is a cone density filter which preserves the volume and performs local averaging. The density filter is employed with the intent of smoothing the geometry of the specimen, avoiding the formation of checkerboard patterns, and saving the algorithm from getting stuck in local minima [14]. Some of the intermediate results of the heterogeneity algorithm regarding $H(\boldsymbol{\rho})$ without the density filter appear to have the undesired checkerboard effect, as seen in Figure 5.6.

The efficiency of the implementation of the filter was also studied on the long term. With boundary conditions of BC1 and a rectangular specimen of 400 elements, for a range of 500 iterations, the algorithm with the filter present performs similarly to the one where the filter was absent, as seen in Figure 5.7. The objective function fluctuates around similar values, so, it is concluded that the presence of the filter is not a detriment to the optimisation procedure, whilst smoothing the geometry of the specimen.

Regarding the results obtained with the implementation of the density filter, it was concluded that its addition to the program is beneficial, resulting in more feasible solutions in terms of manufacturing, while also maintaining the optimisation aspect efficient.

5.1.5 Implementation and analysis of the SIMP – penalisation

The SIMP method is usually employed with the purpose of pushing the intermediate design variables to 0 and 1 in order to obtain a manufacturable solution, and, as a side effect, accelerate the optimisation process. The modified SIMP method applies the penalisation factor in the Young's modulus (as shown in Equation 3.14). This methodology is effective because when the penalisation exponent is activated, the objective function is

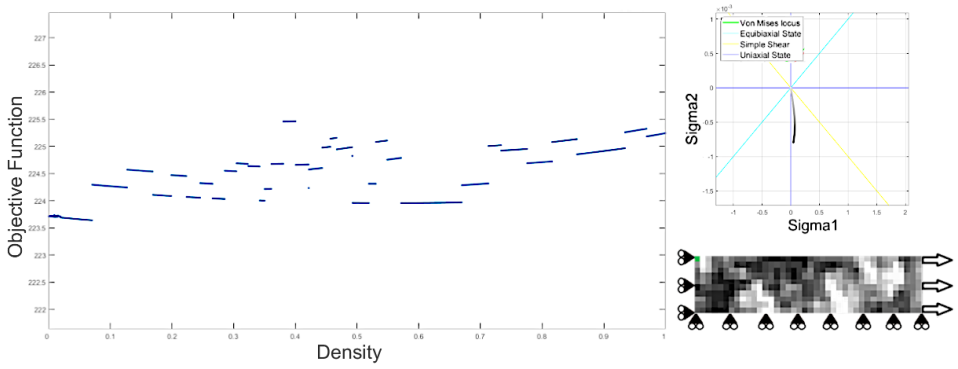

(a)

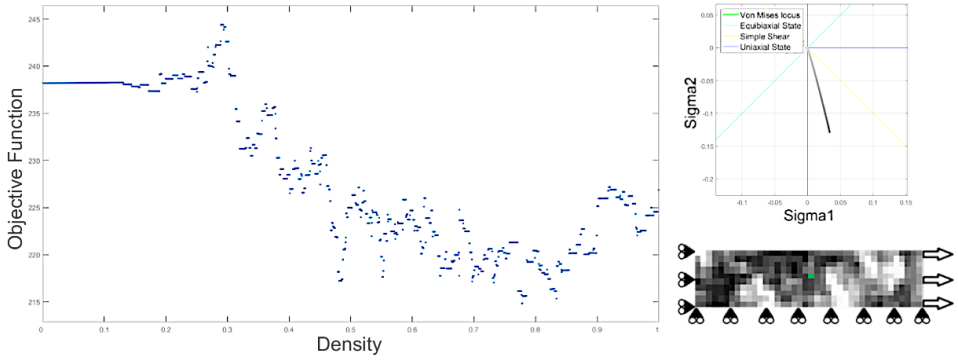

(b)

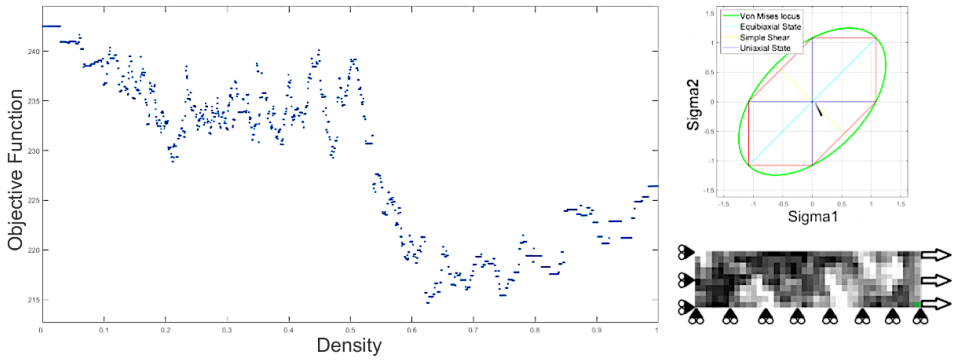

(c)

Figure 5.3: A study on the behaviour of the objective function on a specimen with heterogeneous levels of density and homogeneous boundary conditions, where one of the design variables is swept between 0 and 1: (a) Upper left element; (b) Middle element; (c) Lower right element.

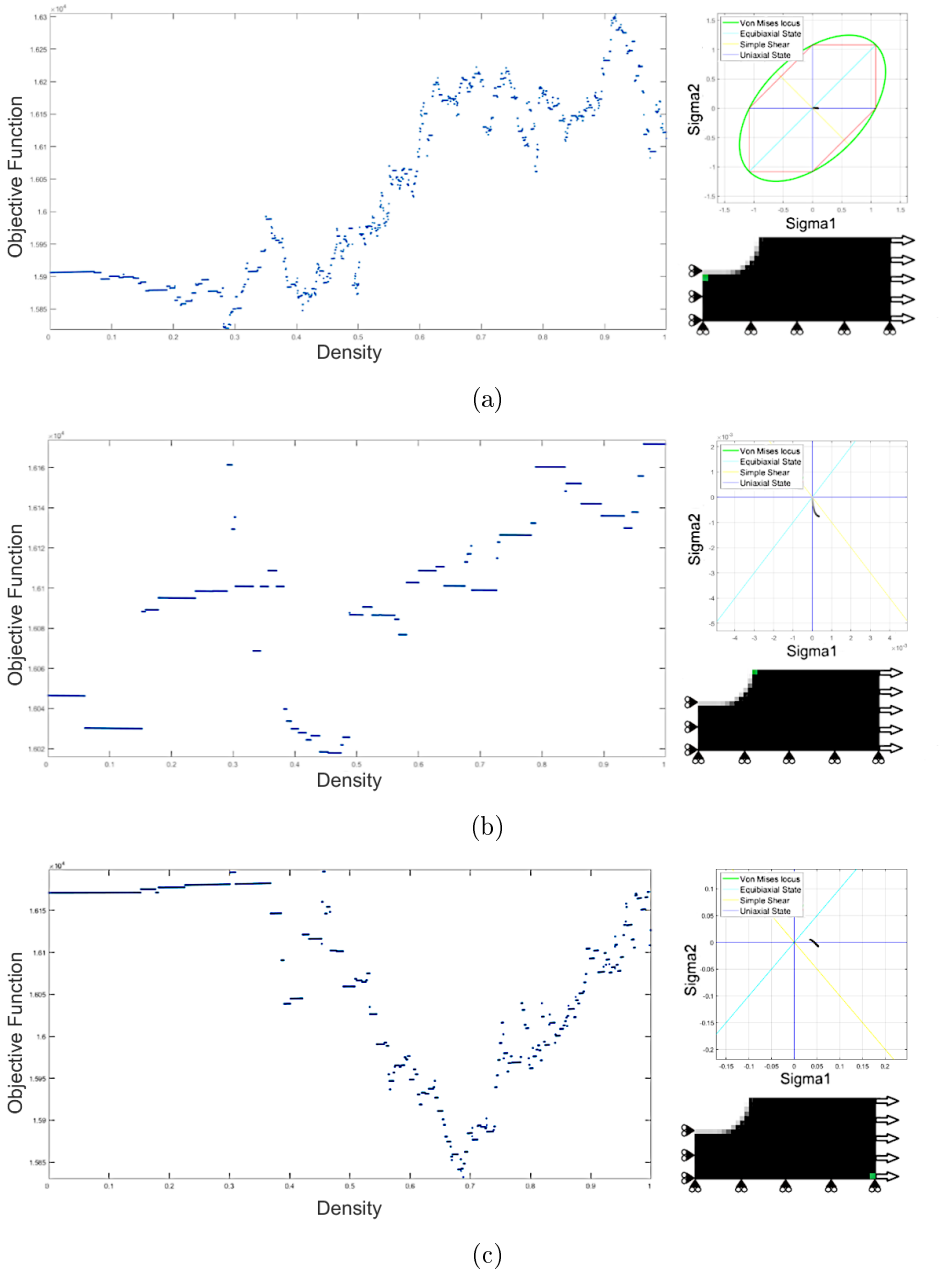

(a)

(b)

(c)

Figure 5.4: A study on the behaviour of the objective function on the specimen present in [25], where one of the design variables is swept between 0 and 1: (a) Upper left element; (b) Middle element; (c) Lower right element.

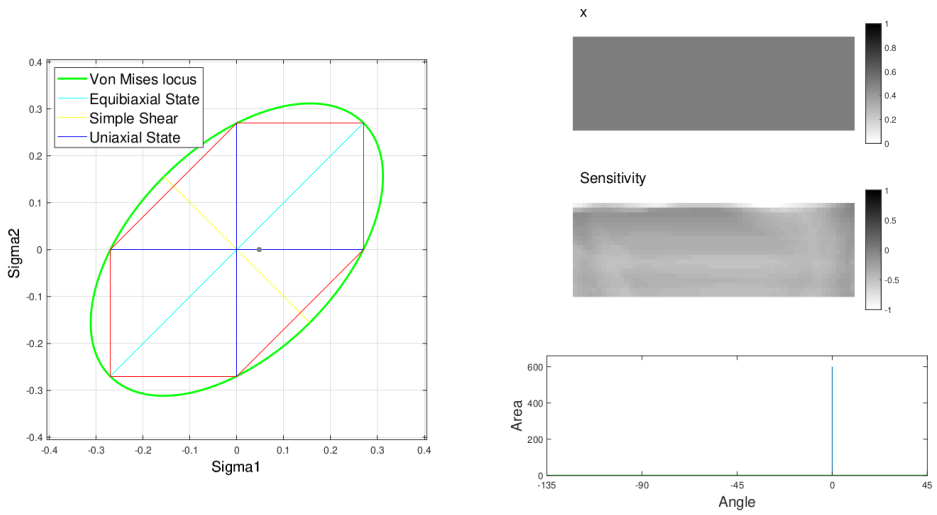

Figure 5.5: A representation of the initial solution of the heterogeneity algorithm regarding $H(\boldsymbol{\rho})$.

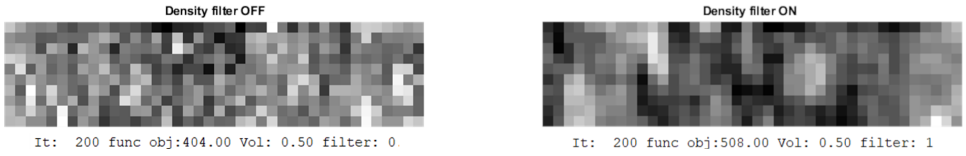

Figure 5.6: Side by side representation of effect of the density filter on the design domain under 200 iterations.

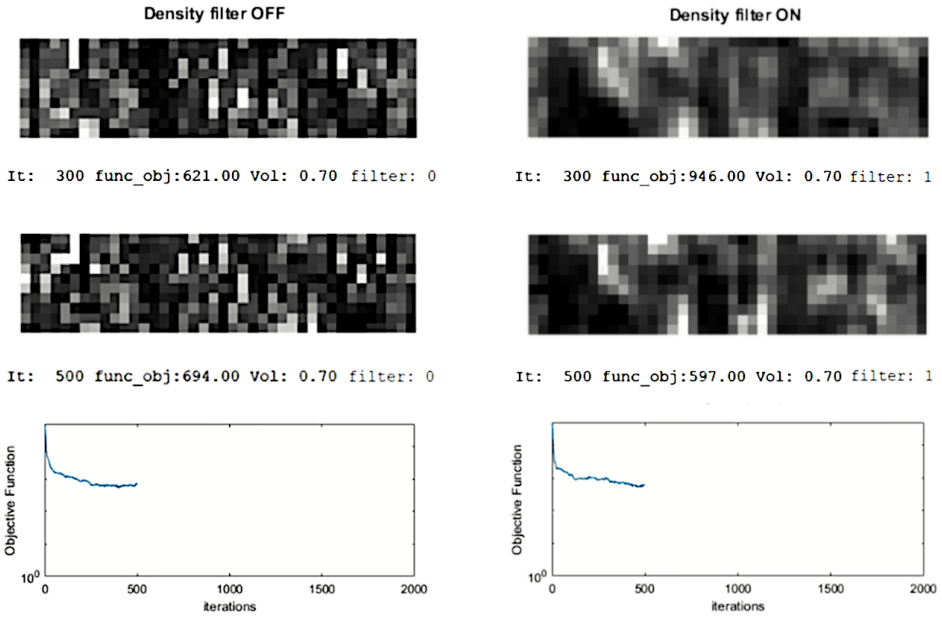

Figure 5.7: Representation of effect of the density filter on the design domain and on the evolution of the objective function.

raised to a factor, which exponentially changes its values and forces the design variables to its extremes. Figure 5.8 shows the effect the SIMP method has on the compliance function of a rectangular specimen composed by 400 elements with BC1 boundary conditions. It is observed that the nature of the compliance function is preserved for different penalization exponents. The penalisation factor changes the magnitude of the compliance function, and for comparison purposes, Figure 5.8 exhibits the functions floored, as different penalisation exponents change the magnitude of the compliance function.

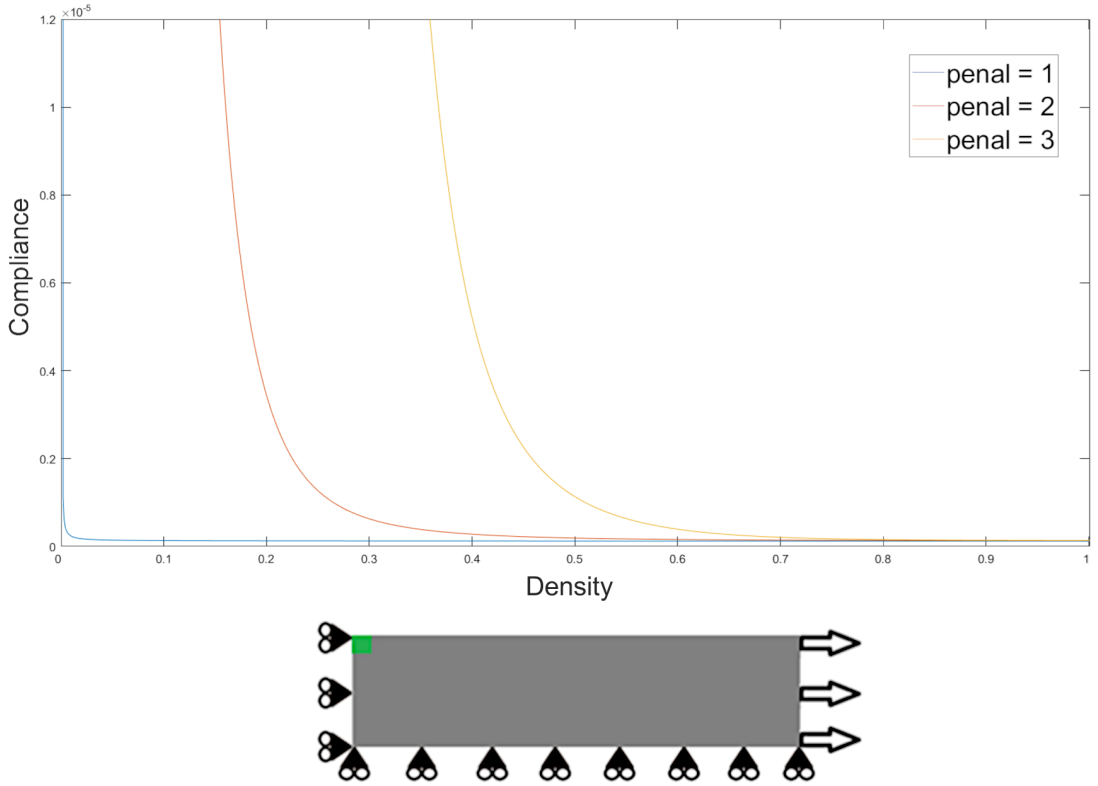

Figure 5.8: Analysis of the effect of the SIMP method's implementation on the objective function of the compliance problem for the upper left element.

The objective function $H(\boldsymbol{\rho})$ is of a different nature, in comparison to the compliance one. Comparing the plots of Figures 5.8 and 5.9, it is observed that the nonlinearity of $H(\boldsymbol{\rho})$ is also apparent in comparison to the compliance function. So, it is imperative to verify the functionality of the SIMP method in the former. Firstly, this study was performed over the upper left element of the same design space and boundary conditions, as seen in Figure 5.9. It is observed that as the value of the penalty exponent is raised, the plot of objective function appears to dampen.

By analysing the lower right element of the design space, shown in Figure 5.10, the same dampening effect is observed. These two analyses may indicate that the penalisation factor is in fact acting with the desired effect of forcing the densities to 0 and 1, whilst contributing to the acceleration of the minimisation process, as the slope of the function appears to increase with the penalization.

The SIMP method was also studied under the optimisation algorithm, in order to

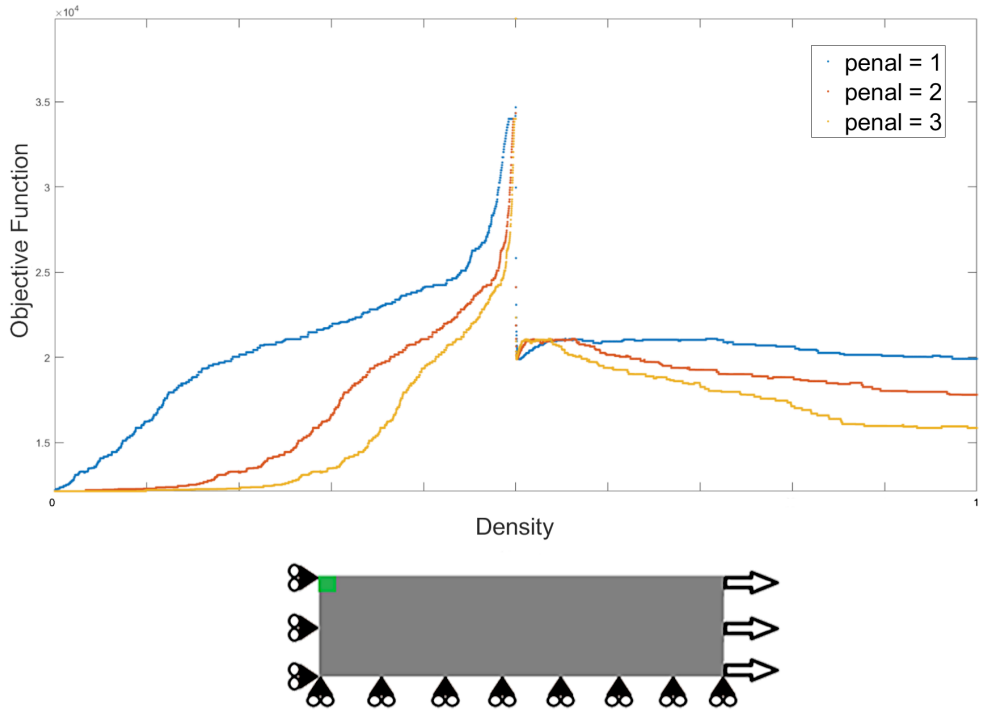

Figure 5.9: Analysis of the effect of the SIMP method's implementation on the objective function $H(\boldsymbol{\rho})$ for the upper left element.

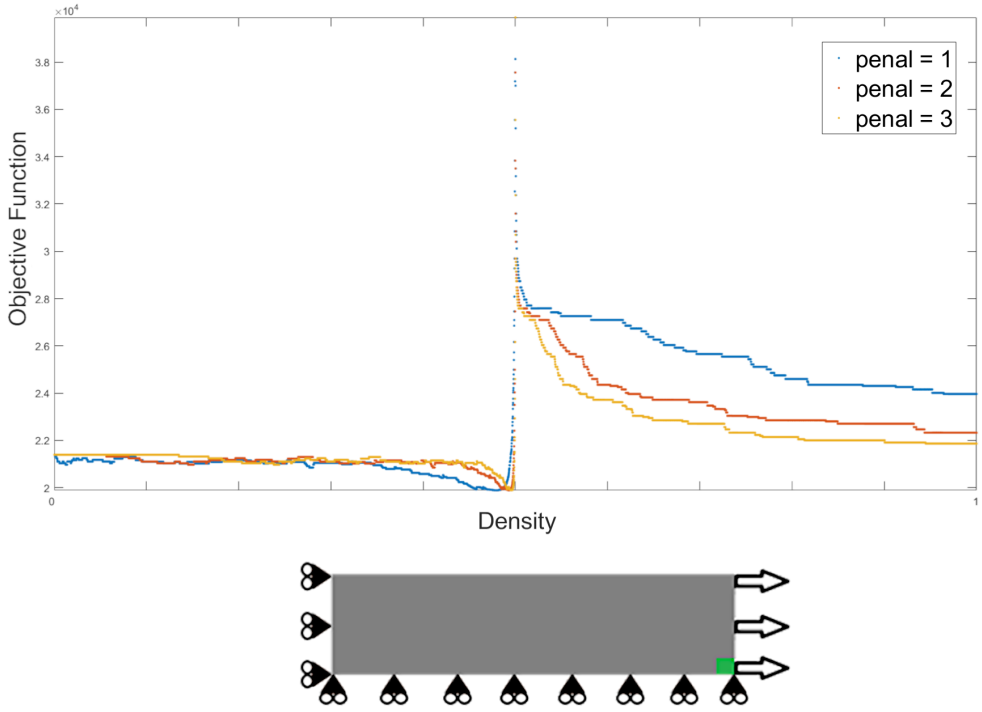

Figure 5.10: Analysis of the effect of the SIMP method's implementation on the objective function $H(\boldsymbol{\rho})$ for the lower right element.

observe its effectiveness on the iterative process. By analysing Figure 5.11, the penalization implementation appears to speed up the optimisation process. Nonetheless, it is not effective in pushing the intermediate densities to 0 and 1.

The defined value of penalisation was 3 due to the fact that, on the one hand, it is the most commonly used in the literature [14,15,24]. On the other hand, as the objective function appears to be greatly nonlinear as seen in Section 5.1.2, adding a high value of penalisation would only aggravate the non-linearity of the objective function and stray the algorithm away from the optimal solution. Not using penalisation would also be non-ideal because it would make the algorithm, which is already slow due to the huge amount of objective function's evaluations per cycle, even slower.

5.1.6 Calibration of the angle resolution

The a_{r} constant defines the interval of resolution of the principal stress angle, as seen in Section 3.1. It is observed that the value of the a_{r} constant scales the magnitude of the objective function, as it changes the thickness of the bars on the density histogram, and the number of elements incorporated per bar changes, as verified in Figure 5.12b. On the other hand, decreasing the a_{r} value seems to increase the nonlinearity of the objective function (Figure 5.12a), which is not ideal in the context of an optimisation problem.

A study was also made regarding a refined mesh. Figure 5.13 shows that for a mesh of 1200 elements, decreasing the a_{r} value will also result in a highly nonlinear function.

The efficiency of different a_{r} values was tested under the heterogeneity algorithm regarding $H(\boldsymbol{\rho})$. Even though the values of the objective function appear to increase as the a_{r} value decreases (Figure 5.14), it is not ideal on the long term to have such a small step. This is due to the fact that the a_{r} value imposes a minimum mesh size required, because the number of bars of the histogram increases as the a_{r} constant decreases, and for every interval of angle, in the utopian solution, there has to be at least one element represented per interval of angle. In the present work, the adopted a_{r} value was 0.5. For an efficient algorithm, refining the mesh is required for a smaller a_{r}.

5.1.7 Calibration of the perturbance of the finite difference method

The step of the finite difference method, $step\_fin\_dif$, represents the size of the disturbance made to the objective function in order to obtain its sensitivity matrix. Its value needs to be chosen in accordance to the sensitivity of the objective function, meaning that the more nonlinear the function is, smaller the step value needs to be. This is due to the fact that the goal is to obtain the approximate derivative of said function, with the best accuracy possible. Given that the objective function is highly nonlinear, the chosen value of $step\_fin\_dif$ was chosen heuristically (see Table 5.1), which is a very small number that hopefully meticulously represents $H(\boldsymbol{\rho})$.

5.1.8 Analysis of the updating step

The updating step δ is an important asset that prevents the algorithm from having an uncontrolled updating process. The updating scheme adopted for the heterogeneity algorithm regarding $H(\boldsymbol{\rho})$ (Equation 4.1) limits the maximum step of the updating of the design variables. This constant, δ, sets the pace of the updating scheme, similarly to the "move" constant present in the TOP88 algorithm [24].

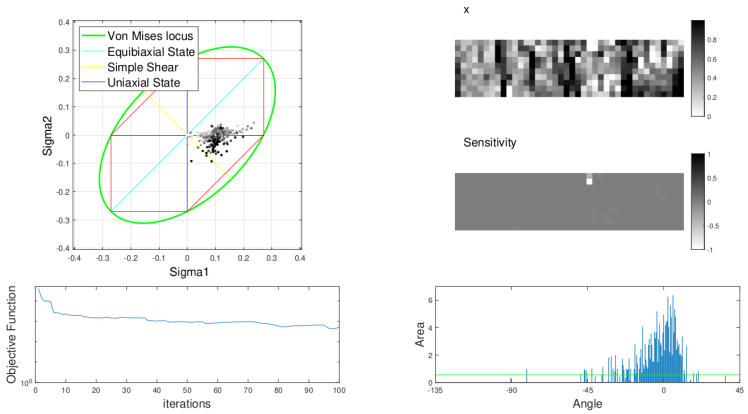

(a)

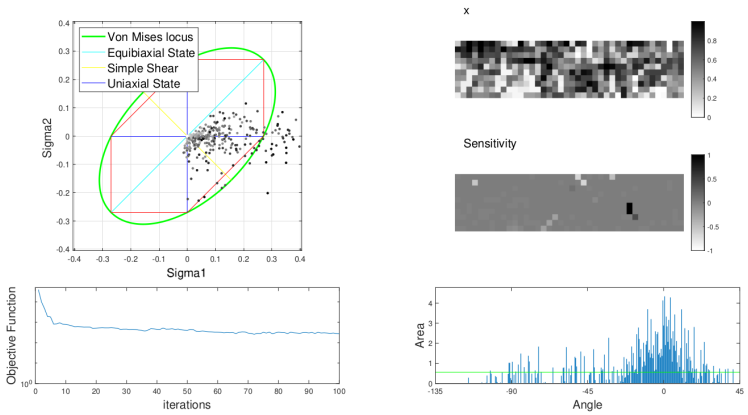

(b)

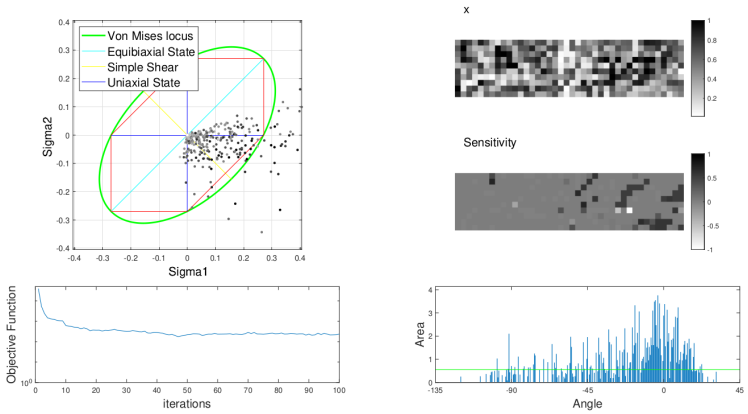

(c)

Figure 5.11: Influence of the SIMP method on the evolution of the optimisation algorithm $H(\boldsymbol{\rho})$ for a volume fraction of 0,5: (a) Without the SIMP penalisation (Objective function = 534); (b) Penalisation factor of 3 (Objective function = 270). (c) Penalisation factor of 5 (Objective function = 235).

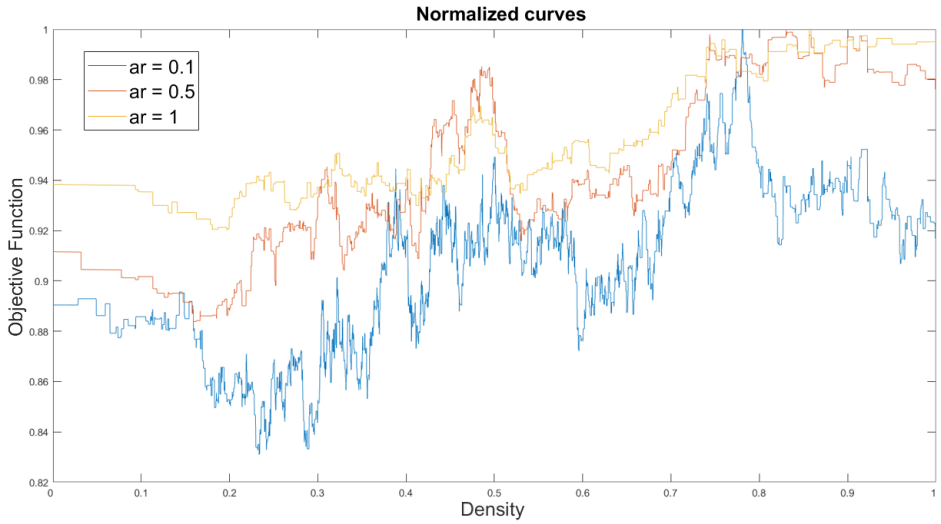

(a)

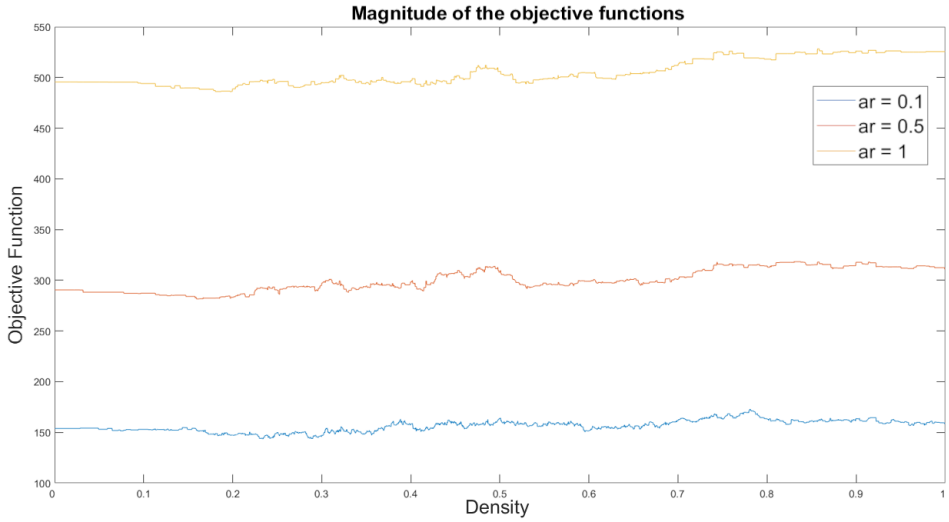

(b) Analysis of the

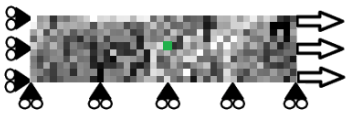

(c)

Figure 5.12: Analysis of the influence of the a_r constant over the objective function:(a) Magnitude of the objective function over different a_r values; (b) change of the behaviour of the objective function under different ar values; (c) Boundary conditions and representation of design variable used (green element) in the analysis of the objective function over the a_r constant.

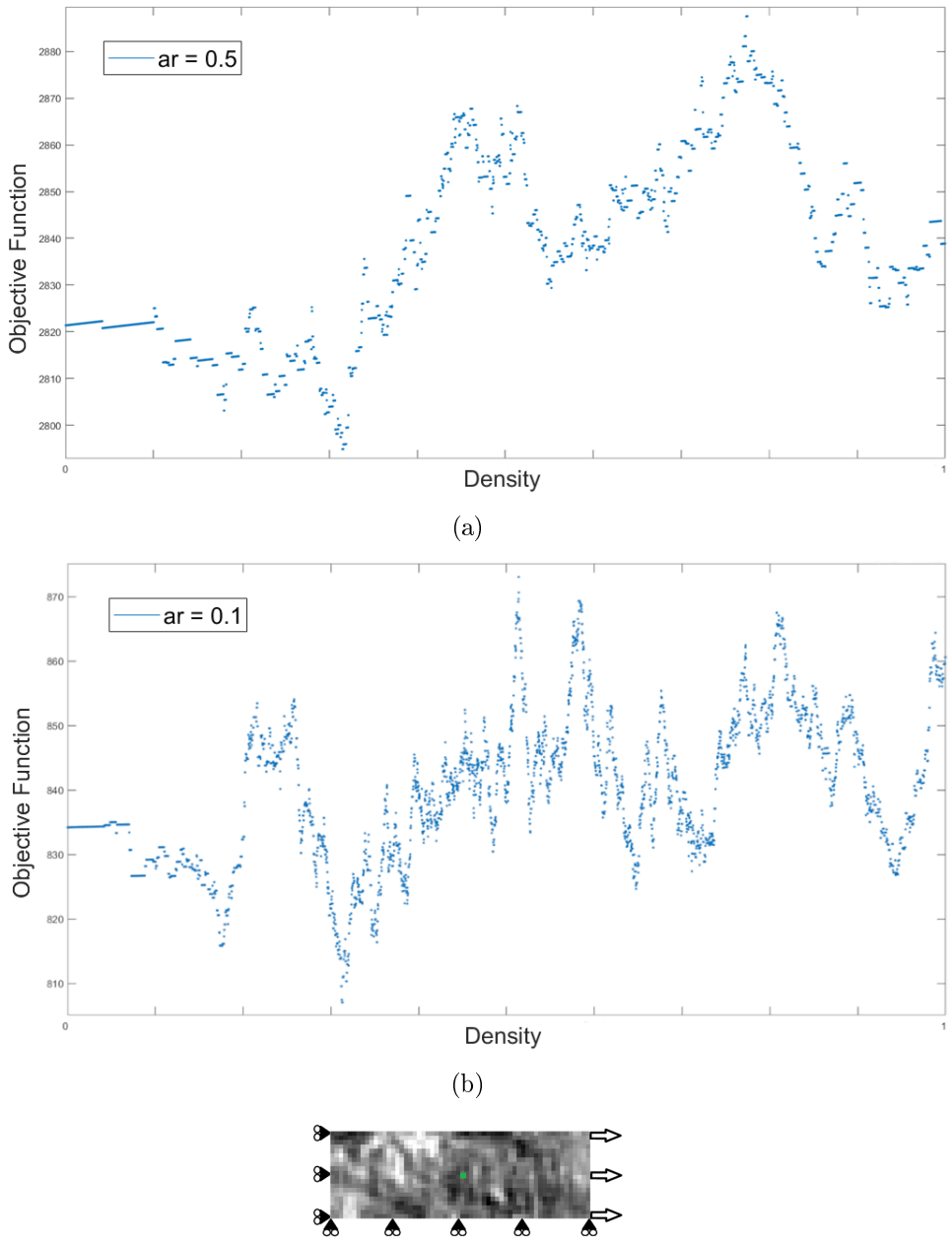

(a)

(b)

(c)

Figure 5.13: Analysis of the influence of the a_r constant over the objective function: (a) a_r value of 0.5; (b) a_r value of 0.1; (c) Boundary conditions and representation of design variable used (green element) in the analysis of the objective function over the a_r constant.

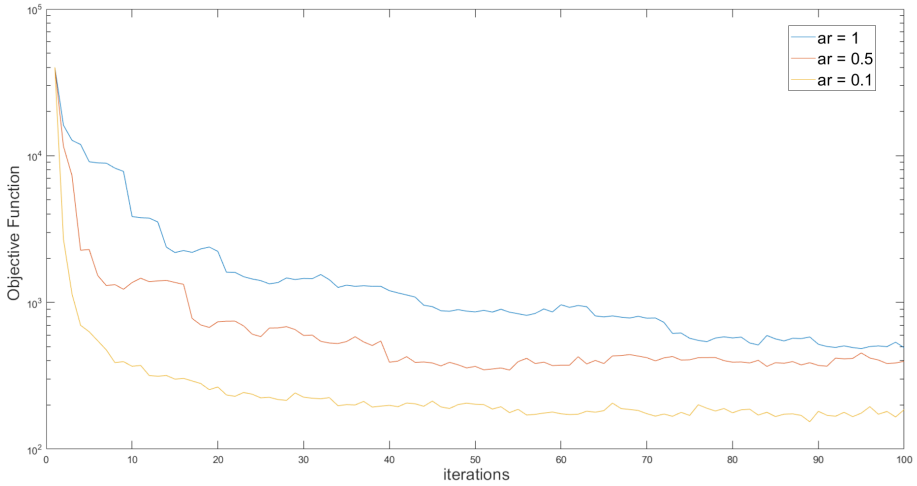

Figure 5.14: Analysis of the effect of the influence of the angle resolution on the heterogeneity algorithm regarding $H(\boldsymbol{\rho})$.

Using BC1 with a rectangular specimen with 400 elements with updating step of δ = 0.01, Figure 5.15 exhibits a slow iterative process, where for 100 iterations the design variables are nowhere near its limits and the objective function decreases slowly per iteration, in comparison to Figures 5.16 and 5.17. A small value of δ would probably make the algorithm reach better values of objective function on the long run, but would also turn the computational process hugely slow. By comparing Figure 5.16 and Figure 5.15, it is concluded that δ=0.1 enhances the minimisation of the objective function and the design variables get closer to its limits, in comparison to δ=0.01. The updating step adopted in [15] is 0.2, in accordance to the TOP88 problem from [24]. Regarding $H(\boldsymbol{\rho})$, as seen in Figure 5.17, a δ value of 0.2 exhibits a favorable balance between the speed of the design variables' updating and its efficiency as an optimiser.

For delta equal to 0.3 (Figure 5.18) it is observed that the algorithm is already struggling to minimise the objective function at 100 iterations. That is a result of the fact that the updating step is too large and oversteps.

Considering all the advantages e disadvantages presented, the updating step of δ=0.2 seems to be the most solid and balanced in terms of both optimisation efficiency and speed.

5.1.9 Analysis of the mesh refinement

The performance of the algorithm using BC1 boundary conditions for the refined mesh of 1200 elements (Figure 5.19) was relatively similar to the one with 400 elements in terms of results (Figure 5.17). It is exponentially computationally more expensive, because it requires more evaluations of the objective function per cycle. Even though the results obtained in terms of heterogeneity are excellent, the geometry of the specimen is not manufacturable due to its intermediate densities. Another significant limitation of the design of the sample in Figure 5.19 is the non-continuity of material from edge to edge, which would break apart under mechanical test conditions, or even fall apart on itself.

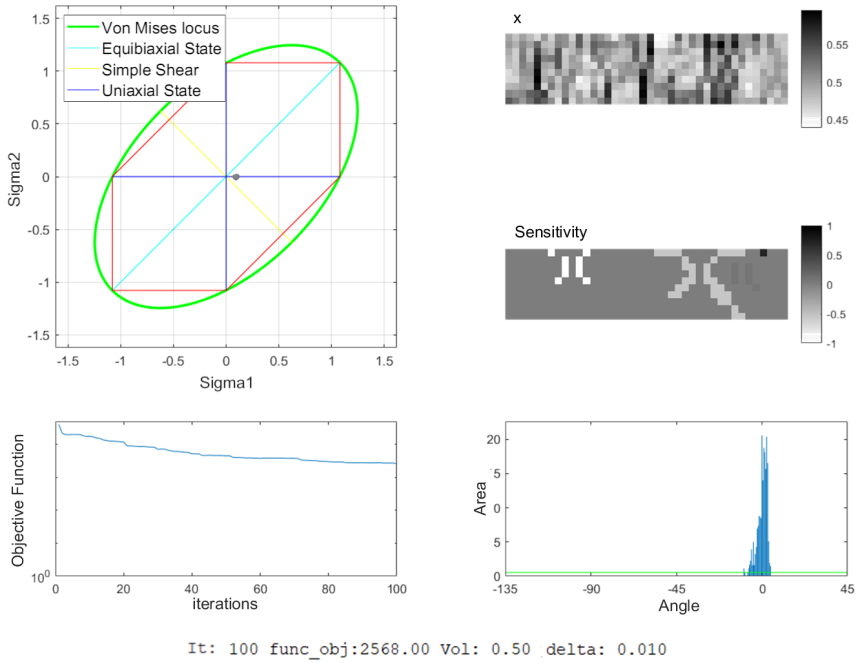

Figure 5.15: Analysis of the behaviour of the heterogeneity algorithm regarding $H(\boldsymbol{\rho})$ under a value of δ=0.01.

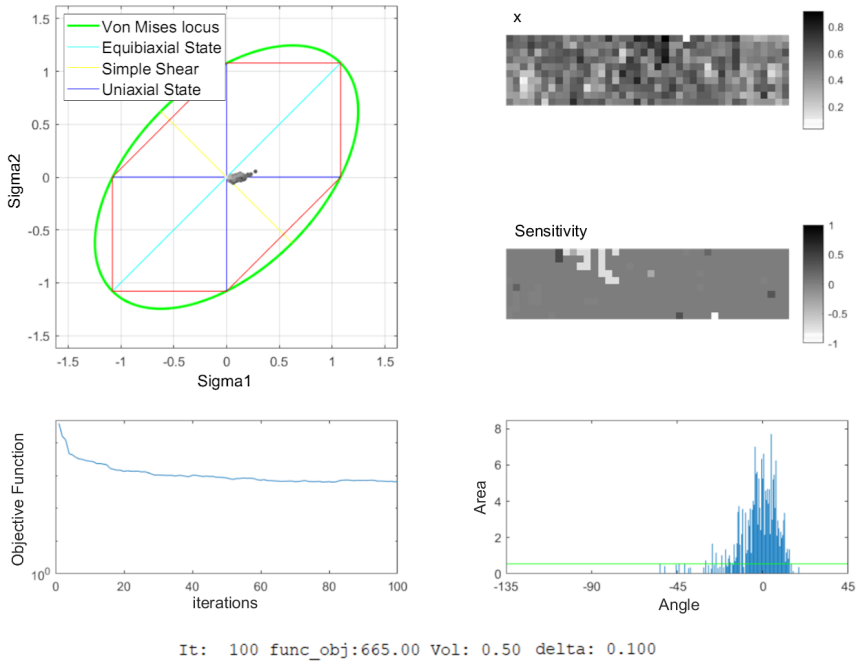

Figure 5.16: Analysis of the behaviour of the heterogeneity algorithm regarding $H(\boldsymbol{\rho})$ under a value of δ=0.1.

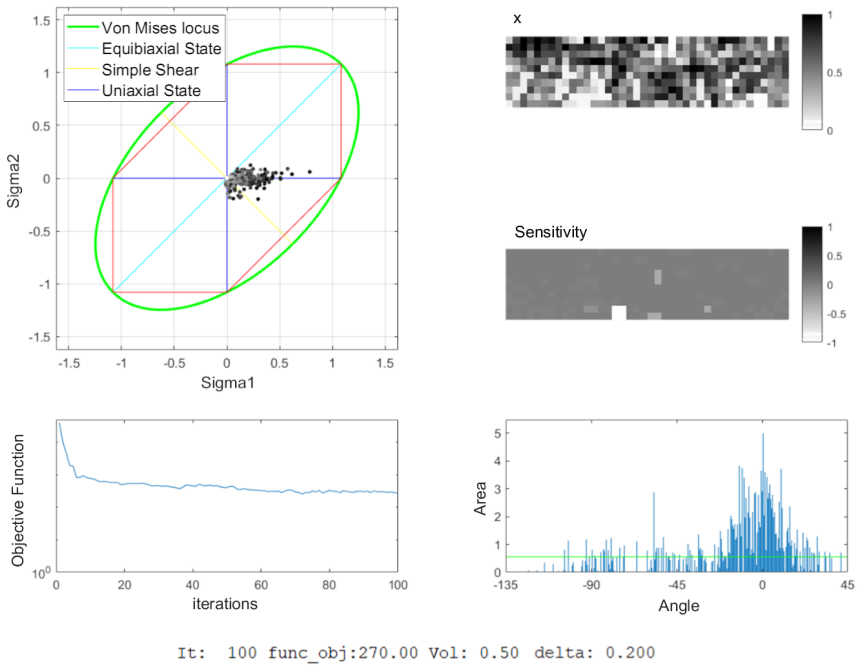

Figure 5.17: Analysis of the behaviour of the heterogeneity algorithm regarding $H(\boldsymbol{\rho})$ under a value of δ=0.2.

5.1.10 Alternative initial solution

As seen in the previous sections, the heterogeneity algorithm regarding $H(\boldsymbol{\rho})$ was able to enhance the heterogeneity of a homogeneous beam. But starting with the worst possible solution may not be the best approach. Therefore, the influence of the initial solution is analysed. The chosen initial solution was a specimen present of [25]. Figure 5.20 exhibits the results of its implementation. It is possible to observe that the heterogeneity level of the principal stress states has enhanced (the value of the objective function decreases as the iterative process proceeds), and the representativity of density per angles also increases as the iterative process proceeds. In spite of that, it is regarded in Figure 5.20 that the geometry of the specimen obtained is also not manufacturable.

5.2 Preliminary analysis

After having studied and optimised all the parameters and methodologies present in the topology optimisation procedure (see Table 5.2), the full potential of the heterogeneity algorithm regarding $H(\boldsymbol{\rho})$ was tested. In the present section, efforts were made towards understanding the definition of heterogeneity, formulating the problem of maximising the heterogeneity of a mechanical test, developing strategies to solve it, and studying the nature of the objective function, the parameters and methodologies embedded in it. Figure 5.21 exhibits a highly heterogeneous specimen with a mesh of 1200 elements, tested under BC1 boundary conditions, with a spectrum of principal stress angles ranging from approximately -115 to 45 degrees (the histogram $dpa(\boldsymbol{\theta})$ is relatively close to the optimal

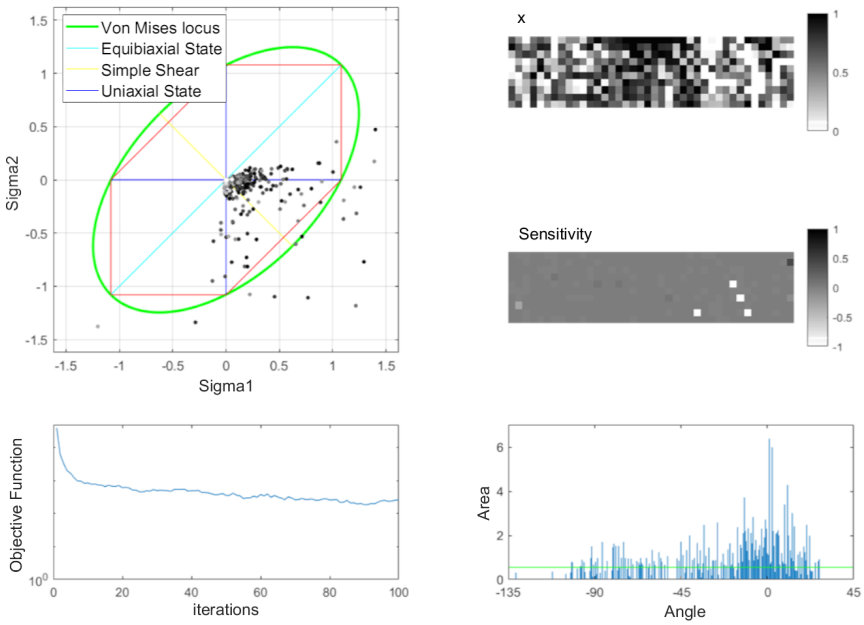


```
It:   95 func_obj:247.00 Vol: 0.50 delta: 0.300
It:   96 func_obj:251.00 Vol: 0.50 delta: 0.300
It:   97 func_obj:236.00 Vol: 0.50 delta: 0.300
It:   98 func_obj:243.00 Vol: 0.50 delta: 0.300
It:   99 func_obj:257.00 Vol: 0.50 delta: 0.300
It:  100 func_obj:264.00 Vol: 0.50 delta: 0.300
```

Figure 5.18: Analysis of the behaviour of the heterogeneity algorithm regarding $H(\boldsymbol{\rho})$ under a value of δ=0.3.

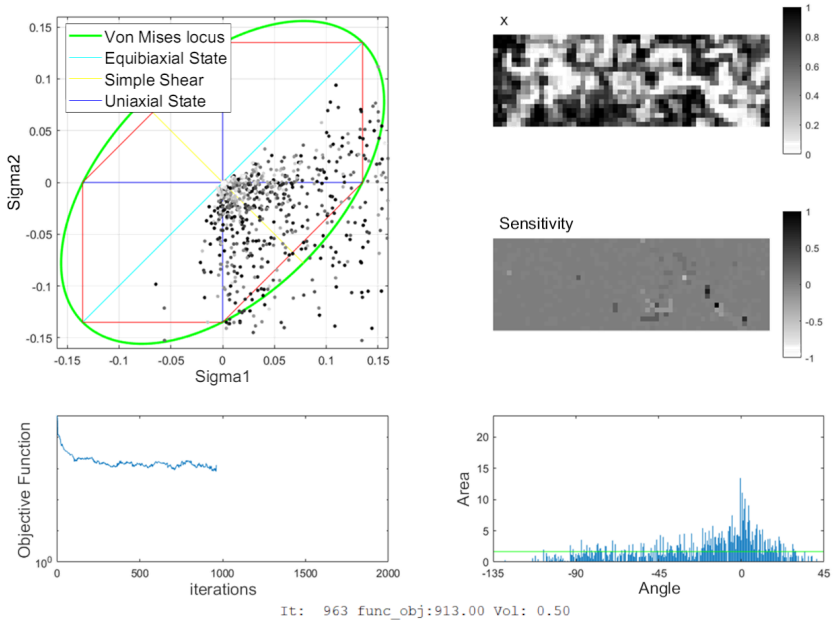


```
It:  963 func_obj:913.00 Vol: 0.50
```

Figure 5.19: Analysis of the mesh refinement over the heterogeneity algorithm regarding $H(\boldsymbol{\rho})$.

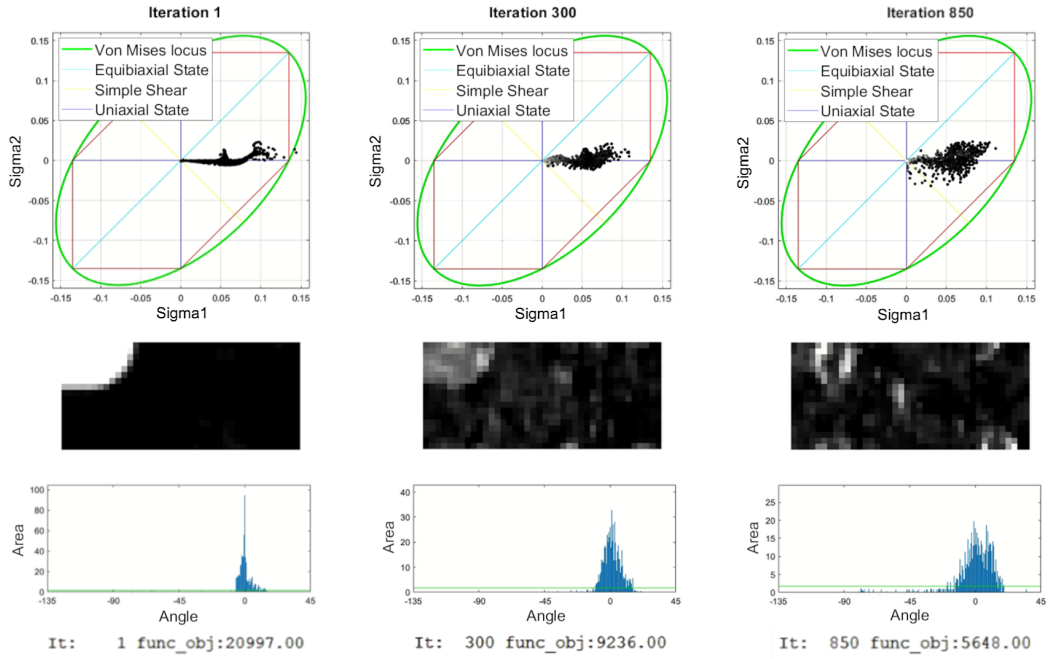

Figure 5.20: A representation of the iterative process of the heterogeneity algorithm regarding $H(\boldsymbol{\rho})$ given the initial solution of a heterogeneous specimen taken from [25].

solution a_o). It is also observed that the range of stress states in the principal stresses distribution is broad, and therefore, a mechanical test with enormous heterogeneity was obtained, which was one of the prerequisites of this work. Figure 5.22 exhibits the evolution of the algorithm for 4000 plus iterations, showing that the heterogeneity levels attained were excellent, but the intermediate densities were not pushed to its desired values. In conclusion, the geometry of the specimen obtained is impossible to manufacture and test. So, the second prerequiste of this work is not fulfilled, as the sample obtained is not suitable for use in the industry.

Table 5.2: List of constants of optimised parameters on the heterogeneity algorithm regarding $H(\boldsymbol{\rho})$.

Final Constants		**Description**
nelx	60	Number of elements in x dimension
nely	20	Number of elements in y dimension
penal	3	SIMP penalisation
vlim	0.5	Volume fraction
ar	0.5°	Angle resolution (degrees)
step_fin_dif	0.0001	Disturbance step - finite difference method
delta_move	0.2	Updating step
filter	1	Density filter – boolean

One of the predominant factors for the non-satisfactory results may be the definition of the objective function. In topology optimisation, the objective function is usually defined as an integral over the design domain. However, the objective function $H(\boldsymbol{\rho})$

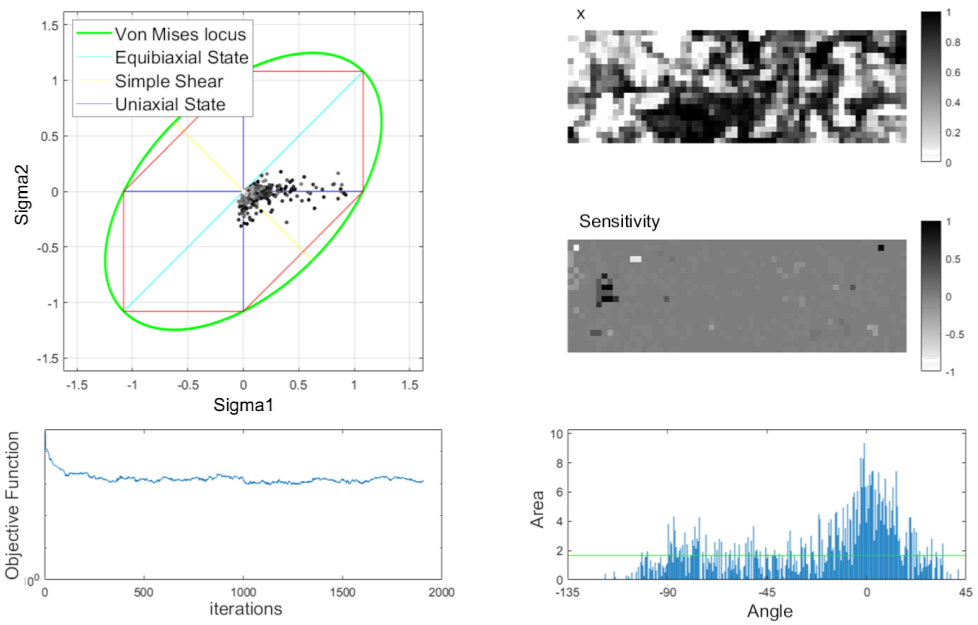

Figure 5.21: Analysis of the final heterogeneity algorithm regarding $H(\boldsymbol{\rho})$ for 1776 iterations.

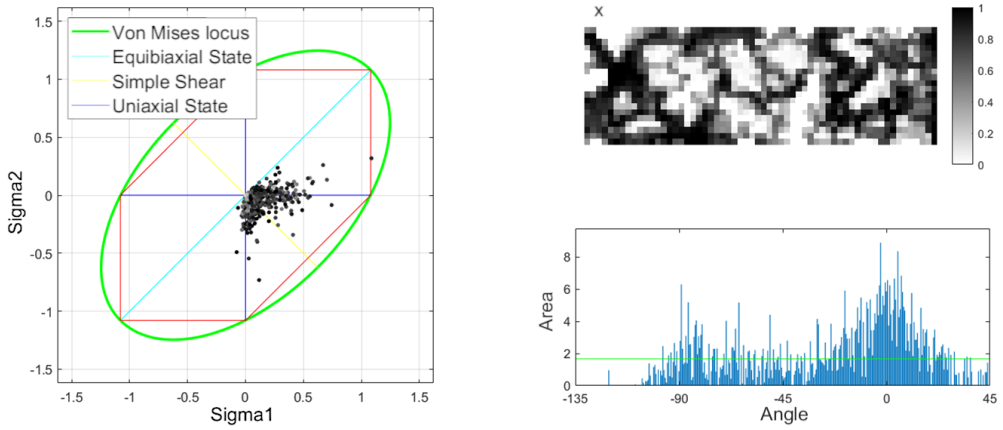

Figure 5.22: Analysis of the final heterogeneity algorithm regarding $H(\boldsymbol{\rho})$ for 4305 iterations.

defines the integral over the principal stress angle θ. On top of that, the resolution of the angles a_r conveys this problem a discrete nature, which is not ideal. Using a more appropriate objective function and defining a more suitable formulation, the goal of this dissertation is completely attainable. Also, the function where the design variable ρ is present, $E(\rho)$ from Equation3.14, is not part of the objective function, and that's the main reason why the SIMP penalisation is not effective in order to push the intermediate densities to 0 and 1. The heterogeneity problem has proven to be highly complex.

5.3 Results regarding the maximisation of the sum of the magnitudes of the principal stress tensors

As seen in the previous section, the results obtained with the heterogeneity algorithm were satisfactory in terms of the heterogeneity levels achieved. Nonetheless, the geometries of the specimens obtained were impossible to manufacture. Being that the purpose of the dissertation is to aid in the characterisation of metals in the real world, a set of complementary objective functions were implemented according to Section 4.3. Initially, it was speculated that, for the formulation S_{m1}, defining the boundary conditions as BC1 (Figure 4.1a) might not be effective because, as all the stress states are equal, the algorithm would not have sensitivity to reach its objective and would be stuck in the initial solution. So, the author tested both BC1 (homogeneous) and BC2 boundary conditions as a way of inducing some heterogeneity to the system.

Figure 5.23 exhibits the results of Section 4.3 using the formulation $S_{m1}(\boldsymbol{\rho})$ present in Equation 3.21, using boundary conditions BC2 for a rectangular specimen with mesh of 80x240, a volume fraction of 0.3 and the penalisation factor equal to 3. It is observed that, even though the algorithm stabilizes in a solution for a geometry that is manufacturable, the result is not ideal in terms of heterogeneity. It is also noticed that changing the penalisation factor showed to be ineffective and the geometry converged to the same solution. This might be due to the fact that the formulation of the problem does not necessarily infer that the angles of the stress states will spread apart. Instead, this formulation will only force the stress states to be as far away as possible from the origin (which favours the elements with the stress states of greater magnitude), and also, the boundary conditions may restrict the algorithm from the beginning.

With the purpose of leading the optimisation algorithm into a solution where its maximum value is on the biaxial stress state, a similar formulation was tested under the set of homogeneous boundary conditions BC1 (Figure 4.1a) using the same rectangular specimen. This formulation is defined as $S_{m2}(\boldsymbol{\rho})$ from Equation 3.22. As seen in Figure 5.24, using boundary conditions BC1 (Figure 4.1a), it is observed that the heterogeneity levels achieved are superior than in Figure 5.23, as the range of stress states covered is broader. These boundary conditions present less of a constraints to the objective function in comparison to BC1 (Figure 4.1a), as these do not guide the algorithm forcefully into some solution that is not the ideal. Also, the geometry obtained is manufacturable.

It was also observed that the size and shape of the design domain changes both the geometry of the final results and the levels of heterogeneity attained. Figure 5.25 exhibits a square design domain with an edge composed by 135 elements using boundary conditions BC1, which yields a feasible solution where the heterogeneity levels are greater than Figure 5.24. More specifically, using the heterogeneity indicator from Section 3.3,

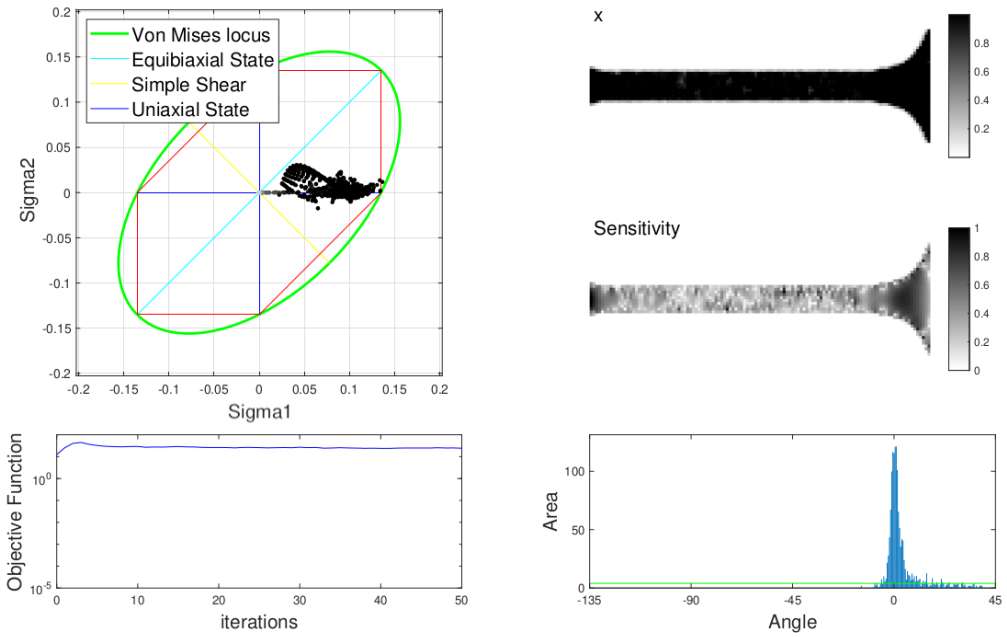

Figure 5.23: A representation of the results of formulation $S_{\mathrm{m1}}(\boldsymbol{\rho})$ for a rectangular specimen with a mesh of 80x240, volume fraction of 0.3, with boundary conditions BC2.

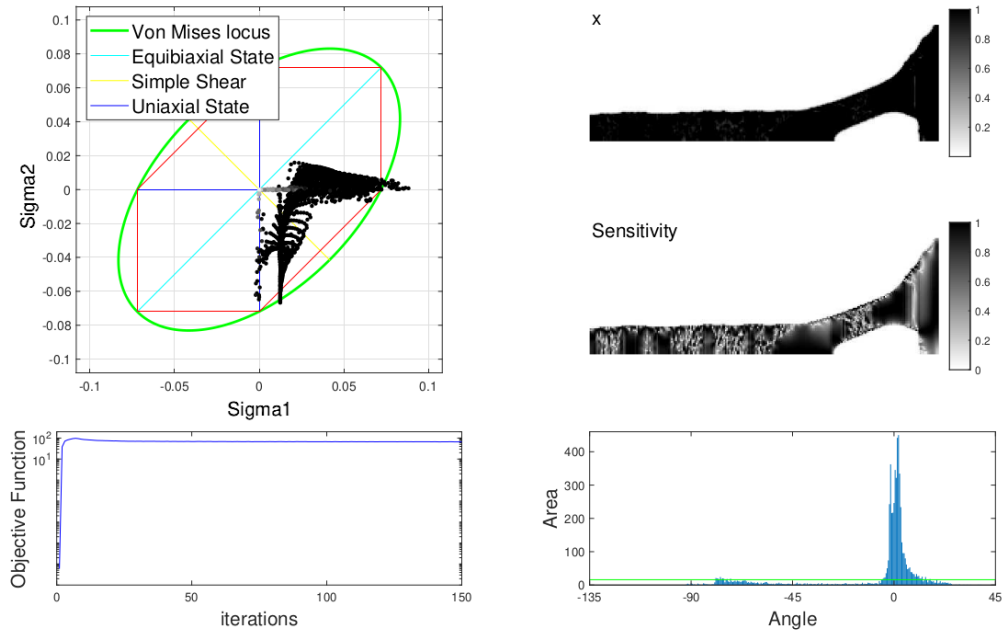

Figure 5.24: A representation of the results of formulation $S_{\mathrm{m2}}(\boldsymbol{\rho})$ for a rectangular specimen with a mesh of 80×240, volume fraction of 0.3, with boundary conditions BC1.

the specimen from Figure 5.24 yields an indicator value I_{h} of 0.0312, whilst the specimen from Figure 5.25 is equal to 0.0137, which correlates to a more heterogeneous mechanical test.

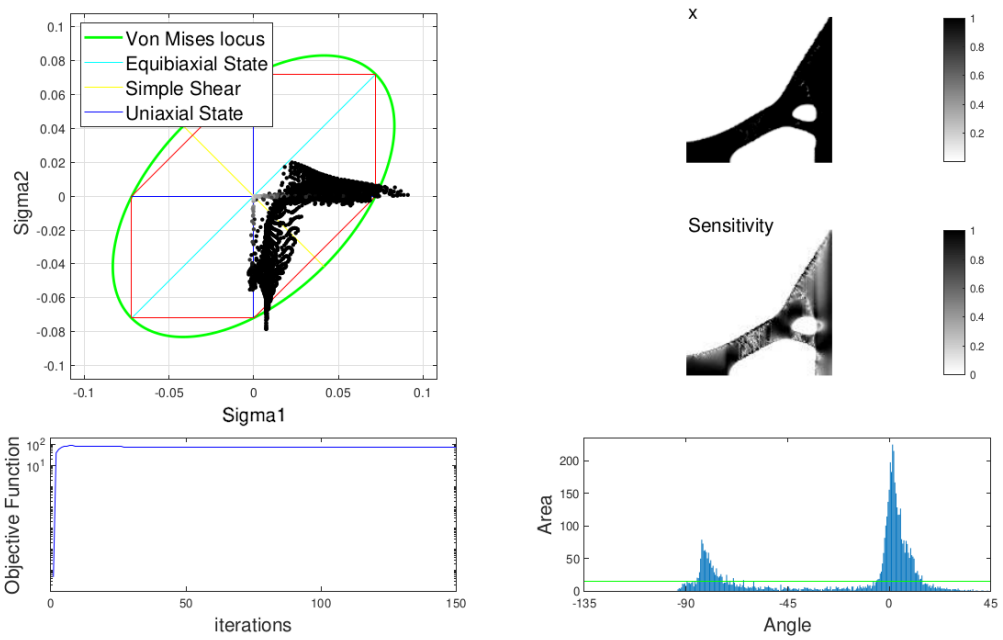

Figure 5.25: A representation of the results of formulation $S_{\mathrm{m2}}(\boldsymbol{\rho})$ for a square specimen with a mesh of 135×135, volume fraction of 0.3, with boundary conditions BC1.

During the optimisation procedure, it was noticed that the intermediate densities of the design contributed greatly to the increase of the heterogeneity of the specimen. In order to assign more weight to these elements, it was opted to divide the principal stress components (from the respective objective function in $S_{\mathrm{m2}}(\boldsymbol{\rho})$) by their respective density levels. Due to the nature of the updating scheme of the PTO, the design variable ρ is never equal to zero, which means that it is possible to divide by its value. Figures 5.26 and 5.27 exhibit the results of this implementation with the two different design domains, the same rectangular and square specimens from before, respectively. It is derived from these results that this second approach correlates to slightly worse results. Specimen from Figure 5.26 yields a heterogeneity indicator of 0.0349, which is worse than the one in specimen from Figure 5.24, and specimen from Figure 5.27 presents an indicator of 0.0144, which is also worse than the one in Figure 5.25.
On a side note, the given results never fully converge within the termination criterion defined on Section 4.2. The density values keep changing slightly from iteration to iteration, so the stop criterion is never satisfied and the iterative process proceeds indefinitely. Nonetheless, the overall geometry of the specimen seems to have stagnated in the exhibited iterative points shown previously.

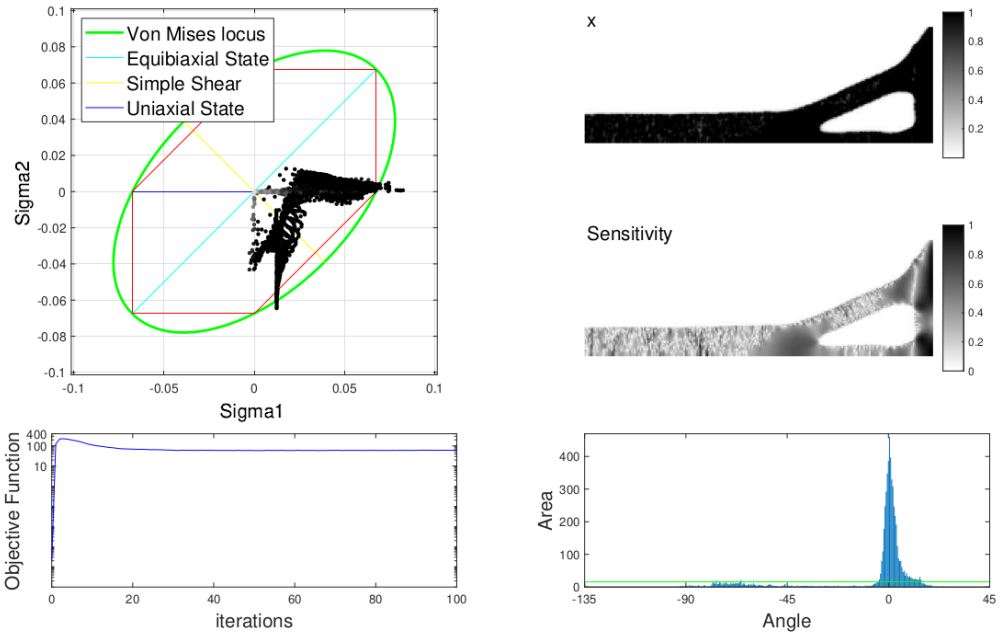

Figure 5.26: A representation of the results of formulation $S_{m2}(\boldsymbol{\rho})$ divided by the respective elemental densities, for a rectangular specimen with a mesh of 80×240, volume fraction of 0.3, with boundary conditions BC1.

5.4 Results regarding the maximisation of the sum of the angles formed by the principal stress tensors

For function $T_1(\boldsymbol{\rho})$ from Section 3.23, defining the boundary conditions as BC1, for a volume fraction of 0.5 and a penalisation factor of 3, the implementation from Section 4.3 managed to push towards a solution that maximises the heterogeneity of the stress field, as seen in Figure 5.28. Despite of that, the resulting geometry is yet non-manufacturable, as the algorithm has the intermediate densities are not pushed to 0 and 1, due to the sensitivity values being unstable from iteration to iteration.

On the other hand, a slightly different formulation was tested, $T_2(\boldsymbol{\rho})$, where instead of using the dot product to calculate the angle, the inverse tangent was employed (for which the values range from -90 to 90 degrees). Defining the homogeneous boundary conditions as BC1, the volume fraction equal to 0.5 and the penalisation factor equal to 3, Figure 5.29 shows that the results using the formulation from Equation 3.24 are more heterogeneous than the previous ones, but still non-manufacturable, which is a crucial prerequisite to this work.

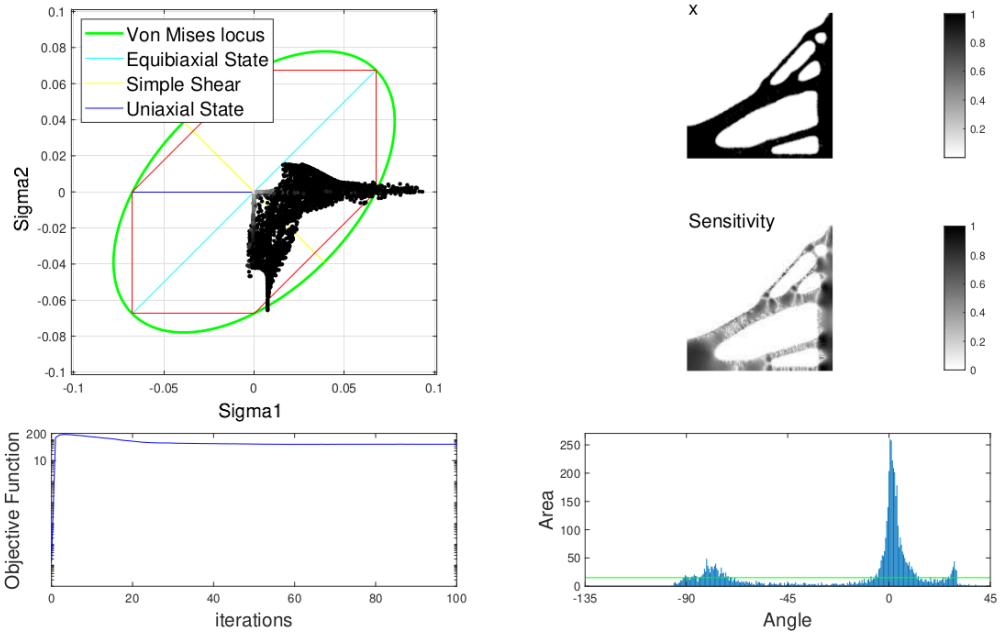

Figure 5.27: A representation of the results of formulation $S_{\mathrm{m2}}(\boldsymbol{\rho})$ divided by the respective elemental densities, for a square specimen with a mesh of 135×135, volume fraction of 0.3, with boundary conditions BC1.

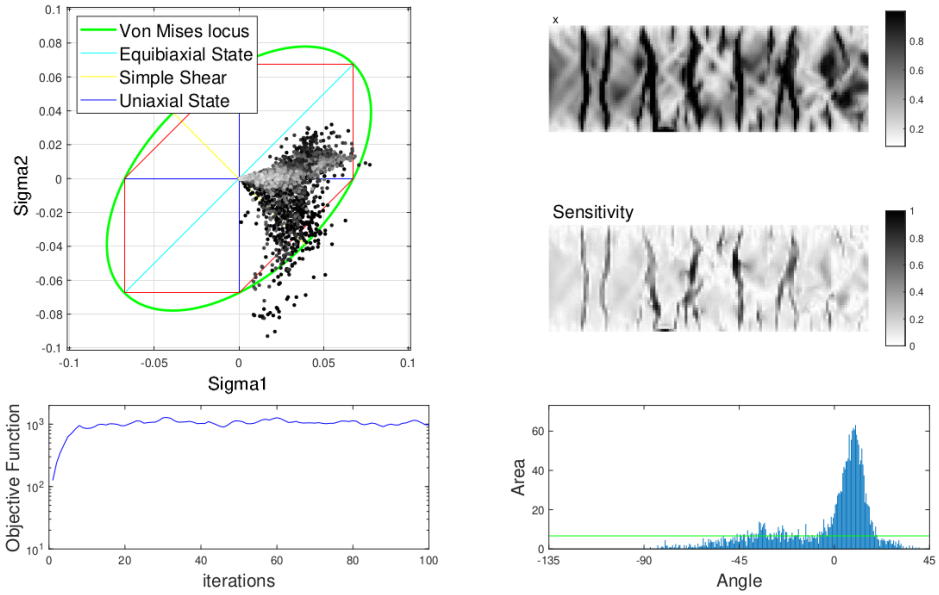

Figure 5.28: A representation of the results of formulation $T_1(\boldsymbol{\rho})$, for a rectangular specimen with a mesh of 40×120, volume fraction of 0.5, with boundary conditions BC1.

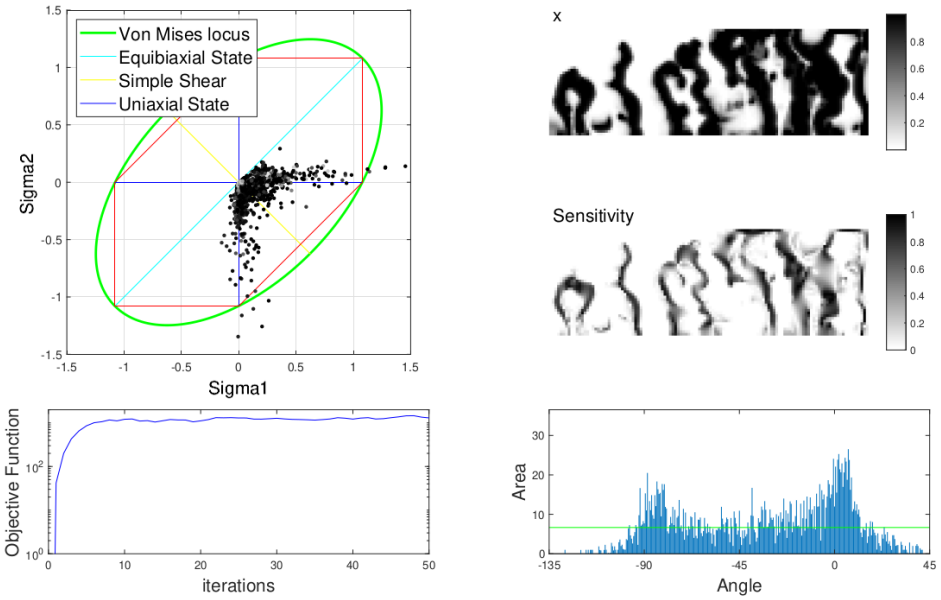

Figure 5.29: A representation of the results of formulation $T_2(\boldsymbol{\rho})$, for a rectangular specimen with a mesh of 40×120, volume fraction of 0.5, with boundary conditions BC1.

5.5 Multiobjective approaches

Heterogeneity algorithm with compliance minimisation

As analysed in Section 5.1, the heterogeneity function $H(\boldsymbol{\rho})$ presents large limitations. Despite of its results being greatly heterogeneous, the geometries obtained are not manufacturable. A multiobjective approach with the minimisation of the compliance, represented in Equation 3.26, comes as a solution to that. These multiojective functions are normalized in relation to their initial solutions, as a way of assigning equivalent magnitudes.

The results of the multiobjective formulation $M_1(\boldsymbol{\rho})$ using BC1, with a mesh of 20×60 and a penalisation factor of 4, with w_1 and w_2 equal to 0.94 and 0.06 respectively, are represented in Figure 5.30. It is concluded that opting for a multiobjective approach resulted in a geometry that is in fact manufacturable and of which the densities culminated in 0 or 1. Nonetheless, the levels of heterogeneity achieved were not superior to other specimens present in the literature (see [23, 25]). The heterogeneity indicator I_{h} from the specimen from Figure 5.30 is equal to 0.0285, which is close to some specimens in the literature. It is also noticed that, during the iterative process, as the intermediate densities are pushed to 0 and 1, the levels of heterogeneity start decreasing. Also, by examining the multiobjective function's plot in Figure 5.30, it is observed that the objective functions are in opposition, meaning that tuning the weights is crucial to find an optimal solution. Each objective function from the multiobjective approach has a different degree of influence in the overall optimisation process depending on the density levels of the geometry, and consequently on the number of iterations the algorithm is currently on. The compliance function is more stable than the heterogeneity function, and its sens-

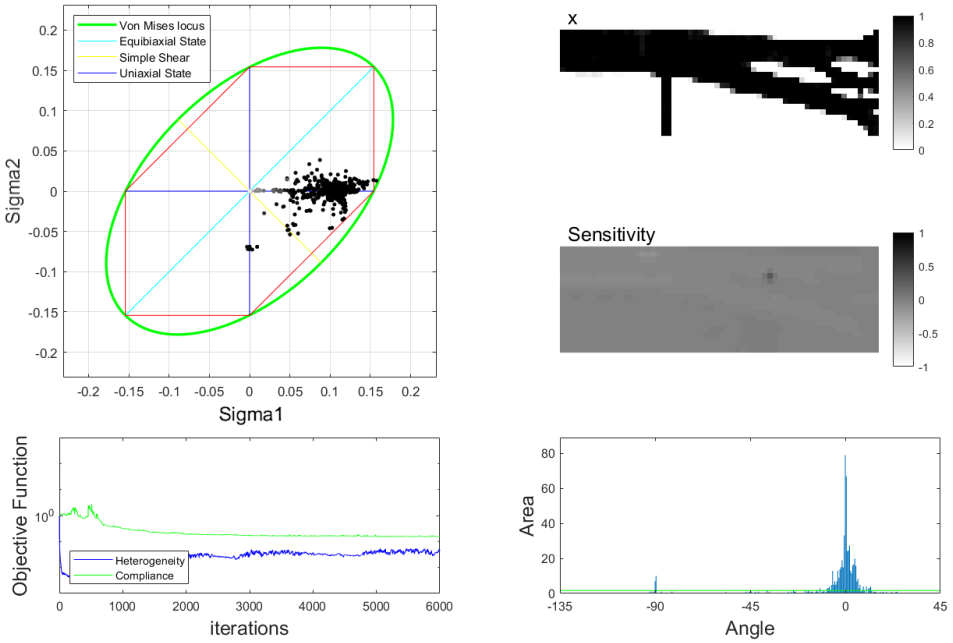

Figure 5.30: A representation of the results of formulation $M_1(\boldsymbol{\rho})$, for a rectangular specimen with a mesh of 20×60, volume fraction of 0.5, with boundary conditions BC1.

itivities will lead to a solution with less iterations. It was deducted that the heterogeneity function should have a larger weight in the initial iterations, so that the algorithm does not prematurely lead to a solution that favours the minimisation of the compliance and end up with a non-heterogeneous solution. Despite of that, if the algorithm favours the heterogeneity function, the solutions do not culminate into a solution of densities of 0 and 1. For that reason, as seen in Figure 5.31, it was opted for a heuristic methodology where the weights change linearly as the iterative process goes (the weight of the heterogeneity function decreases and the compliance increases slightly), always keeping the sum of these weights equal to 1. The results of this implementation are represented in Figure 5.32. It is observed that the solution is manufacturable and the heterogeneity levels are acceptable, with I_{h} equal to 0.0170, which is actually superior to Figure 5.30. The plot of the objective functions shows that the heterogeneity function is predominant in the initial iterations and afterwards a balance is achieved. It is observed that this result was forcefully stoped at an iteration where there was a compromise between manufacturability and heterogeneity.

For the results to fully converge into a geometry of zeros and ones regarding its density values, it is necessary to attribute a weight value to the heterogeneity portion of the multiobjective approach, which almost completely overshadows the effect of the compliance function, as seen in Figure 5.31. Also, given the high level of nonlinearity of the heterogeneity function, it is proven in this section that the structural portion of the multiobjective approach is essential to obtain a manufacturable solution, which is imperative in order to meet the goals of this work.

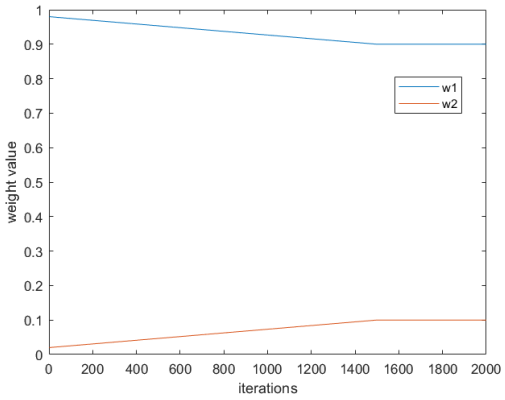

Figure 5.31: A representation of the heuristic approach of changing the weights over the iterations.

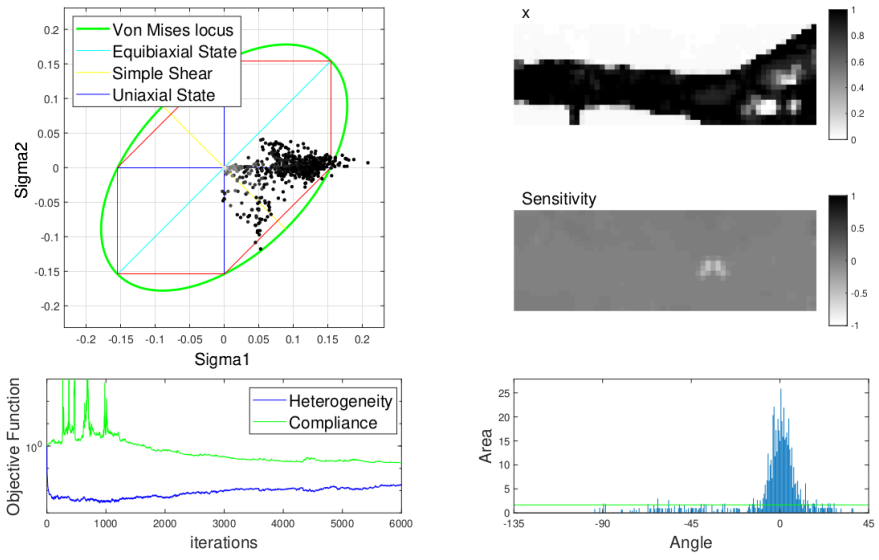

Figure 5.32: A representation of the results of formulation $M_1(\boldsymbol{\rho})$, for a rectangular specimen with a mesh of 20×60, volume fraction of 0.5, with boundary conditions BC1, using the varying weights approach.

Magnitude of the angles with compliance minimisation

As the solutions presented in Section 5.4 did not converge into 0 and 1 in terms of their density levels, the multiobjective approach with the structural feature is mandatory. The formulation of the multiobjective function, $M_2(\boldsymbol{\rho})$, combining $T_2(\boldsymbol{\rho})$ and the minimisation of the compliance is defined in Equation 3.28.

The implementation used was the one from Section 4.3, where the proportion matrices of the objective functions were floored, and then normalized using its respective maximum values in order to obtain values ranging from 0 to 1. Also, the elements with intermediate densities that had a great value of T_2 persisted, even though they are undesired. With the purpose of forcing these intermediate densities to disappear, the proportion matrix of the T_2 function was multiplied by the density matrix affected by the penalisation. Figure 5.33 exhibits the results using the homogeneous boundary conditions BC1, using a rectangular specimen with a mesh of 40x120, a penalisation factor of 6, w_1 and w_2 equal to 0,8760 and 0,1240 respectively, and a volume fraction of 0.6. It is noticed that changing the weights results either in a specimen favouring the heterogeneity or the compliance function, without any middle ground. The geometry of the specimen obtained is not manufacturable.

With the purpose of correcting the issues present on the previous approach, the author implemented the heuristic methodology of linearly changing the multiobjective weights as the design variables are updated (in a similar way to Figure 5.31). The weight ramp is represented in Figure 5.34b, and it is concluded that the geometry of the specimen is manufacturable, specially with the advancements in additive manufacturing over the years. Also, the heterogeneity levels attained in Figure 5.34a are formidable, with an indicator I_{h} equal to 0.0100. It is noticed that the execution of the *Matlab*® program had to be stopped without ever converging.

5.6 Final comparisons

The specimens obtained with the developed formulations across the present work were evaluated under the heterogeneity indicator I_{h} from Equation 3.16, as seen in Table 5.3. For comparison purposes, Table 5.4 exhibits some of the state of the art specimens present in the literature and their respective ranks regarding said indicator. It is concluded that the heterogeneity levels yielded by the specimens developed during this work are similar to those on the literature. In fact, the specimen from figure 5.34a yielded a superior heterogeneity level than the heterogeneous specimens taken from the literature in this particular work.

Additionally, some of the obtained specimens resulting from the exploratory work on this chapter are not represented on the respective sections. Appendix A encompasses a selection of said alternative results.

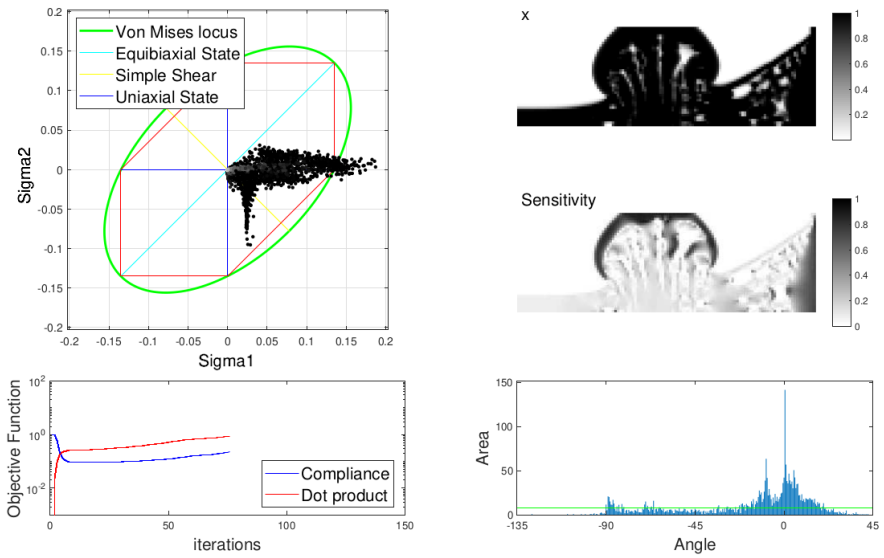

(a)

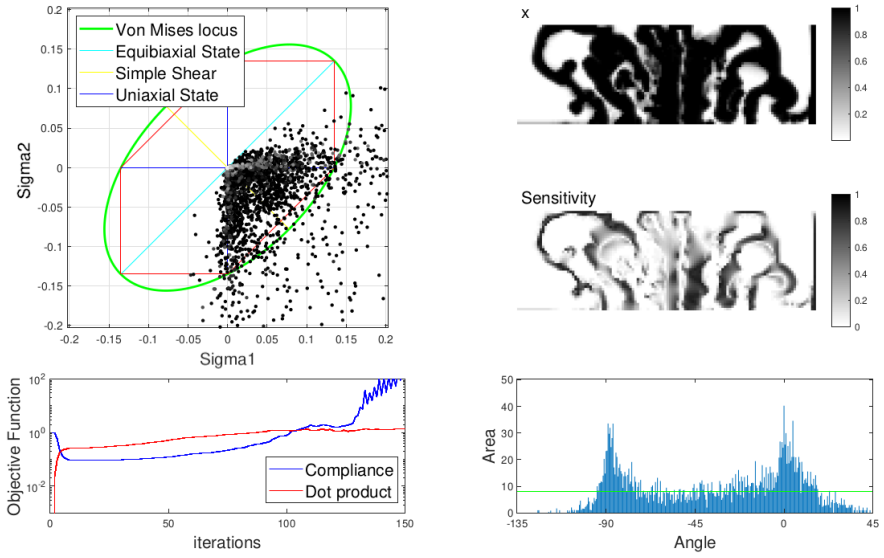

(b)

Figure 5.33: A representation of the results of formulation $M_2(\boldsymbol{\rho})$, for a rectangular specimen with a mesh of 40×120, volume fraction of 0.6, with boundary conditions BC1: (a) Specimen obtained with 75 iterations; (b) Specimen obtained with 150 iterations.

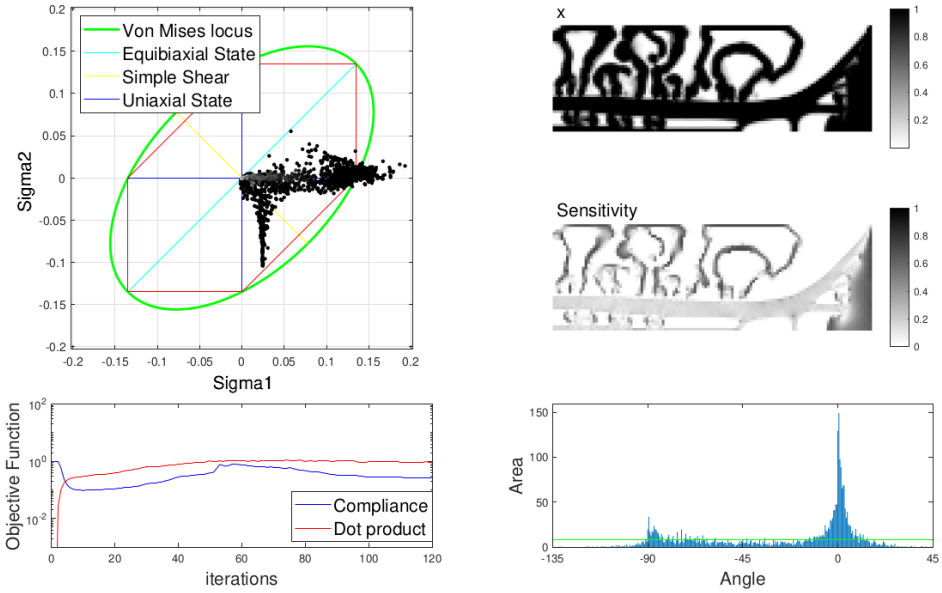

(a)

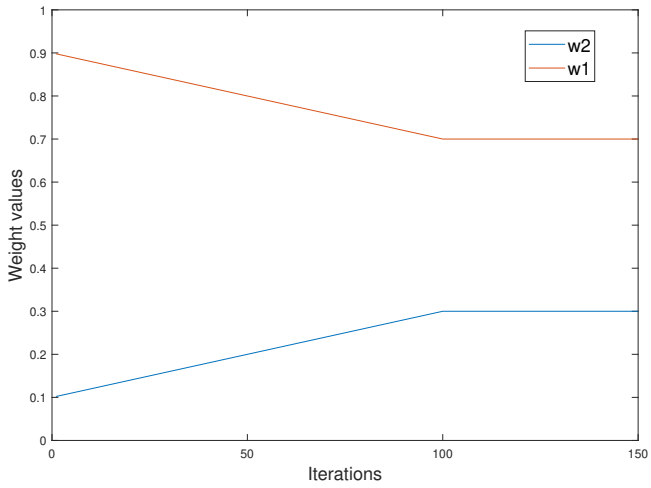

(b)

Figure 5.34: A representation of the results of formulation $M_2(\boldsymbol{\rho})$, with the variation of the weights: (a) A representation of the specimen obtained; (b) A representation of the variation of the weights from the multiobjective function.

Specimen	Histogram	Heterogeneity indicator
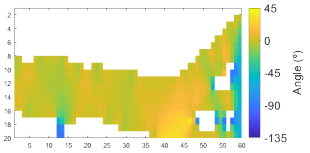	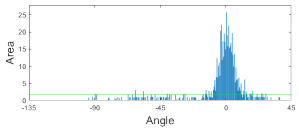	• $M_1(\boldsymbol{\rho})$ • BC1 • Figure 5.32 • $I_{\mathrm{h}} = 0.0170$
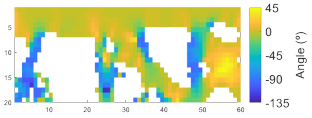	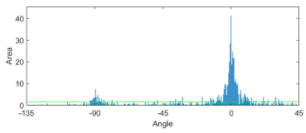	• $M_1(\boldsymbol{\rho})$ • BC1 • Figure A.1: • $I_{\mathrm{h}} = 0.0131$
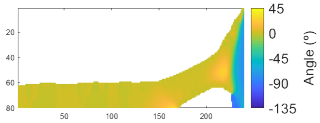	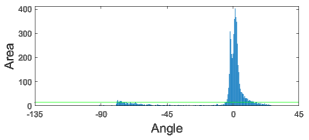	• S_{m2} • BC1 • Figure 5.24: • $I_{\mathrm{h}} = 0.0312$
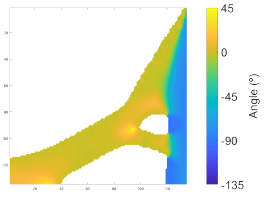	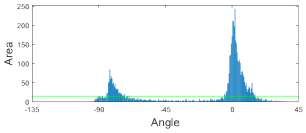	• S_{m2} • BC1 • Figure 5.25: • $I_{\mathrm{h}} = 0.0137$
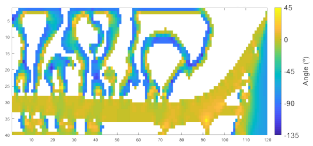	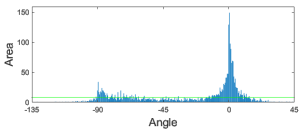	• M_2 • BC1 • Figure 5.34: • $I_{\mathrm{h}} = 0.0100$

Table 5.3: A representation between the developed specimens regarding the heterogeneity indicator.

Specimen	Histogram	Heterogeneity indicator
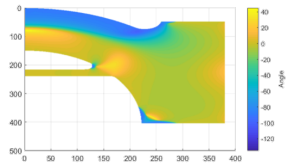	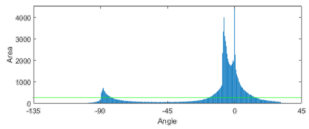	• Specimen Jones et. al [23]: • $I_h = 0.0121$
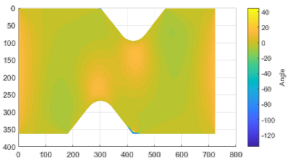	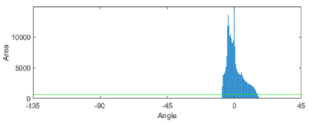	• Specimen 1 from Haddadi et. al [25]: • $I_h = 0.0286$
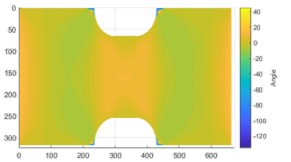	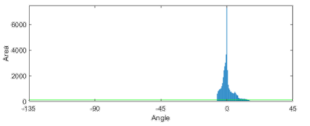	• Specimen 2 from Haddadi et. al [25]: • $I_h = 0.0558$

Table 5.4: A representation of different specimens from the literature regarding the heterogeneity indicator.

Intentionally blank page.

Chapter 6

Final Remarks

In conclusion, the overall goals of this dissertation were achieved. In the present work, an accurate heterogeneity indicator and a set of efficient algorithms were developed. Taking into account the complexity of this research problem, the solutions presented were satisfactory. More importantly, the methodologies developed hold scientific interest. These new topology optimisation formulations managed to generate geometries of manufacturable specimens with high levels of heterogeneity. Some of the specimens obtained with the different formulations developed within this dissertation yield heterogeneity levels similar to some specimens present in the literature, as seen in Tables 5.3 and 5.4. However, it is regarded that the full potential of topology optimisation was not attained. The topology optimisation procedure is not bound by any predefined geometry. In fact, some of the non-manufacturable solutions obtained yielded heterogeneity levels superior than some of the state of the art samples (e.g. Figures 5.22 and 5.29). Having such a great level of freedom in the design of the geometry with this optimisation procedure presents huge challenges. The principal challenge found in applying topology optimisation to this particular problem lays on the formulation of the objective function and its constraints. The nature of the heterogeneity objective functions defined is highly non-linear, which implies that it is difficult to push the intermediate density variables to a manufacturable solution with density levels of zeros and ones. The gray elements in the iterative process make some of the black elements have different stress states, and have heterogeneous states themselves. As they disappear, the other elements seem to shift into states closer to the uniaxial state. That is why the heterogeneity levels seem to decrease as the iterative process proceeds. In fact, obtaining a non-manufacturable specimem with fantastic heterogeneity is rather useless to the industry. It was concluded that, in order to obtain a manufacturable heterogeneous specimen, it is essential to either use a formulation of direct maximisation of heterogeneity, allied with a structural formulation or constraint (Section 3.5), or to use a formulation that indirectly induces heterogeneity in the specimen but which does not perfectly reflect the problem and does not necessarily produce the optimal results (Section 3.4.1).

For future work it is important to find a more efficient formulation for this problem, as it was proven to be the most difficult task. It is also important to assess the fact that topology optimisation may not be the best solution for said problem, as the intermediate densities are an adversity to the optimisation procedure. One solution might be to use evolutionary (or genetic) algorithm allied with topology optimisation, in order to avoid the intermediate densities. Also, other optimisation procedures may be more efficient

and accurate than topology optimisation. In shape optimisation, design variables are the parameters that define some boundary of the design (and not the whole area as in topology optimisation). As a consequence, the complexity and non-linearity of the problem in comparison to topology optimisation can be lower.

On a side note, depending on the formulation and on the usage of sensitivities, the computational work using *Matlab*® seemed to be expensive, and using a faster programming language may be essential.

Appendices

Appendix A

Additional results

Figure A.1 represents a solution using $M_1(\boldsymbol{\rho})$ from Equation 3.26, where the algorithm obtained a geometry with great heterogeneity, but if the program had not been stopped, the gray densities, which present a great role on the overall heterogeneity of the specimen, would disappear.

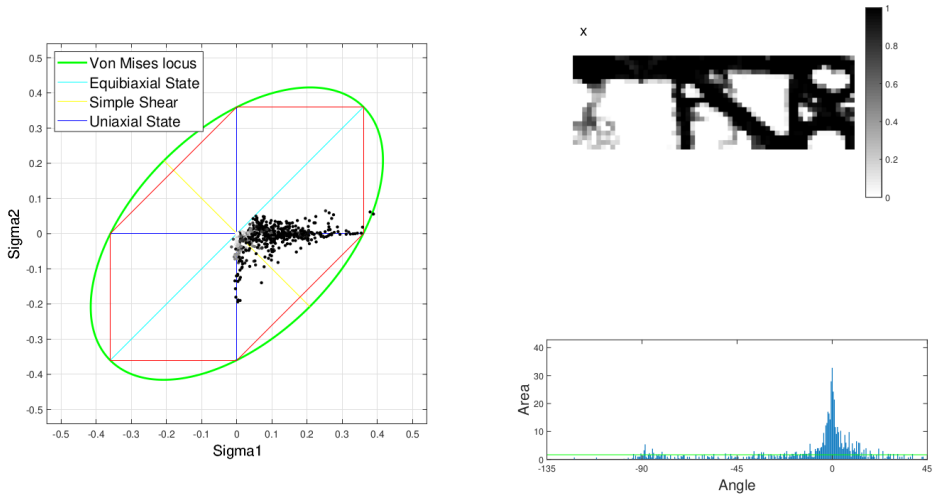

Figure A.1: A representation of a specimen developed with formulation $M_1(\boldsymbol{\rho})$ for a mesh size of 10×40, penalty exponent equal to 4, with BC1 boundary conditions, using a particular varying weights approach.

Figures A.2, A.3, A.4, A.5, A.6 and A.7 represent a set of complementary manufacturable heterogeneous solutions using formulation $M_1(\boldsymbol{\rho})$ with different multiobjective weights. These alternatives were part of the exploratory procedure, where the weights were tuned in order to obtain the optimal solution.

Figure A.8 exhibits a complementary solution to the formulation $M_1(\boldsymbol{\rho})$ with a different set of weights. Even though the heterogeneity levels attained are high, the geometry is difficult to manufacture and does not appear to have a great deal of stiffness.

Figure A.9 represents a solution using a multiobjective approach with $S_{\mathrm{m1}}(\boldsymbol{\rho})$ and compliance, with BC2 boundary conditions. In this case, even though the specimen is

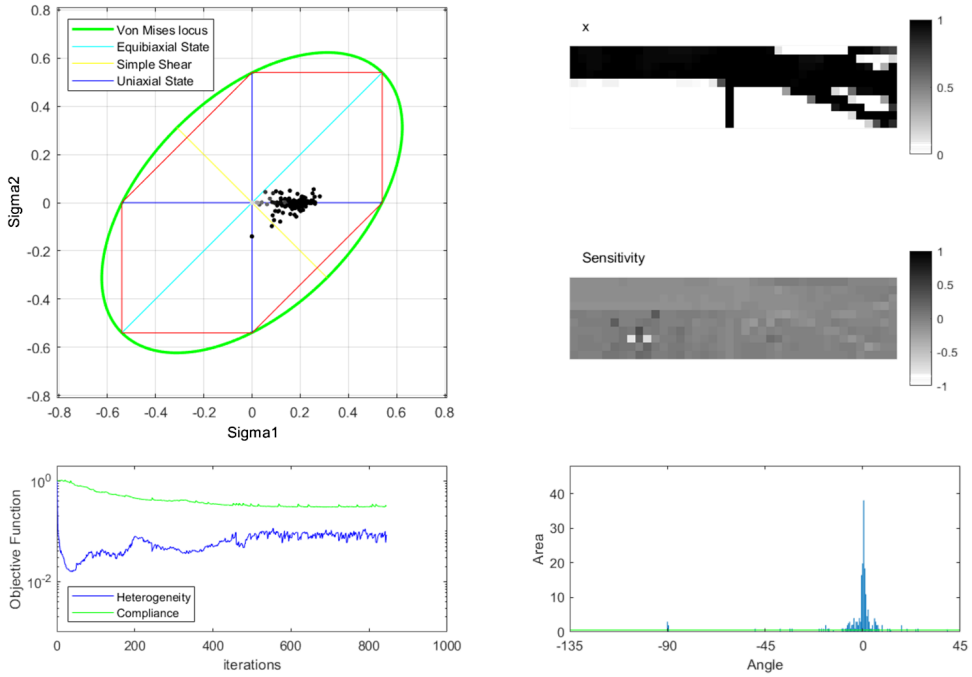

Figure A.2: An alternative solution of using the multiobjective function $M_1(\boldsymbol{\rho})$, with BC1 boundary conditions and a mesh size of 10×40.

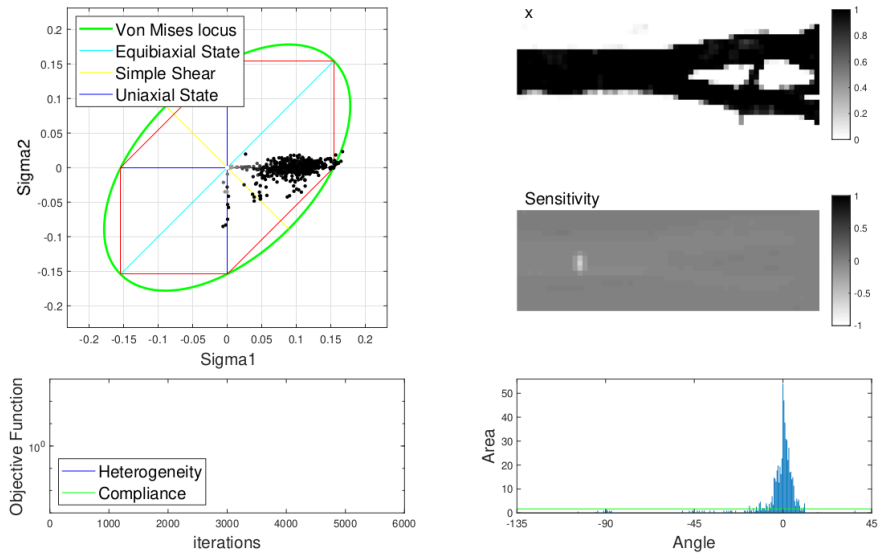

Figure A.3: A representation of the results of formulation $M_1(\boldsymbol{\rho})$, for a rectangular specimen with a mesh of 20×60, volume fraction of 0.5, with boundary conditions BC1, using a particular varying weights approach.

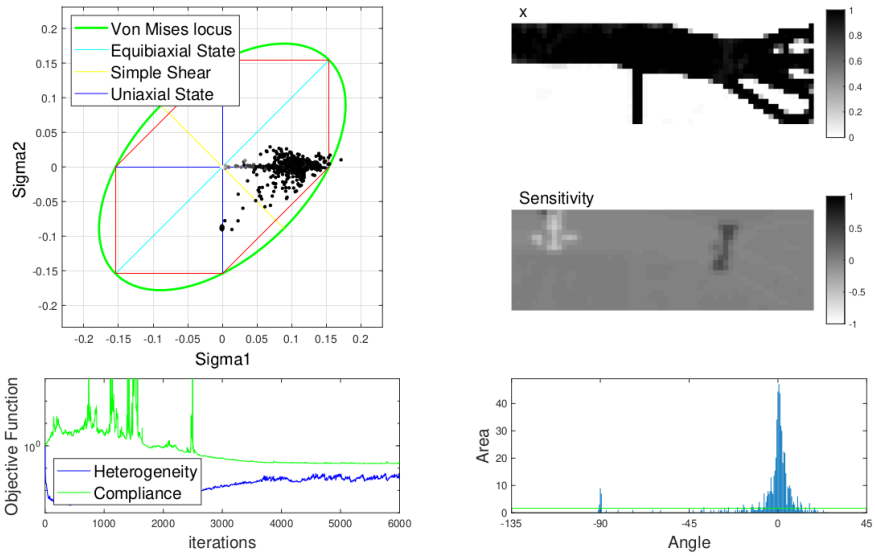

Figure A.4: A representation of the results of formulation $M_1(\boldsymbol{\rho})$, for a rectangular specimen with a mesh of 20×60, volume fraction of 0.5, with boundary conditions BC1, using a particular varying weights approach.

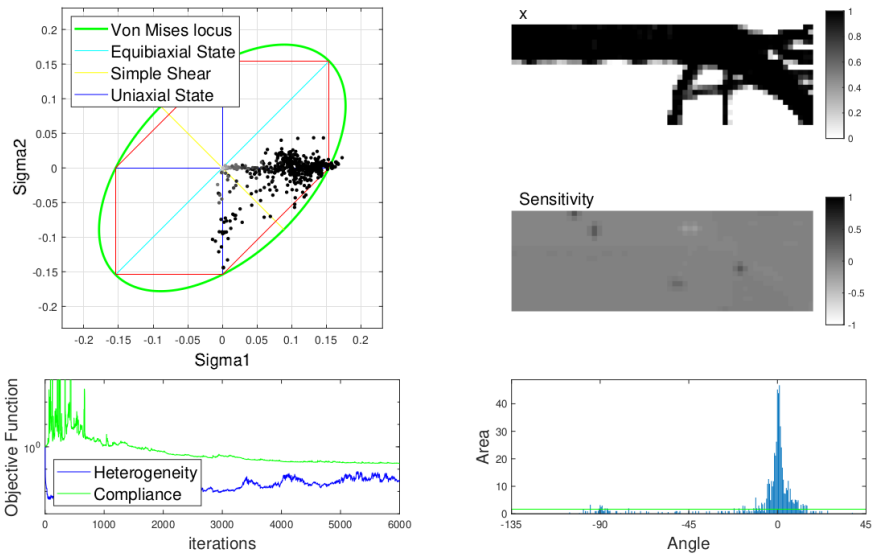

Figure A.5: A representation of the results of formulation $M_1(\boldsymbol{\rho})$, for a rectangular specimen with a mesh of 20×60, volume fraction of 0.5, with boundary conditions BC1, using a particular varying weights approach.

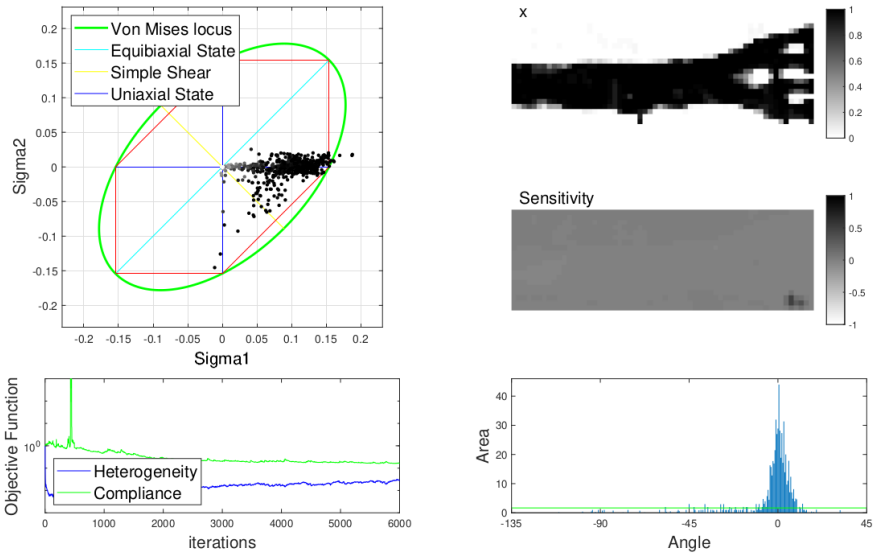

Figure A.6: A representation of the results of formulation $M_1(\boldsymbol{\rho})$, for a rectangular specimen with a mesh of 20×60, volume fraction of 0.5, with boundary conditions BC1, using a particular varying weights approach.

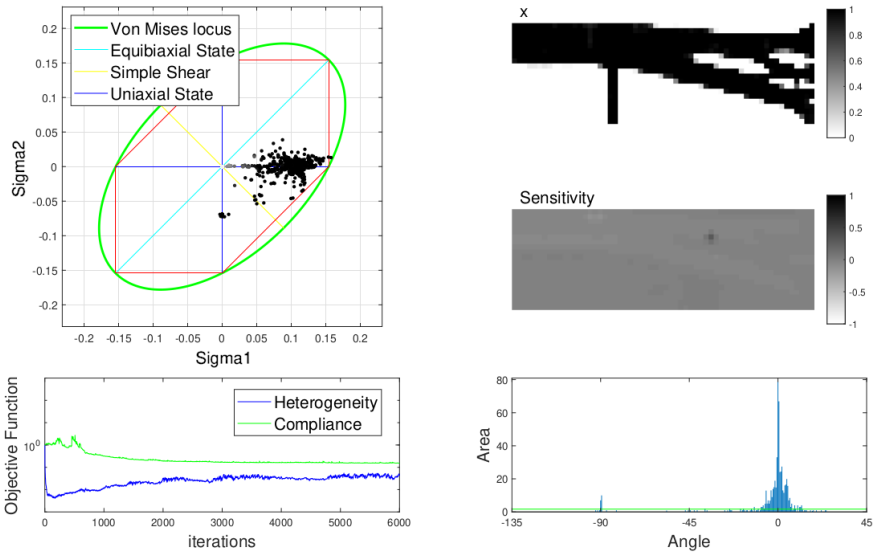

Figure A.7: A representation of the results of formulation $M_1(\boldsymbol{\rho})$, for a rectangular specimen with a mesh of 20×60, volume fraction of 0.5, with boundary conditions BC1, using a particular varying weights approach.

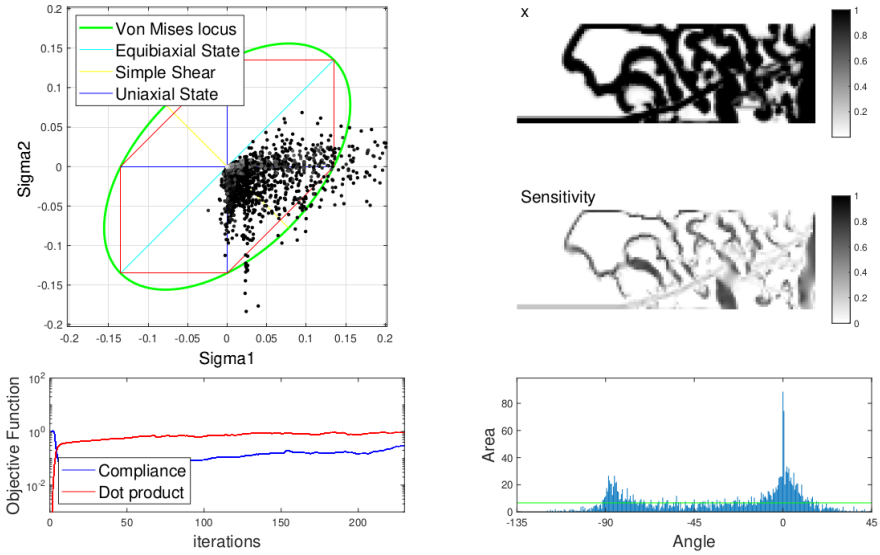

Figure A.8: A representation of the specimen obtained from Formulation $M_1(\boldsymbol{\rho})$, with BC1 boundary conditions, non-varying weights of w_1 and w_2 of 0,75 and 0,25 respectively, penalty factor of 6, a volume fraction of 0,5 and an indicator I_h of 0.0047.

manufacturable, the heterogeneity level is poor.

Figure A.10 represents a multiobjective approach using formulation $T_1(\boldsymbol{\rho})$ and the compliance function, with BC2 boundary conditions. Adding the compliance function to $T_1(\boldsymbol{\rho})$ was ineffective, as the intermediate densities persisted and the heterogeneity level is low.

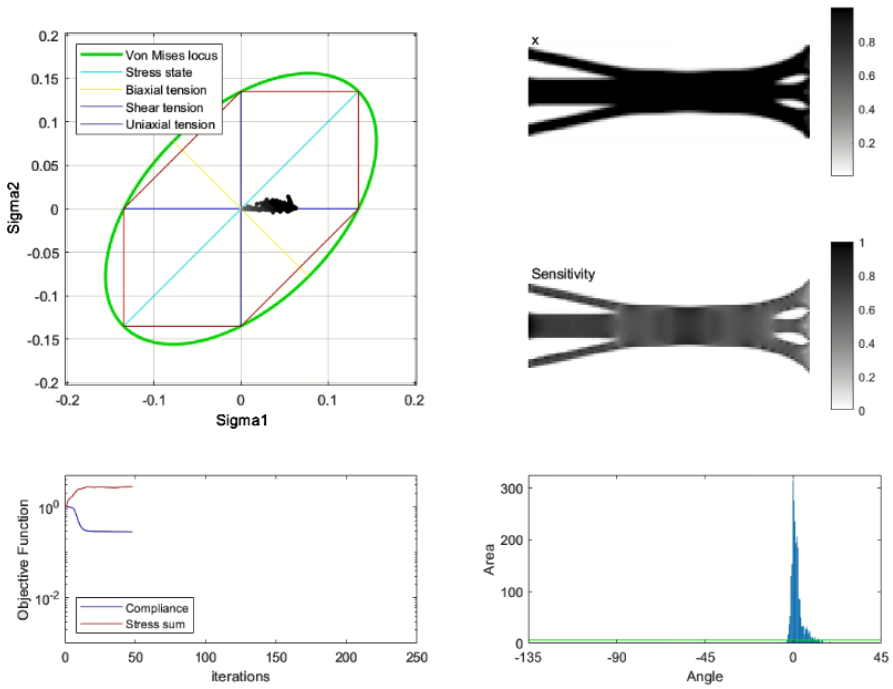

Figure A.9: A solution for a multiobjective approach using formulation $S_{\mathrm{m1}}(\boldsymbol{\rho})$ and the compliance function, with BC2 boundary conditions, a mesh size of 80×240, with the weights set to 0.01 and 0.99 respectively.

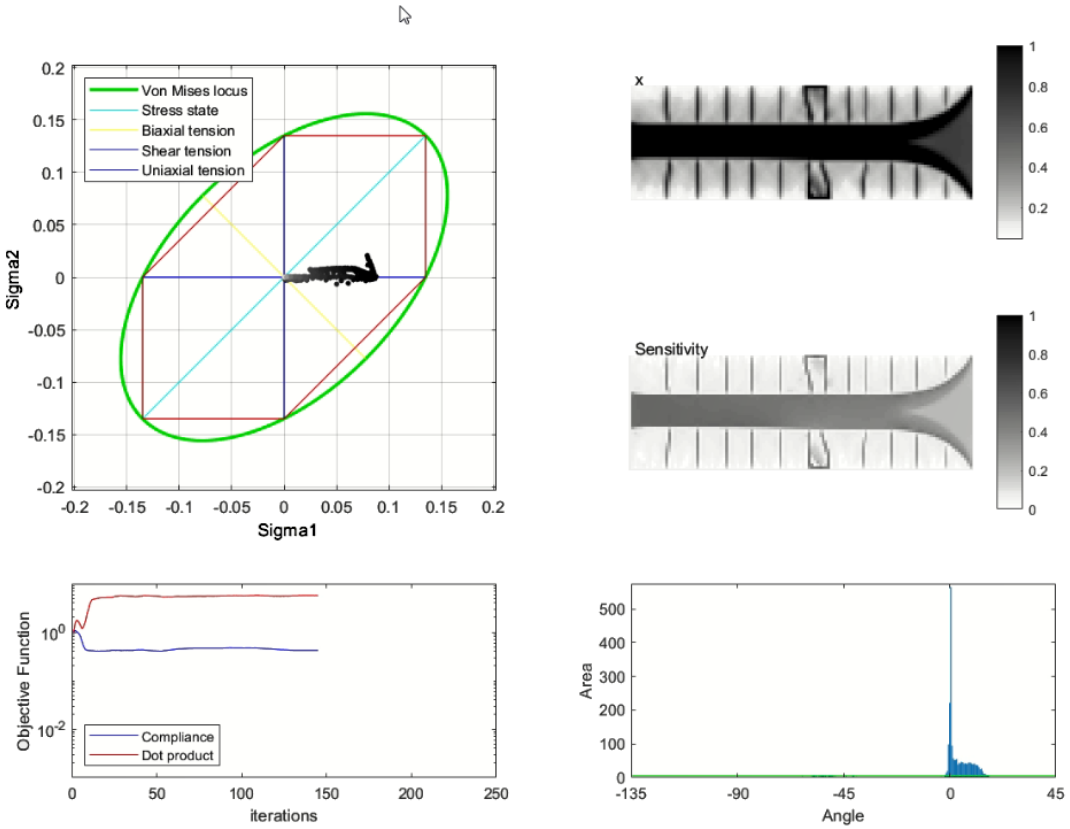

Figure A.10: A solution for a multiobjective approach using formulation $T_1(\boldsymbol{\rho})$ and the compliance function, with BC2 boundary conditions, a mesh size of 40×120, with both weights set to 0.5.

Intentionally blank page.

Bibliography

[1] P. A. Prates, A. F. Pereira, N. A. Sakharova, M. C. Oliveira, and J. V. Fernandes, "Inverse Strategies for Identifying the Parameters of Constitutive Laws of Metal Sheets", *Advances in Materials Science and Engineering*, pp. 1–16, 2016.

[2] S. Cooreman, D. Lecompte, H. Sol, J. Vantomme, and D. Debruyne, "Identification of mechanical material behavior through inverse modeling and DIC", *Experimental Mechanics*, vol. 48, pp. 421–433, 2008.

[3] N. M. Souto, *Computational design of a mechanical test for material characterization by inverse analysis.* PhD thesis, Department of Mechanical Engineering, University of Aveiro, pp. 1–226, 2015.

[4] G. Vladimír, "Plane Stress Finite Element Analysis and Experimental Measurement", Bratislava, 2013.

[5] D. Mohr and S. Henn, "Calibration of stress-triaxiality dependent crack formation criteria: A new hybrid experimental-numerical method", *Experimental Mechanics*, vol. 47, pp. 805–820, 2007.

[6] A. Brosius, Q. Yin, A. Güner, and A. E. Tekkaya, "A new shear test for sheet metal characterization", *Steel Research International*, vol. 82, pp. 323–328, 2011.

[7] Z. Marciniak, J. Duncan, and S. Hu, *Mechanics of Sheet Metal Forming.* London, 1992: Butterworth-Heinemann, 2002.

[8] K. Mattiasson, "Material Characterization and Modeling for Industrial Sheet Forming Simulations", vol. 875, pp. 875–880, 2004.

[9] M. Arcan, Z. Hashin, and A. Voloshin, "A method to produce uniform plane-stress states with applications to fiber-reinforced materials - A specially designed specimen yields material properties under pure shear or uniform plane-stress conditions", *Experimental Mechanics*, vol. 18, pp. 141–146, 1978.

[10] R. El-Hajjar and R. Haj-Ali, "In-plane shear testing of thick-section pultruded FRP composites using a modified Arcan fixture", *Composites Part B: Engineering*, vol. 35, pp. 421–428, 2004.

[11] T. Pottier, P. Vacher, F. Toussaint, H. Louche, and T. Coudert, "Out-of-plane Testing Procedure for Inverse Identification Purpose: Application in Sheet Metal Plasticity", *Experimental Mechanics*, vol. 52, pp. 951–963, 2012.

[12] M. P. Bendsøe and O. Sigmund, *Topology optimization: theory, methods, and applications*, Springer, 2003.

[13] K. Liu and A. Tovar, "An efficient 3D topology optimization code written in Matlab", *Structural and Multidisciplinary Optimization*, vol. 50, pp. 1175–1196, 2014.

[14] E. Biyikli and A. C. To, "Proportional Topology Optimization : A New Non-Sensitivity Method for Solving Stress Constrained and Minimum Compliance Problems and Its Implementation in MATLAB", *PLoS ONE*, vol. 10, pp. 1–23, 2015.

[15] O. Sigmund, "A 99 line topology optimization code written in matlab", *Structural and Multidisciplinary Optimization*, vol. 21, pp. 120–127, 2001.

[16] S. H. Jeong, S. H. Park, D. H. Choi, and G. H. Yoon, "Toward a stress-based topology optimization procedure with indirect calculation of internal finite element information", *Computers and Mathematics with Applications*, vol. 66, pp. 1065–1081, 2013.

[17] R. Yang and J. Du, "Microstructural topology optimization with respect to sound power radiation", *Structural and Multidisciplinary Optimization*, vol. 47, pp. 191–206, 2013.

[18] A. K. Nandy and C. S. Jog, "Optimization of vibrating structures to reduce radiated noise", *Structural and Multidisciplinary Optimization*, vol. 45, pp. 717–728, 2012.

[19] X. Huang, Y. M. Xie, B. Jia, Q. Li, and S. W. Zhou, "Evolutionary topology optimization of periodic composites for extremal magnetic permeability and electrical permittivity", *Structural and Multidisciplinary Optimization*, vol. 46, pp. 385–398, 2012.

[20] B. Zheng, C. J. Chang, and H. C. Gea, "Topology optimization of energy harvesting devices using piezoelectric materials", *Structural and Multidisciplinary Optimization*, vol. 38, pp. 17–23, 2009.

[21] Q. Li, G. P. Steven, Y. M. Xie, and O. M. Querin, "Evolutionary topology optimization for temperature reduction of heat conducting fields", *International Journal of Heat and Mass Transfer*, vol. 47, pp. 5071–5083, 2004.

[22] C. Zhuang, Z. Xiong, and H. Ding, "A level set method for topology optimization of heat conduction problem under multiple load cases", *Computer Methods in Applied Mechanics and Engineering*, vol. 196, pp. 1074–1084, 2007.

[23] E. M. Jones, K. N. Karlson, and P. L. Reu, "Investigation of assumptions and approximations in the virtual fields method for a viscoplastic material model", *Strain*, pp. 1–30, 2019.

[24] E. Andreassen, A. Clausen, M. Schevenels, and B. S. Lazarov, "Efficient topology optimization in MATLAB using 88 lines of code Efficient topology optimization in MATLAB using 88 lines of code", pp. 1–15, 2011.

[25] H. Haddadi and S. Belhabib, "Improving the characterization of a hardening law using digital image correlation over an enhanced heterogeneous tensile test", *International Journal of Mechanical Sciences*, vol. 62, pp. 47–56, 2012.